

Statistical Mechanics of Protein Solutions

Statistical Mechanics of Protein Solutions

PROEFSCHRIFT

ter verkrijging van de graad van doctor
aan de Technische Universiteit Delft,
op gezag van de Rector Magnificus Prof. dr. ir. J. T. Fokkema,
voorzitter van het College voor Promoties,
in het openbaar te verdedigen op dinsdag 20 november 2007 om 15:00 uur

door Peter PRINSEN

natuurkundig ingenieur en wiskundig ingenieur
geboren te 's-Hertogenbosch.

Dit proefschrift is goedgekeurd door de promotor:

Prof. dr. T. Odijk

Samenstelling promotiecommissie:

Rector Magnificus	voorzitter
Prof. dr. T. Odijk	Technische Universiteit Delft, promotor
Prof. dr. M. O. Coppens	Technische Universiteit Delft
Prof. dr. D. Frenkel	AMOLF
Prof. dr. W. Kegel	Universiteit Utrecht
Prof. dr. H. Schiessel	Universiteit Leiden
Prof. dr. S. de Vries	Technische Universiteit Delft
Prof. dr. D. R. M. Williams	Australian National University

ISBN 978-90-9022310-0

Cover design by Janine Kiers

Colofon: Thesis typeset in L^AT_EX, pictures prepared with MATLAB 7.4 and converted to the appropriate format with laprint.m

Author email: peter@p8r.nl

Experiment is the sole source of truth. It alone can teach us something new; it alone can give us certainty. - Henri Poincaré (1854-1912)

Equations are more important to me, because politics is for the present, but an equation is something for eternity. - Albert Einstein (1879-1955)



Contents

1	Introduction	1
1.1	Proteins	1
1.2	Theoretical preliminaries: a pedestrian approach	3
1.2.1	Introduction	3
1.2.2	Effective one-component description	4
1.2.3	Virial expansion	6
1.2.4	The Baxter potential	9
1.2.5	Higher concentrations	9
1.3	Theoretical preliminaries: rigorous treatment	12
1.3.1	Introduction	12
1.3.2	Effective one-component description	13
1.3.3	Virial expansion	15
1.3.4	Distribution function theories	18
1.3.5	The Baxter potential	20
1.4	Outline of the thesis	22
2	Optimized Baxter model of protein solutions: Electrostatics versus adhesion	29
2.1	Introduction	29
2.2	Second virial coefficient	30
2.2.1	Theory	30
2.2.1.1	Second virial coefficient	30
2.2.1.2	Effective attractive well	32
2.2.1.3	Attractive well in the Baxter limit	35
2.2.2	Application to lysozyme	36
2.2.2.1	Experimental Data	36
2.2.2.2	Theory	36

2.3	Liquid state theory at higher densities	42
2.3.1	Theory	42
2.3.1.1	Density dependent attractive well in the Baxter limit	42
2.3.1.2	Approximate radial distribution function for the Baxter potential	44
2.3.1.3	Determination of the effective adhesion	45
2.3.2	Application to lysozyme	47
2.4	Discussion	47
2.5	Appendix	50
2.5.1	Effective charge	50
2.5.2	Dependence of B_2 on ionic strength	51
2.5.3	Corrections to the free energy	52
3	Application of the optimized Baxter model to the hard-core attractive Yukawa system	59
3.1	Introduction	59
3.2	Theory	61
3.3	Simulations	63
3.4	Results and discussion	65
3.4.1	Phase equilibrium	65
3.4.2	Consistency test in the fluid phase	67
3.5	Appendix	72
3.5.1	Finite size effects	72
3.5.2	Second-order correction to the free energy	74
4	Fluid-crystal coexistence for proteins and inorganic nanocolloids: Dependence on ionic strength	79
4.1	Introduction	79
4.2	Optimized Baxter model	81
4.3	Solubility curves: chemical potential of the fluid phases	84
4.3.1	Method	84
4.3.2	Lysozyme	84
4.3.3	Silicotungstates (STA)	87
4.4	Crystal model: Donnan effect	91
4.4.1	Comparison with experiment	95
4.4.1.1	Lysozyme crystal	95
4.4.1.2	STA crystals	96
4.4.1.3	$H_4STA.31H_2O$	96
4.4.1.4	$Li_4STA.24H_2O/Li_4STA.26H_2O$	97
4.4.1.5	$Na_4STA.18H_2O$	98
4.5	Discussion	98

4.6	Appendix	101
4.6.1	Phase diagram of hard spheres interacting by attractive Yukawa forces	101
4.6.2	Poisson-Boltzmann equation in a crystal or porous medium	101
5	Collective diffusion coefficient of proteins with hydrodynamic, electrostatic and adhesive interactions	105
5.1	Introduction	105
5.2	Theory	106
5.2.1	Effective interaction	106
5.2.2	Stickiness parameter	108
5.2.3	General expression for λ_C	109
5.2.4	Hydrodynamics	111
5.2.5	Determination of λ_C	114
5.3	Comparison with experiment	115
5.4	Discussion	118
	Bibliography	121
	Summary	135
	Samenvatting	139
	Curriculum Vitae	143
	List of Publications	145
	Dankwoord	147

Chapter 1

Introduction

1.1 Proteins

Proteins are among the key components in cells of living organisms. They perform a broad range of different tasks, from the catalyzation of reactions by enzymes to the packaging of DNA by histone proteins and from the transport of molecules through membranes by membrane-bound transporters or inside the cell by motor proteins, to the spatial organization of the cell by cytoskeletal filaments [1]. In fact, one of the main functions of DNA, the carrier of genetic information, is to store the information on how to build the different proteins that a cell needs. The number of different proteins in a living organism ranges from typically a few thousand in prokaryotes (eubacteria and archaea) to a few tens of thousands in multicellular eukaryotes (animals, plants and fungi) [1].

The basic building blocks of proteins are amino acids. There are hundreds of types of naturally occurring amino acids [2] but only 20 are commonly used by organisms to build proteins [1]. An amino acid consists of a carboxyl group, an amino group and a side chain all linked to the same carbon atom. The carboxyl group links covalently to the amino group of another amino acid, forming the (linear) backbone of the protein. Except for the ends, the backbone is uncharged. The side chain of an amino acid can be either polar or nonpolar (hydrophilic or hydrophobic). The polar side chains can be basic, acidic or neutral (positively charged, negatively charged or neutral, depending on the pH). The backbone of the protein and some of the side chains can also form hydrogen bonds, and the amino acid cysteine can form a disulfide bond with another cysteine [1].

The molar mass of amino acids in proteins ranges from 75 Da (1 Dalton (Da) is equivalent to 1 g mol^{-1}) for glycine to 204 Da for tryptophan [3]. The minimum number of amino acids in a protein is about 20 to 30. Smaller amino acid chains generally do not have a unique, well-defined structure and are called peptides [4]. One of the largest known proteins is titin, a protein that is relatively abundant in

striated muscle. It has a molar mass of about 2.6 – 2.8 MDa [5]. A typical protein consists of a few hundred amino acids, has a molar mass of a few tens of kDa and a radius of a few nanometers. In yeast, for example, a protein on average consists of 466 amino acids and weighs 52.7 kDa [4].

Unlike linear polymers in good solvents, proteins generally fold into a dense and unique three-dimensional structure. Biologists distinguish four levels of organization herein [1]. The first level, the primary structure, is the amino acid sequence. Parts of the amino acid chain can form localized regular repeating structures that are stabilized by hydrogen bonds. These structures are called secondary structures and the most important ones are the α helix and the β sheet. Usually, the full three-dimensional or global structure of a protein is called the tertiary structure. If a protein forms a complex with other proteins the complete structure of this complex is called the quaternary structure.

Since the side chains of amino acids have such different properties, the surface of a protein can be very heterogeneous. There may be charged patches, neutral hydrophilic patches and hydrophobic patches. In fact, the heterogeneous nature of the protein surface, together with the overall shape of the protein, makes proteins very suitable for performing specific tasks in a cell. Fig. 1.1 on the flap on the back cover shows an example of a protein, lysozyme obtained from hen egg white. The shape of the surface is shown as well as the distribution of charged and hydrophobic amino acids. Whenever we compare theoretical predictions of properties of protein solutions in this thesis with experimental results on proteins, we turn to lysozyme, since this is one of the best-studied proteins. The main reason for that is that lysozyme from hen egg white is easy to obtain and easy to purify, because it crystallizes relatively easily.

To understand the specific interactions between proteins or between a protein and other biological material in a cell, like for example DNA, RNA or membranes, it is important to know the three-dimensional structure of the protein and the distribution of side chains near the surface. These can be determined by X-ray diffraction on a protein crystal or nuclear magnetic resonance (NMR) spectroscopy on a protein solution. Due to technical limitations, structure determination of proteins by NMR spectroscopy is primarily limited to small proteins, usually smaller than 25 kDa, although structures of proteins as large as 30 to 40 kDa have been determined [9]. By contrast, X-ray diffraction can be used for structure determination of much larger proteins. The biggest difficulty with this method is that the protein has to be crystallized. This crystallization is generally not easy to achieve since one does not know a priori if and under which conditions a protein will crystallize [10]. The main goal of this thesis—a better understanding of the thermodynamic behavior of protein solutions—may help in finding the proper crystallization conditions.

Proteins also have wide application in the food industry. Some examples are soy proteins (known under collective names such as α -conglycinin, β -conglycinin, γ -conglycinin and glycinin), milk proteins like caseins and the whey proteins (β -lactoglobulin, α -lactalbumin, bovine serum albumin, immunoglobulins and

proteose-peptones) and egg proteins (like for example ovalbumin, ovotransferrin, ovomucoid, lysozyme, ovoglobulin and ovomucin in egg white and livetins and lipoproteins in egg yolk) [11]. A better understanding of the thermodynamic behavior of these proteins in solution will help to develop new products.

1.2 Theoretical preliminaries: a pedestrian approach

The goal of this thesis is to develop a simple description of protein solutions, i.e. solutions of one kind of protein in water with added monovalent salt, that can be used to predict their thermodynamic properties with as little input data from experiment as possible. In this section we introduce preliminaries to the theory, which is mainly developed in Chapter 2 and then applied in Chapters 3, 4 and 5. This section should suffice as an introduction but we refer the reader interested in a more rigorous treatment of some aspects to Section 1.3.

1.2.1 Introduction

If one wishes to gain insight into the thermodynamic properties of protein solutions, one usually measures the osmotic pressure. Other thermodynamic properties, such as the chemical potential or the osmotic compressibility, for example, can then be determined by simple analysis. At very low concentrations of protein, the interactions between the protein molecules may be neglected and the solution behaves ideally. In that case the osmotic pressure Π of the solution is given by Van 't Hoff's law (see for example Ref. [12])

$$\Pi = \rho k_B T, \quad (1.1)$$

which is formally equivalent to the ideal gas law for gases. Here ρ is the number of particles per unit volume, T is the absolute temperature and k_B is Boltzmann's constant.

The osmotic pressure is a quantity that can be determined experimentally by membrane osmometry (see for example Ref. [13]). There are two compartments that are separated by a semipermeable membrane that is permeable to the solvent (water) but not to the solute (protein), see Fig. 1.2. One chamber (I) contains pure solvent while the other (II) contains solvent and solute. Since the solvent is free to diffuse from one compartment to the other, the chemical potential $\mu_w(p_{II}, x_w)$ of the solvent in compartment II, should be equal to the chemical potential of the pure solvent in compartment I, $\mu_w(p_I, 1)$. Here x_w is the mole fraction of solvent in compartment II and p_i is the pressure in compartment i , which can be measured with a pressure sensor, for example. The mole fraction of solvent in compartment I equals unity, of course. The pressures in both compartments are not identical, in principle, and their difference is the osmotic pressure. This pressure must be imposed on compartment II by external means in order to assure

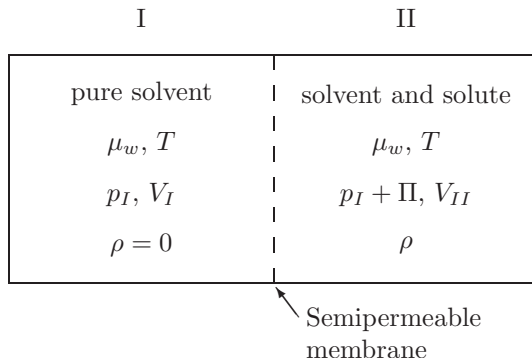


Figure 1.2: *Principle of membrane osmometry. Both compartments, of volume V_I and V_{II} , contain solvent (water), but only the right one (II) contains the solute (protein), at density ρ . The temperature T is the same for both compartments. The membrane separating the two compartments is permeable to the solvent, so the chemical potential μ_w of the solvent is the same in both compartments. At equilibrium, the pressure difference between the two compartments is equal to Π .*

mechanical equilibrium. One can derive Van 't Hoff's law (Eq. (1.1)) if one notes that x_w is close to unity in compartment II because the solution is dilute.

1.2.2 Effective one-component description

Van 't Hoff's law is generally valid for all solutions of uncharged species at vanishingly low concentrations of solute. We are interested in protein solutions at higher concentrations however. In that case interactions between particles are important and we have to include them in our description. The protein solutions we study contain several kinds of molecules. First of all we have the proteins and the solvent water. Moreover, the proteins are charged and the counterions are dissolved in the water, and monovalent salt is present. All these molecules interact with each other and a full description of all these interactions is complicated. We want a simplified description in which we only have proteins interacting with each other through an effective interaction that may depend on the other components.

The protein molecules cannot overlap so the effective interaction between the protein molecules consists first of all of the steric interaction. For simplicity, we assume that the interactions between the protein molecules are isotropic and we model the proteins as incompressible hard spheres (for proteins that are spherical, more or less, this is a good approximation though, obviously, the theory will not work for very elongated proteins). We set the volume of a sphere equal to the

volume of a protein. The hard sphere interaction potential $U_{HS}(r)$ is given by

$$\frac{U_{HS}(r)}{k_B T} = \begin{cases} \infty & 0 \leq r < 2a \\ 0 & r \geq 2a \end{cases}, \quad (1.2)$$

where a is the radius of the sphere. Eq. (1.2) shows that two spheres cannot interpenetrate if the distance between their centers r is less than the sphere diameter $2a$.

Since the proteins are charged there are electrostatic interactions between them. We assume that the pH is far from the isoelectric point so dipole and higher order multipole interactions of the fluctuational type can be neglected. We model the electrostatic interaction between two proteins with a Debye-Hückel potential [14]

$$U_{DH}(r) = \frac{Z_p^2}{\epsilon r} \frac{e^{-\omega(r/a-2)}}{(1+\omega)^2}. \quad (1.3)$$

Here, Z_p is the protein charge, ϵ is the permittivity of water, $\omega \equiv \kappa a$, κ^{-1} is the Debye length defined by $\kappa^2 = 8\pi QI$, I is the ionic strength, $Q = q^2/\epsilon k_B T$ is the Bjerrum length, which equals 0.71 nm in water at 298 K, and q is the elementary charge. Note that one part of the Debye-Hückel potential is equivalent to Coulomb's law for the interaction between two charges in a dielectric of permittivity ϵ . The second factor describes the screening of the interaction by the salt ions; here we suppose there is an excess of salt so we may neglect counterions arising from the proteins themselves. Thus, we see how the effective interaction between the proteins explicitly depends on properties of the other components, namely those of water and salt. The Debye-Hückel potential, Eq. (1.3), is valid at large distances and low charge densities. The fact that the potential is less accurate at close distances does not influence the results much since the Boltzmann factor $\exp(-U/k_B T)$ arises in our calculations and this only depends weakly on U if $U/k_B T \gg 1$, which is the case only at close distances. In Chapter 2 we determine an effective charge to correct for the fact that the surface charge of proteins is relatively high using the Poisson-Boltzmann approximation to account for nonlinear screening.

Finally, there are several other interactions, like the hydrophobic and the polarization interactions that we have not discussed yet. It is still unclear what the status of these forces is and how these interactions should be incorporated in a quantitative theory. It will become apparent in the next section that we are forced to include a salt-independent attraction of short range to describe the experimental data relating to the second virial coefficient.

Furthermore, we have implicitly assumed that the interactions between proteins are pairwise additive. This means that the interaction between a certain number of particles is equal to the sum of interactions between all pairs of particles. This is not necessarily always the case. A charged protein, for example, may change the distribution of ions around two other proteins, thus influencing

the screening between those two proteins. However, we assume that these effects are unimportant. For more details on the effective one-component description we refer to Section 1.3.

1.2.3 Virial expansion

One useful approach at moderate concentrations of protein is to write a Taylor expansion of the osmotic pressure [15]

$$\Pi = \rho k_B T (1 + B_2 \rho + B_3 \rho^2 + \dots). \quad (1.4)$$

The coefficients B_n are called the virial coefficients and the series is called a virial expansion. If the density ρ is low enough, higher order terms can be neglected and, usually, one only retains the first few terms in the expansion.

Once the two-particle interaction potential U is known, the virial coefficients can be calculated. For example, if we assume that the interaction between the particles only depends on the distance r between the centers of two particles, the second virial coefficient B_2 is given by [15]

$$B_2 = 2\pi \int_0^\infty r^2 dr \left(1 - e^{-U(r)/k_B T} \right). \quad (1.5)$$

One can see that if there is no interaction between the particles ($U \equiv 0$) then $B_2 = 0$. Furthermore, a purely attractive interaction ($U(r) \leq 0$) leads to a negative B_2 and an osmotic pressure lower than in the ideal case, and a purely repulsive interaction ($U(r) \geq 0$) leads to a positive B_2 and a higher osmotic pressure. If we set $U = U_{HS} + U_{DH}$ (see Eqs. (1.2) and (1.3)) then B_2 is positive.

We want to introduce as few relevant data as possible, for example only the protein size and its charge, and we want to replace the protein solution by another system that is simpler if possible. The parameters in the latter depend on those of the original system (for example the protein parameters and salt concentration). One example of an effective system is a fluid of hard spheres (see Eq. (1.2)). The second virial coefficient of the hard sphere system is given by $B_2^{HS} = 4v_0$, where $v_0 = 4\pi a^3/3$ is the volume of a single sphere.

One simple-minded procedure could then be to measure experimentally the second virial coefficient of the protein solution as a function of solution conditions (for example ionic strength and pH) and choose the only parameter in the hard sphere system, the radius a , by equating the respective second virials. This yields a hard sphere radius that depends on these solution conditions (but not on the protein concentration!). Since the virial coefficients of the hard sphere system and the protein solution are equal, the osmotic pressures are identical up to second order in the density (see Eq. (1.4)). This means that the thermodynamic properties are the same, at least at low concentrations of protein.

The second virial coefficient can be determined from light scattering experiments. One shines laser light on a sample and measures the light that is scattered

in a certain direction. The difference between the scattered intensity of the solution with protein and the scattered intensity of the solution without protein, I_θ , depends on the protein concentration and at low concentrations we have (see for example Ref. [16])

$$\frac{Ac_p}{I_\theta} \simeq \frac{1}{M} + \frac{2B_2N_Ac_p}{M^2}. \quad (1.6)$$

Here M is the molar mass of the protein, c_p is the concentration of protein, N_A is Avogadro's number and A is a constant that depends on the optical properties of the solvent and of the protein solution and the wavelength of the laser. To determine the second virial coefficient, one prepares samples at various protein concentrations under the same solution conditions. One then plots Ac_p/I_θ as a function of c_p and a linear function is fitted through the data. The ordinate of the point where the line crosses the vertical axis ($c_p = 0$) is equal to $1/M$ and B_2 can be determined from the slope of the line.

Fig. 1.3 shows the second virial coefficient of lysozyme as a function of ionic strength at pH 4.5, determined by light scattering experiments. At this pH the protein is positively charged and one expects an electrostatic repulsion between the protein molecules that becomes less strong with increasing ionic strength, due to screening by the salt ions (see Eq. (1.3): at fixed distance r , U_{DH} decreases if I increases). As described earlier, in a naive procedure, we might want to replace the protein solution by an effective hard sphere system. We choose the radius of the spheres in such a way that the second virial coefficients are equal. Since we have repulsion both from the actual hard interaction between the protein molecules and from the electrostatic interaction, we would expect the adjustable radius of the hard spheres to be somewhat larger than the real (effective) protein radius. We also expect that this hard sphere radius decreases with increasing salt concentration to a limiting value that is equal to the real (effective) radius of the protein, since U_{DH} is negligible at very large ionic strengths (see Eq. (1.3)). However, from Fig. 1.3 we see that for large enough values of the ionic strength ($I \gtrsim 0.1$ M), the second virial coefficient is smaller than the value one would expect if there were no electrostatic interaction ($B_2/B_2^{HS} < 1$, where B_2^{HS} is the second virial coefficient of spheres with a radius equal to the effective protein radius). In other words, in that case the radius of the spheres in the hard sphere system has to be less than the (effective) radius of the proteins. For larger values of the ionic strength ($I \gtrsim 0.2$ M) the second virial coefficient becomes negative even, implying a negative radius!

We draw two conclusions from these results. First of all, the sum of a hard interaction plus an electrostatic repulsion only is not enough to describe the interaction between the proteins. Apparently, there is also an attractive interaction between the proteins and we have to include this in our description to explain the experiments. This is what we do in the first part of Chapter 2. We introduce an

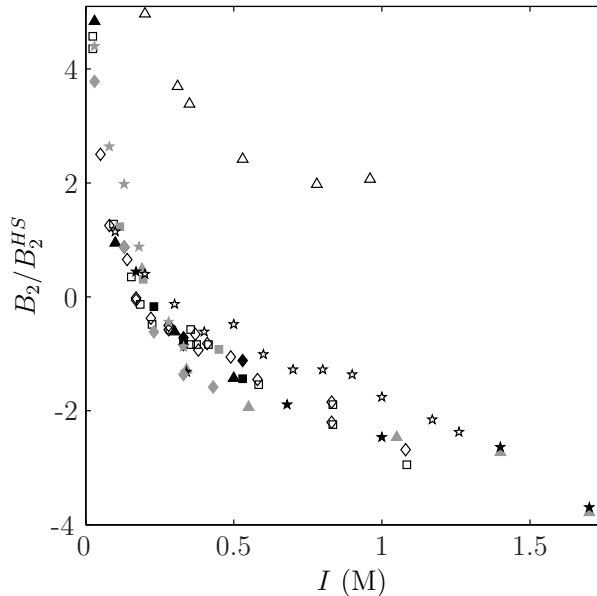


Figure 1.3: Experimental data of the second virial coefficient B_2 of lysozyme as a function of the ionic strength I at a pH of about 4.5. The second virial coefficient is scaled by the hard sphere value B_2^{HS} . Black squares: Bonneté et al. [17], pH 4.5, 20°C; grey triangles: Curtis et al. [18], pH 4.5, 20°C; grey squares: Muschol et al. [19], pH 4.7, 20°C; black stars: Curtis et al. [20], pH 4.5, 25°C; black diamonds: Bonneté et al. [17], pH 4.5, 25°C; black triangles: Velez et al. [21], pH 4.5, 25°C; white squares: Rosenbaum et al. [22], pH 4.6, 25°C; white diamonds: Rosenbaum et al. [23], pH 4.6, 25°C; grey stars: Bloustine et al. [24], pH 4.6, 25°C; white stars: Piazza et al. [25], pH 4.7, 25°C; white triangles: Behlke et al. [26], pH 4.5; grey diamonds: Bloustine et al. [24], pH 4.7. In all cases, the electrolyte is NaCl, often with a small amount of Na acetate added.

attractive square well interaction of short range

$$U_{SW}(r) = \begin{cases} 0 & 0 \leq r < 2a \\ -U_A & 2a \leq r \leq 2a + \delta a \\ 0 & r > 2a + \delta a \end{cases}, \quad (1.7)$$

and we use a variety of measurements of the second virial coefficient by a large number of groups to determine the strength U_A and range δa of this interaction. We assume that these parameters are independent of the ionic strength and we show that they are probably also independent of the pH. The second conclusion is that the hard sphere system is not suitable as a model system here. We therefore introduce the adhesive hard sphere system in the next section.

1.2.4 The Baxter potential

In the Baxter or adhesive hard sphere (AHS) model the particles behave as hard spheres, but they also have a sticky interaction. The interaction potential U_{AHS} is given by [27]

$$\frac{U_{AHS}(r)}{k_B T} = \begin{cases} \infty & 0 \leq r < 2a \\ \ln \frac{12\tau\zeta a}{2a+\zeta a} & 2a \leq r \leq 2a + \zeta a \\ 0 & r > 2a + \zeta a \end{cases}, \quad (1.8)$$

where τ is a constant and the limit $\zeta \downarrow 0$ has to be taken after all integrations have been done. In other words, we have a hard sphere system with a square well attraction of vanishing width and infinite depth in such a way that the second virial coefficient remains finite

$$B_2^{AHS} = B_2^{HS} \left(1 - \frac{1}{4\tau} \right). \quad (1.9)$$

This is derived by inserting Eq. (1.8) into Eq. (1.5). Here $B_2^{HS} = 4v_0$ is the second virial coefficient pertaining to hard spheres without the attraction. One sees that for small enough values of τ the second virial coefficient is negative.

In Chapter 2 we approximate the protein solution by a system of adhesive hard spheres. We set the radius of the spheres equal to the effective radius of the proteins and we choose the stickiness parameter $\tau = \tau_0$ in such a way that the virial coefficients of the AHS system and the protein solution are the same taking into account the electrostatic interactions. (For clarity, τ_0 refers to the value of τ at low concentrations, when its value is determined by matching second virial coefficients, and τ refers to the value that is also valid at higher concentrations, and which is determined differently (see the next sections and Chapter 2)). The stickiness parameter τ_0 is then a function of solution conditions such as, for example, the ionic strength and pH (protein charge) and it depends on parameters like the strength and the range of the short range attraction: $\tau_0 = \tau_0(Z, I; U_A, \delta)$. Thermodynamic properties of the system can then be determined from the osmotic pressure

$$\frac{\Pi}{k_B T} = \rho + B_2^{AHS}(\tau_0)\rho^2 \quad (1.10)$$

where τ_0 is a known function of the solution conditions and B_2^{AHS} is given by Eq. (1.9). We emphasize that this replacement is valid at low enough concentrations i.e. when virials beyond the second may be neglected.

1.2.5 Higher concentrations

At higher concentrations the approximation of the osmotic pressure by the first two terms in the virial expansion deteriorates. For comparison, we show the sum

of the first two terms of the virial expansion and the “exact” osmotic pressure from simulations [28] as a function of protein volume fraction $\eta \equiv \rho v_0$ at various values of the stickiness parameter τ_0 in Fig. 1.4. We see that the difference between the two curves is appreciable even at relatively small protein volume fractions. Note also the strong dependence of the osmotic pressure on the stickiness τ_0 .

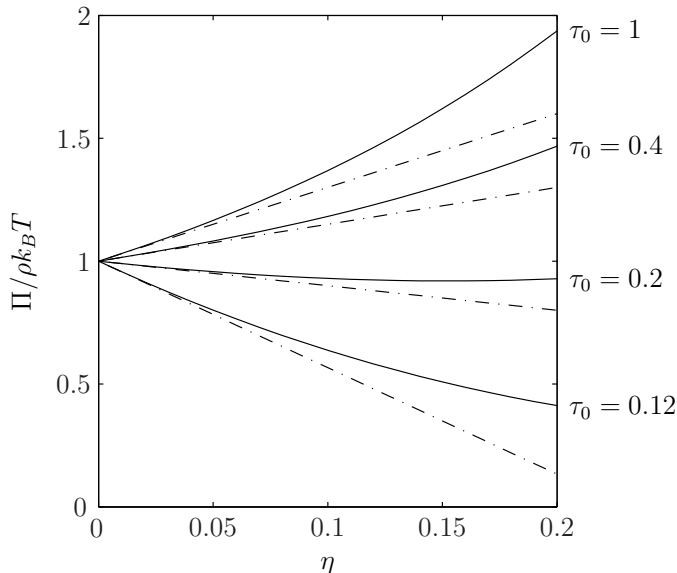


Figure 1.4: Comparison between the osmotic pressure Π as a function of volume fraction of particles η from the first two terms in the virial expansion, Eq. (1.4), with the second virial coefficient from Eq. (1.9) (dash-dotted lines), and the “exact” result from simulations [28] (solid lines), at various values of the stickiness τ_0 . For both dash-dotted and solid lines we have from bottom to top $\tau_0 = 0.12$, $\tau_0 = 0.2$, $\tau_0 = 0.4$ and $\tau_0 = 1$.

One strategy to deal with higher concentrations is to include more terms in the virial expansion. However, the higher virial coefficients are increasingly more difficult to compute. Another approach is to focus on correlations between the particles in the liquid. A quantity that is often used, and that can be measured relatively easily by scattering techniques, is the radial distribution function $g(r)$, which describes the correlation between two particles (see for example Ref. [29]). More specifically, $4\pi r^2 \rho g(r) dr$ equals the average number of particles in a shell of thickness dr at a distance r from a particle. Once the radial distribution function is known, one can determine thermodynamic properties of the system by using the compressibility equation [30]

$$k_B T \left(\frac{\partial \rho}{\partial \Pi} \right)_{\langle N \rangle, T} = 1 + 4\pi \rho \int r^2 dr [g(r) - 1], \quad (1.11)$$

the virial equation

$$\Pi = \rho k_B T - \frac{2\pi\rho^2}{3} \int r^3 dr \frac{dU(r)}{dr} g(r), \quad (1.12)$$

or the energy equation

$$\frac{E}{V} = \frac{3}{2}\rho k_B T + 2\pi\rho^2 \int r^2 dr U(r)g(r). \quad (1.13)$$

Here E is the average energy of the system, N is the number of particles and V is the volume of the system. If $g(r)$ is known exactly, all three equations yield identical thermodynamics. For example, in the ideal case $U \equiv 0$ we have $g(r) \equiv 0$ and we find $\Pi = \rho k_B T$ and $E = \frac{3}{2}Nk_B T$. For low particle densities, when only two particle interactions are important, we have a Boltzmann distribution $g(r) = \exp[-U(r)/k_B T]$ and we find from Eq. (1.11) or Eq. (1.12), in combination with Eq. (1.5), $\Pi/\rho k_B T = 1 + B_2\rho$.

In most cases one does not have an exact expression for $g(r)$ however, and one tries to solve $g(r)$ from an approximate integral equation. A famous example that gives accurate results for short-range potentials is the Percus-Yevick equation [31]

$$e^{U(r_1)/k_B T} g(r_1) = 1 + \rho \int d\mathbf{r}_2 [g(r_{12}) - 1] \left[1 - e^{U(r_2)/k_B T} \right] g(r_2), \quad (1.14)$$

where $r_{12} \equiv |\mathbf{r}_2 - \mathbf{r}_1|$. Note that for vanishing particle density ρ we recover the exact result $g(r) = \exp[-U(r)/k_B T]$. For most interaction potentials the Percus-Yevick equation cannot be solved exactly and one has to resort to approximate methods or numerical solutions, but in some cases, for example in the case of hard spheres [32] and also in the case of adhesive hard spheres [27], the Percus-Yevick equation admits an analytical solution. This makes the adhesive hard sphere system useful as a reference system. Note that because the expression for $g(r)$ from the Percus-Yevick equation is merely approximate, the three results from the compressibility equation, the virial equation and the energy equation are not entirely consistent (see Section 1.3.5).

Now, instead of trying to solve the Percus-Yevick equation, or some other integral equation, for the complicated interaction potential of our original system ($U = U_{HS} + U_{DH} + U_{SW}$, see Eqs. (1.2), (1.3) and (1.7)), we again want to replace ours by a system of Baxter spheres. We can then use the solution of the adhesive hard sphere system in the Percus-Yevick approximation to determine thermodynamic properties of the original system. The second part of Chapter 2 describes how to do this. We again set the radius of the spheres equal to the effective radius of the proteins but we now choose the stickiness parameter τ in such a way that the *free energy* of the AHS system and the protein solution is the same, at least to an excellent approximation. Then the stickiness parameter τ not only depends on the solution conditions, such as the ionic strength and pH, but also on the protein concentration. In order to do this, we only need the pair

distribution function of the Baxter model and not of the original system. In other words, we first determine $\tau = \tau(Z, I, \eta; U_A, \delta)$. Then we can determine thermodynamic properties from the expressions for these thermodynamic properties for the AHS model (see for example Section 1.3.5 for expressions for the osmotic pressure and the chemical potential).

1.3 Theoretical preliminaries: rigorous treatment

1.3.1 Introduction

Even in the relatively simple case of a protein solution that contains only water, a single type of protein, and monovalent salt, the interactions between the proteins can be quite complicated. Since protein molecules cannot overlap, they first of all interact sterically. Although proteins are quite dense objects, they can in principle be slightly deformed. Next, some amino acids are acidic or basic. This means that proteins are charged in water and this charge fluctuates due to the constant binding and unbinding of protons to these amino acids [33]. The equilibrium constants associated with these processes depend on the electrostatic potential at the binding site. This means that surrounding charges influence the binding constant at a particular site and the charge of a protein cannot be determined by solely considering the values of the equilibrium constants of the separate amino acids, although such an estimate is usually not wide off the mark. For accurate estimates on the protein charge titration experiments have to be performed.

The charges on a protein are not distributed homogeneously so the sign of the charge and its density can differ from place to place, which complicates matters. The salt ions in the solution interact with the charges on the protein, effectively screening the interactions and making them of shorter range. Since the electrostatic interactions are screened by the salt, the binding constants for the protonation and deprotonation of the basic and acidic amino acids depend on the salt concentration. In other words, the titration curves depend on the salt concentration.

Apart from the steric interactions between the protein molecules and the screened Coulomb interactions between their charges, there are also polarization forces between the protein molecules, which are essentially also electrostatic in origin [34]. These forces are of short range but there is no accurate quantitative theory to describe them for complicated molecules such as proteins. Finally, there is the solvent, water, the exact effects of which are not very well known. It is claimed that water structuring around the protein and the salt ions influences the interactions [34], but there is no quantitative theory to describe this.

Another issue that makes calculating the properties of protein solutions non-trivial is the fact that, in principle, the interactions between proteins depend on their orientation. However, in order to develop an analytical theory, one resorts to approximations. Here we assume the interactions to be isotropic i.e. the pro-

tein molecules are spherical and the charge is distributed homogeneously on the surface. This means that our theory cannot be used for proteins with a large aspect ratio, such as bovine serum albumin, or proteins with a greatly asymmetric charge distribution or at a pH close to the isoelectric point of the protein. We come back to all this in more detail in the next chapter, but for the remainder of this chapter it is important to note that the effective interaction between the proteins only depends on the distance r between their centers of mass.

We do not take the water molecules and the salt ions as such explicitly into account. We integrate out the degrees of freedom of these particles and we are left with particles of one type, the proteins, that interact through an effective two-particle interaction. We discuss this effective one-component description next.

1.3.2 Effective one-component description

We are interested in the thermodynamic properties of protein solutions. As described in the previous section, the interactions between the protein molecules are influenced by the other molecules present in the solution, that is, the water molecules, the ions of the monovalent salt and possibly other molecules that are present. This means that, in principle, in a description of the total system all the particles have to be taken into account. However, in order to simplify the description, we want to get rid of the explicit dependence of the interaction on these other molecules and we want to describe the system effectively as a one-component system of only proteins. A convenient framework in which to carry this out is the McMillan-Mayer solution theory [35] (see Ref. [29] for an extensive discussion of this theory).

Let us start by considering an open system, that is, a system where the temperature T and volume V are constant and where particles can be exchanged with a reservoir. Suppose we have K species of molecules in the solution. The activity of species k ($k \in \{1, 2, \dots, K\}$) is defined by $z_k \equiv \exp(\mu_k/k_B T)/\Lambda_k^3$ where μ_k is the chemical potential of species k , k_B is Boltzmann's constant and $\Lambda_k = h/\sqrt{2\pi m_k k_B T}$ is the thermal wavelength. Here h is Planck's constant and m_k is the particle mass. Now suppose the number of molecules of species k in a certain configuration equals N_k and suppose the coordinates of the N_k molecules of species k in that configuration are denoted by $\mathbf{x}_k \equiv \{\mathbf{x}_k^1, \mathbf{x}_k^2, \dots, \mathbf{x}_k^{N_k}\}$, where \mathbf{x}_k^i are the coordinates of molecule number i of species k . For convenience we write $\mathbf{x} \equiv \{\mathbf{x}_1, \mathbf{x}_2, \dots, \mathbf{x}_K\}$. The interaction potential in a certain configuration depends on the coordinates of all the molecules and we denote it by $\tilde{U}(\mathbf{x})$. Then the grand partition function Ξ of the system is defined by

$$\Xi(\mathbf{z}, V, T) \equiv \sum_{N_1=0}^{\infty} \sum_{N_2=0}^{\infty} \dots \sum_{N_K=0}^{\infty} \left(\prod_{k=1}^K \frac{z_k^{N_k}}{N_k!} \right) \int d\mathbf{x} e^{-\tilde{U}(\mathbf{x})/k_B T}, \quad (1.15)$$

where the integral extends over all possible configurations of that particular collection of molecules and where we used the shorthand notation $\mathbf{z} \equiv \{z_1, z_2, \dots, z_K\}$.

From the grand potential all thermodynamic properties can be derived such as the average pressure

$$p = k_B T \frac{\ln \Xi(\mathbf{z}, V, T)}{V} \quad (1.16)$$

and the average number of particles of species k

$$\langle N_k \rangle = z_k \left(\frac{\partial \ln \Xi(\mathbf{z}, V, T)}{\partial z_k} \right)_{V, T, \{z_i\}_{i \neq k}}. \quad (1.17)$$

Now let species 1 denote the protein. We are interested in the properties of the solution compared to that of a similar solution without the proteins present. In other words, we compare our original system with a system at the same temperature T and volume V with the same activities for all the molecule species except that $z_1 = 0$. Since the grand potential $-pV$ is proportional to $\ln \Xi$, we are interested in $\Xi(\mathbf{z}, V, T)/\Xi(\tilde{\mathbf{z}}, V, T)$, where $\tilde{\mathbf{z}} \equiv \{0, z_2, z_3, \dots, z_K\}$. We rewrite Eq. (1.15) as

$$\begin{aligned} \frac{\Xi(\mathbf{z}, V, T)}{\Xi(\tilde{\mathbf{z}}, V, T)} &= \sum_{N_1=0}^{\infty} \frac{(z_1/\gamma_1^0)^{N_1}}{N_1!} \\ &\times \int d\mathbf{x}_1 \left[\frac{(\gamma_1^0)^{N_1}}{\Xi(\tilde{\mathbf{z}}, V, T)} \sum_{N_2=0}^{\infty} \dots \sum_{N_K=0}^{\infty} \left(\prod_{k=2}^K \frac{z_k^{N_k}}{N_k!} \right) \int d\tilde{\mathbf{x}} e^{-\tilde{U}(\mathbf{x})/k_B T} \right]. \end{aligned} \quad (1.18)$$

Here $\tilde{\mathbf{x}} \equiv \{\mathbf{x}_2, \mathbf{x}_3, \dots, \mathbf{x}_K\}$ and γ_1^0 denotes the limiting value of the activity coefficient γ_1 as $z_1 \rightarrow 0$, where γ_1 is defined by $\gamma_1 \equiv z_1/\rho_1$ and $\rho_1 \equiv \langle N_1 \rangle/V$. Since we are looking for a one-component description, we need to find an effective interaction such that Eq. (1.18) resembles the grand partition function of a one-component system. The way in which Eq. (1.18) has been written already suggests a possible choice. We define an effective interaction (or potential of mean force) $\Phi^{(N_1)}(\mathbf{x}_1, \tilde{\mathbf{z}}, T)$ between particles of species 1 by

$$\begin{aligned} &e^{-\Phi^{(N_1)}(\mathbf{x}_1, \tilde{\mathbf{z}}, T)/k_B T} \\ &\equiv \frac{(\gamma_1^0)^{N_1}}{\Xi(\tilde{\mathbf{z}}, V, T)} \sum_{N_2=0}^{\infty} \dots \sum_{N_K=0}^{\infty} \left(\prod_{k=2}^K \frac{z_k^{N_k}}{N_k!} \right) \int d\tilde{\mathbf{x}} e^{-\tilde{U}(\mathbf{x})/k_B T}. \end{aligned} \quad (1.19)$$

We first have to prove that this is indeed the potential from which the force between the proteins can be derived. Suppose q is an arbitrary coordinate associated with one of the particles of species 1. Then the force F experienced by that particle along the direction of coordinate q is the force experienced in a certain configuration of molecules averaged over all possible configurations of particles with the particles of species 1 fixed

$$F = - \left\langle \frac{\partial \tilde{U}}{\partial q} \right\rangle = \frac{\int d\tilde{\mathbf{x}} \left(\frac{\partial \tilde{U}}{\partial q} \right) e^{-\tilde{U}(\mathbf{x})/k_B T}}{\int d\tilde{\mathbf{x}} e^{-\tilde{U}(\mathbf{x})/k_B T}}. \quad (1.20)$$

It is not difficult to show that (see for example Ref. [29])

$$-\frac{\partial \Phi^{(N_1)}}{\partial q} = -\left\langle \frac{\partial \tilde{U}}{\partial q} \right\rangle. \quad (1.21)$$

This equation shows that the average force is derivable from a potential and that this potential is $\Phi^{(N_1)}$. In principle one could add an arbitrary constant to $\Phi^{(N_1)}$ and still have a function that obeys Eq. (1.21). However, we note that in the limit $\mathbf{z} \rightarrow \mathbf{0}$, $\Phi^{(N_1)} \rightarrow \tilde{U}$ so Eq. (1.19) is the correct expression for the potential of mean force.

If we now substitute the expression for the potential of mean force, Eq. (1.19), in Eq. (1.18) we find

$$\begin{aligned} \Xi^*(\mathbf{z}, V, T) &\equiv \frac{\Xi(\mathbf{z}, V, T)}{\Xi(\tilde{\mathbf{z}}, V, T)} = e^{(p(\mathbf{z}) - p(\tilde{\mathbf{z}}))/k_B T} \\ &= \sum_{N_1=0}^{\infty} \frac{(z_1/\gamma_1^0)^{N_1}}{N_1!} \int d\mathbf{x}_1 e^{-\Phi^{(N_1)}(\mathbf{x}_1, \tilde{\mathbf{z}}, T)/k_B T}. \end{aligned} \quad (1.22)$$

This is the main result of this section and it shows that we can describe the protein solution as a one-component solution if we make the substitutions $z_1 \rightarrow z_1/\gamma_1^0$, $p \rightarrow \Pi = p(\mathbf{z}) - p(\tilde{\mathbf{z}})$, $\Xi \rightarrow \Xi^*$ and if we use Eq. (1.19) for the interaction. Π is the osmotic pressure and γ_1/γ_1^0 can be considered as a ‘‘concentration activity coefficient’’ and z_1/γ_1^0 as a ‘‘concentration activity’’ with $\gamma_1/\gamma_1^0 \rightarrow 1$ and $z_1/\gamma_1^0 \rightarrow \rho_1$ as $\rho_1 \rightarrow 0$. A very practical consequence of this result is that one can use all the methods developed for the theoretical description of gases (virial expansions, integral equations for distribution functions etc.) to describe the protein solution without any further modifications.

The two main difficulties now lie in finding the potential of mean force $\Phi^{(N_1)}(\mathbf{x}_1, \tilde{\mathbf{z}}, T)$ and calculating Eq. (1.22). Usually the interaction potential $\tilde{U}(\mathbf{x})$ is not known and even if it is, the integrals in Eq. (1.19) cannot be performed analytically in general. One therefore has to find some approximate potential of mean force. We come back to this problem in Chapter 2. We discuss approximate methods to calculate Eq. (1.22) in the next sections.

1.3.3 Virial expansion

For convenience, we drop the subscript 1 from now on and write $N \equiv N_1$, $z \equiv z_1$ etc. We also drop the explicit mention of dependencies on fugacity $\tilde{\mathbf{z}}$, volume V and temperature T , and we define $z^* \equiv z/\gamma^0$. For clarity we denote the positions of the N proteins in a certain configuration by $\mathbf{r}^N = \{\mathbf{r}_i\}_{i=1}^N$, where \mathbf{r}_i is the position of protein i .

In principle, in order to calculate the grand partition function Eq. (1.22), one has to calculate expressions of the form

$$Z_N^* \equiv \int d\mathbf{r}^N e^{-\Phi^{(N)}(\mathbf{r}^N)/k_B T}. \quad (1.23)$$

In practice these integrals cannot be performed analytically, even if relatively simple approximations for the functions $\Phi^{(N)}(\mathbf{r}^N)$ are used, and the configuration space is too large for a brute force numerical calculation. Therefore one has to resort to approximate methods. The first of these we discuss is the virial expansion. Since it produces a systematic expansion of the thermodynamic quantities of interest for small values of the density $\rho \equiv \langle N \rangle / V$, this method is very useful at low concentrations of particles.

We assume that the interaction between the particles is pairwise additive

$$\Phi(\mathbf{r}^N) = \sum_{i=1}^N \sum_{j>i}^N U(r_{ij}). \quad (1.24)$$

Here $\mathbf{r}_{ij} \equiv \mathbf{r}_i - \mathbf{r}_j$ and $r_{ij} \equiv |\mathbf{r}_{ij}|$ is the distance between particles i and j . We start by introducing the Mayer function

$$f(r_{ij}) = e^{-U(r_{ij})/k_B T} - 1 \quad (1.25)$$

and write the configurational integral in Eq. (1.23) as

$$Z_N^* = \int d\mathbf{r}^N \prod_{i=1}^N \prod_{j>i}^N [f(r_{ij}) + 1]. \quad (1.26)$$

From its definition, Eq. (1.25), it is clear that the Mayer function is small if the interaction between the particles is small, so for short-range potentials it seems natural to expand the product in the integrand of Eq. (1.26). If one then substitutes this expansion in Eq. (1.22) and collects terms with the same number of Mayer functions one finds, after some algebra,

$$\Xi^* = e^{V \sum_{N=1}^{\infty} b_N (z^*)^N}, \quad (1.27)$$

and

$$\frac{\Pi}{k_B T} = \sum_{N=1}^{\infty} b_N (z^*)^N. \quad (1.28)$$

The first three of the cluster integrals b_N are given by (see Ref. [36] for more details)

$$b_1 = 1, \quad (1.29)$$

$$b_2 = \frac{1}{2V} \int d\mathbf{r}_1 \int d\mathbf{r}_2 f(r_{12}) \quad (1.30)$$

and

$$b_3 = \frac{1}{6V} \int d\mathbf{r}_1 \int d\mathbf{r}_2 \int d\mathbf{r}_3 [f(r_{31})f(r_{21}) + f(r_{32})f(r_{31}) + f(r_{32})f(r_{21}) + f(r_{32})f(r_{31})f(r_{21})]. \quad (1.31)$$

We then use Eq. (1.17) to find an expression for the density as a function of the activity

$$\rho = \sum_{N=1}^{\infty} N b_N (z^*)^N. \quad (1.32)$$

For a comparison with experiments, it is often convenient to have expressions for thermodynamic quantities as a function of the density instead of the activity. We therefore invert Eq. (1.32) to get an expression for the activity as a function of the density which we then substitute in the equation for the osmotic pressure, Eq. (1.28). The final expressions for the osmotic pressure and the chemical potential are

$$\frac{\Pi}{k_B T} = \rho \left(1 - \sum_{N=1}^{\infty} \frac{N}{N+1} \beta_N \rho^N \right) \quad (1.33)$$

and

$$\frac{\mu}{k_B T} = 3 \ln \Lambda + \ln \rho - \sum_{N=1}^{\infty} \beta_N \rho^N. \quad (1.34)$$

The isothermal compressibility κ is given by

$$\kappa = \left(\rho \frac{\partial \Pi}{\partial \rho} \right)_T^{-1} = \frac{1}{k_B T} \left(1 - \sum_{N=1}^{\infty} N \beta_N \rho^N \right)^{-1}. \quad (1.35)$$

One can prove [36] that these expressions are valid as long as $\rho < \rho_s$, where ρ_s is the first singularity of $\sum \beta_N \rho^N$ on the positive real axis, and $\sum_{N=1}^{\infty} N \beta_N \rho^N < 1$. The first two coefficients β_N are related to the b_N by

$$\beta_1 = 2b_2 \quad (1.36)$$

and

$$\beta_2 = 3(b_3 - 2b_2^2). \quad (1.37)$$

The virial coefficients B_N are related to the coefficients β_N by

$$B_N = -\frac{N-1}{N} \beta_{N-1}. \quad (1.38)$$

It is clear that in order to get more accurate expressions for higher concentrations, one should calculate more cluster integrals b_N . These cluster integrals contain integrals over products of Mayer functions, which become increasingly more difficult to compute as the number of Mayer functions increases and usually these integrals have to be performed numerically. Moreover, the expansion converges poorly at high densities so at higher concentrations of particles the virial expansion method is inadequate and we have to use other methods. We describe one of these methods in the next section.

1.3.4 Distribution function theories

Another approach to developing liquid state theories focuses on correlations between the particles in the liquid. In the grand canonical ensemble, the radial distribution function, which was introduced in Section 1.2.5, can be determined from the total interaction potential by the expression [29]

$$\rho^2 g(r) = \rho^{(2)}(r) = \frac{1}{\Xi^*} \sum_{N=2}^{\infty} \frac{(z^*)^N}{(N-2)!} \int d\mathbf{r}_3 \cdots \int d\mathbf{r}_N e^{-\Phi(\mathbf{r}^N)/k_B T}, \quad (1.39)$$

where $\rho^{(2)}(r)$ is the two-particle distribution function. Next one determines the thermodynamic properties of the system by using the compressibility equation, the virial equation or the energy equation (Eqs. (1.11)-(1.13)). In the case of the compressibility equation the total interaction potential does not have to be pairwise additive, in the other two cases it does.

The expressions Eqs. (1.11)-(1.13) look considerably more simple than Eq. (1.22), but they are not. In fact, up until now we have only written Eq. (1.22) differently. The real difficulty now lies in finding an (approximate) expression for $g(r)$. In the literature there are many approaches to devising analytical or numerical approximations of the two-particle distribution function or other multi-particle distribution functions. One class consists of formulating integral equations that relate various multi-particle correlation functions. These equations define a hierarchy of relations between the functions. At some point this hierarchy has to be broken. This is usually done by positing an approximate relation between the $(n+1)$ -particle distribution function and the n -particle distribution function. A famous example is the Kirkwood superposition approximation which gives an approximate relation between the three-particle and two-particle distribution functions [37].

We will focus here on approximate integral equations for the radial distribution function in the case when the total interaction potential is pairwise additive since this is relevant for the next section. In a method due to Percus [38], we imagine that one particle is fixed at the origin and we consider the interaction of this particle with the other particles as an external field $W(r)$ that acts on the other particles. In that case the grand partition function is

$$\Xi^*(W) = \sum_{N=0}^{\infty} \frac{(z^*)^N}{N!} \int d\mathbf{r}^N e^{-\sum_{i=1}^N W(r_i)/k_B T} e^{-\Phi^{(N)}(\mathbf{r}^N)/k_B T}, \quad (1.40)$$

where $\Xi^*(0)$ denotes the grand partition function in the absence of the external field and $r_i = |\mathbf{r}_i|$. From this we can easily see that

$$\Xi^*(U) = \Xi^*(0) \frac{\rho}{z^*}. \quad (1.41)$$

The one-particle density $\rho^{(1)}(r; W)$ only depends on the distance r from the fixed particle (at the origin). Its value for $W = U$ can be found by keeping

one particle fixed at distance r from the origin and integrating over all possible configurations of the other particles weighted by their Boltzmann weight

$$\begin{aligned}\rho^{(1)}(r; U) &= \frac{1}{\Xi^*(U)} \sum_{N=1}^{\infty} \frac{(z^*)^N}{(N-1)!} \int d\mathbf{r}_2 \cdots \int d\mathbf{r}_N e^{-\sum_{i=1}^N U(r_i)/k_B T} e^{-\Phi(\mathbf{r}^N)/k_B T} \\ &= \rho g(r).\end{aligned}\tag{1.42}$$

The last equality follows from Eqs. (1.39) and (1.41). If we now suppose that the interaction due to the particle at the origin is gradually switched on, the interaction varies by $\Delta W(r) = U(r)$ and its response, the one-particle density, varies by $\Delta \rho^{(1)}(r) = \rho^{(1)}(r; U) - \rho^{(1)}(r; 0) = \rho h(r)$. Here, we have introduced the total correlation function $h(r) \equiv g(r) - 1$ and we have used the fact that $\rho^{(1)}(r; 0) = \rho$.

Various approximate integral equations can now be derived by viewing $U(r)$ as a perturbation and considering functional Taylor expansions of various functionals of U with respect to ΔW or $\Delta \rho^{(1)}$. Some of these integral equations can then be solved analytically for certain interaction potentials to find the radial distribution function $g(r)$. Others have to be solved by numerical methods.

For convenience we first introduce the direct correlation function

$$c(r_{12}) = \lim_{W \rightarrow 0} \frac{\delta \ln [\rho^{(1)}(r_1; W)/ze^{-W(r_1)/k_B T}]}{\delta \rho^{(1)}(r_2; W)}.\tag{1.43}$$

One can show that the direct correlation function is related to the total correlation function by the Ornstein-Zernike relation [39]

$$h(r_1) = c(r_1) + \rho \int d\mathbf{r}_2 c(r_{12}) h(r_2).\tag{1.44}$$

Expanding $\Delta \rho^{(1)}$ in powers of ΔW to first order leads to the Yvon equation which is equivalent to the Ornstein-Zernike equation Eq. (1.44) together with the following approximation for the direct correlation function

$$c(r) = -U(r)/k_B T.\tag{1.45}$$

The Yvon equation is not very suitable for potentials that are strongly repulsive at short range [30].

Expansion of $\rho^{(1)}(r_1; U)/ze^{-U(r_1)/k_B T}$ in terms of $\Delta \rho^{(1)}$ to first order leads to the Percus-Yevick equation

$$e^{U(r_1)/k_B T} g(r_1) = 1 + \rho \int d\mathbf{r}_2 [g(r_{12}) - 1] \left[1 - e^{U(r_2)/k_B T} \right] g(r_2),\tag{1.46}$$

which is equivalent to the Ornstein-Zernike equation Eq. (1.44) together with the approximation for the direct correlation function

$$c(r) = \left(1 - e^{U(r)/k_B T} \right) g(r).\tag{1.47}$$

It is the most successful first-order integral equation when the interaction is of short range. It has been solved for the hard sphere case [32] (see Eq. (1.2)), and also for the Baxter potential [27] (see the next section).

As a final example we mention the hypernetted chain (HNC) theory in which the direct correlation function is approximated by [40]

$$c(r) = -U(r)/k_B T + g(r) - 1 - \ln g(r). \quad (1.48)$$

It is obtained by expanding $\ln [\rho^{(1)}(r_1; U)/ze^{-U(r_1)/k_B T}]$ to first order with respect to $\Delta\rho^{(1)}$.

1.3.5 The Baxter potential

One of the simplest extensions of the hard sphere potential that incorporates attractive interactions is the adhesive hard sphere (AHS) potential, which was introduced by Baxter in 1968 [27], and which we described briefly in Section 1.2.4. A big advantage of the Baxter potential over other interactions such as the square well attraction of finite depth and finite range, is that it has been solved in the Percus-Yevick approximation [27]. This makes calculating properties of the Baxter fluid, such as the pressure and the chemical potential, relatively easy. Since we make extensive use of the AHS potential in the rest of this thesis, we report the pressures Π_c^{AHS} and chemical potentials μ^{AHS} one obtains by inserting the Percus-Yevick approximation for $g(r)$ in the compressibility equation, the virial equation and the energy equation (Eqs. (1.11)-(1.13)) respectively.

From the compressibility equation (Eq. (1.11)) we find for the pressure Π_c^{AHS} [27]

$$\frac{\Pi_c^{AHS}}{\rho k_B T} = \frac{1 + \eta + \eta^2}{(1 - \eta)^3} - \frac{\eta(1 + \eta/2)}{(1 - \eta)^2} \lambda + \frac{\eta^2}{36} \lambda^3. \quad (1.49)$$

Here $\eta = \rho v_0$ is the volume fraction of particles, $v_0 = 4\pi a^3/3$ is the volume of a sphere and λ is given by the smallest root of

$$\tau = \frac{1 + \eta/2}{(1 - \eta)^2} \frac{1}{\lambda} - \frac{\eta}{1 - \eta} + \frac{\eta}{12} \lambda. \quad (1.50)$$

When the roots of Eq. (1.50) are complex, the pressure cannot be determined for the physical realization of the liquid state breaks down, at least within the Percus-Yevick approximation. The chemical potential μ of the spherical particles is determined by using the pressure from Eq. (1.49) and the Gibbs-Duhem equation at constant temperature [41]

$$\frac{\mu_c^{AHS} - \mu_0}{k_B T} = \ln \eta - 1 - \ln(1 - \eta) + \frac{3\eta(2 - \eta)}{2(1 - \eta)^2} + \frac{1 + \eta + \eta^2}{(1 - \eta)^3} + J_c(\eta, \tau). \quad (1.51)$$

Here

$$J_c(\eta, \tau) = \frac{1}{36}\eta^3\lambda^3 + \frac{3}{2}\eta^2\lambda^2 - \frac{\eta(6 + 20\eta - 23\eta^2)}{2(1-\eta)^2}\lambda + \frac{6\eta(2+\eta)}{(1-\eta)^2} - \frac{18\eta}{1-\eta}\tau \quad (1.52)$$

$$- \frac{6(\tau - \tau_c)^2}{\tau_c(1-6\tau_c)} \ln \left| \frac{\lambda(1-\eta) - \tau_c^{-1}}{\tau^{-1} - \tau_c^{-1}} \right| + \frac{6\tau_c(18\tau\tau_c - 1)^2}{1-6\tau_c} \ln \left| \frac{\lambda(1-\eta) - 18\tau_c}{\tau^{-1} - 18\tau_c} \right|$$

is the contribution to the chemical potential that vanishes in the hard-sphere limit ($\tau \rightarrow \infty$) and

$$\frac{\mu_0}{k_B T} = \ln \frac{1}{v_0} \left(\frac{h^2}{2\pi m k_B T} \right)^{3/2}, \quad (1.53)$$

where m is the mass of a sphere. The critical value of τ below which there is a range of densities where there is no real solution of λ , is given by

$$\tau_c = \frac{2 - \sqrt{2}}{6}. \quad (1.54)$$

The pressure Π_v^{AHS} one finds from the virial equation is given by

$$\frac{\Pi_v^{AHS}}{\rho k_B T} = \frac{1 + 2\eta + 3\eta^2}{(1-\eta)^2} + \eta J_v(\eta, \tau), \quad (1.55)$$

with

$$J_v(\eta, \tau) = -\frac{4\eta}{1-\eta}\lambda + \frac{\eta}{3}\lambda^2 - \frac{1}{3\tau} \left[3(1+\eta)\alpha_1 + 4\alpha_2 + \frac{1}{6}\eta\lambda^2 + \frac{1}{24}\eta^2\lambda^3 \right], \quad (1.56)$$

$$\alpha_1 = \frac{(1 + 2\eta - \lambda\eta(1-\eta))^2}{(1-\eta)^4} \quad (1.57)$$

and

$$\alpha_2 = \frac{-3\eta(2+\eta)^2 + 2\lambda\eta(1-\eta)(1+7\eta+\eta^2) - \lambda^2\eta^2(1-\eta)^2(2+\eta)}{2(1-\eta)^4}. \quad (1.58)$$

The chemical potential is given by

$$\frac{\mu_v^{AHS} - \mu_0}{k_B T} = \ln \eta - 1 + 2 \ln(1-\eta) + \frac{6\eta}{1-\eta} + \frac{1 + 2\eta + 3\eta^2}{(1-\eta)^2} + \eta J_v(\eta, \tau)$$

$$+ \int_0^\eta d\eta' J_v(\eta', \tau). \quad (1.59)$$

Finally, we present the thermodynamic properties computed via the energy equation. Since there is no solution of the energy equation in the Percus-Yevick

approximation for hard spheres, the expressions for the AHS system are given relative to those for purely hard spheres [42]. For the pressure Π_e^{AHS} we have

$$\frac{\Pi_e^{AHS} - \Pi^{HS}}{\rho k_B T} = \frac{6\eta}{(1-\eta)^2} \ln \left[\frac{2\tau\lambda(1-\eta)^2}{2+\eta} \right] - \frac{1-4\eta}{(1-\eta)^2} \sqrt{\frac{6\eta}{|2-5\eta|}} J_e(\eta, \tau), \quad (1.60)$$

where

$$J_e(\eta, \tau) = \begin{cases} \arcsin \sqrt{\frac{6\eta}{2+\eta}} - \arcsin \left[\sqrt{\frac{6\eta}{2+\eta}} \left(1 - \frac{2-5\eta}{6\tau(1-\eta)} \right) \right] & \eta \leq 0.4 \\ \ln \left[1 + \frac{\lambda\eta(5\eta-2)}{6\tau(2+\eta)} + \frac{\eta}{\tau(1-\eta)} \sqrt{\frac{5\eta-2}{6\eta}} \left(1 - \frac{\lambda\eta(1-\eta)}{2+\eta} \right) \right] & \eta > 0.4 \end{cases} \quad (1.61)$$

For the pressure of the hard sphere system we use the accurate Carnahan-Starling expression [43]

$$\frac{\Pi_{cs}^{HS}}{\rho k_B T} = \frac{1 + \eta + \eta^2 - \eta^3}{(1-\eta)^3}. \quad (1.62)$$

The chemical potential is given by the expression

$$\frac{\mu_e^{AHS} - \mu^{HS}}{k_B T} = \eta\lambda + \frac{6\eta(2-\eta)}{(1-\eta)^2} \ln \left[\frac{2\tau\lambda(1-\eta)^2}{2+\eta} \right] - \frac{3-11\eta+5\eta^2}{(1-\eta)^2} J_e(\eta, \tau), \quad (1.63)$$

where we again use the Carnahan-Starling result for the chemical potential of the hard sphere system

$$\frac{\mu_{CS}^{HS} - \mu_0}{k_B T} = \ln \eta - 1 + \eta \frac{4-3\eta}{(1-\eta)^2} + \frac{1+\eta+\eta^2-\eta^3}{(1-\eta)^3}. \quad (1.64)$$

Recently, the equation of state has also been determined with the help of computer simulations [28]. In Figs. 1.5 on page 25 and 1.6 on page 27 we compare the results of the simulations for the pressure and the chemical potential for various values of the stickiness parameter τ as a function of volume fraction η with the results of the compressibility equation, the virial equation and the energy equation.

1.4 Outline of the thesis

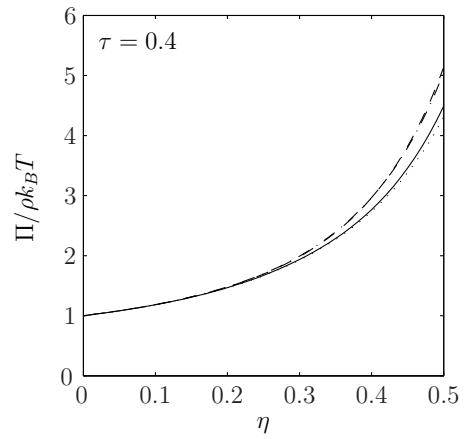
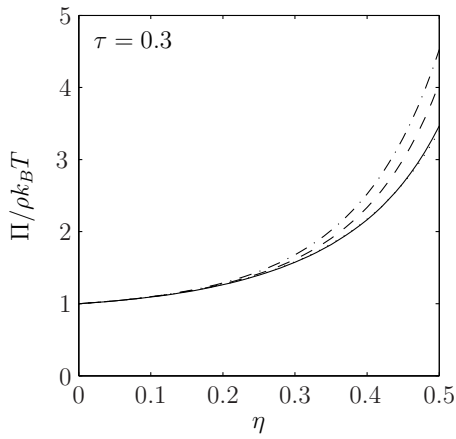
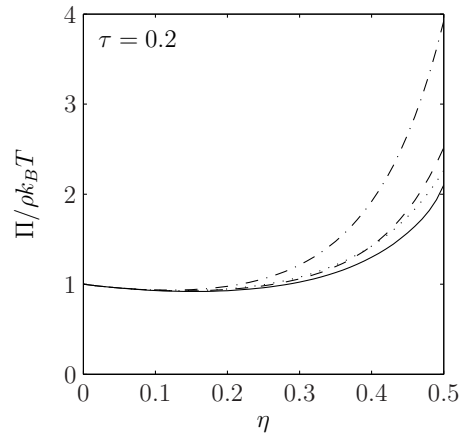
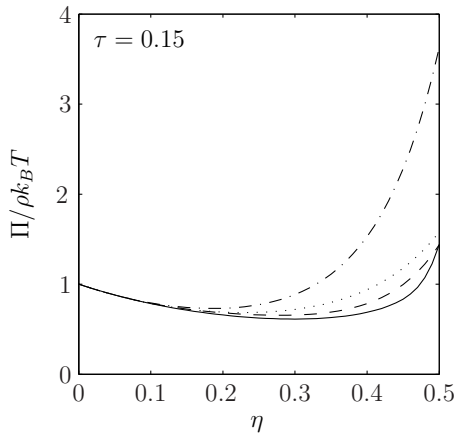
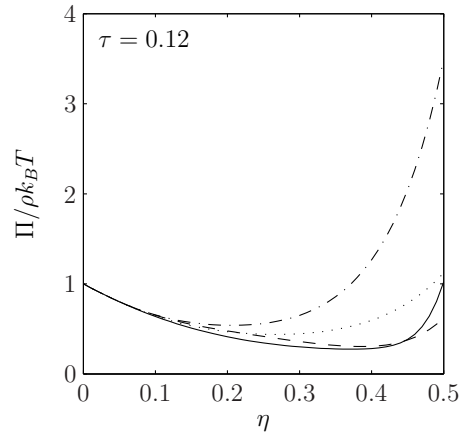
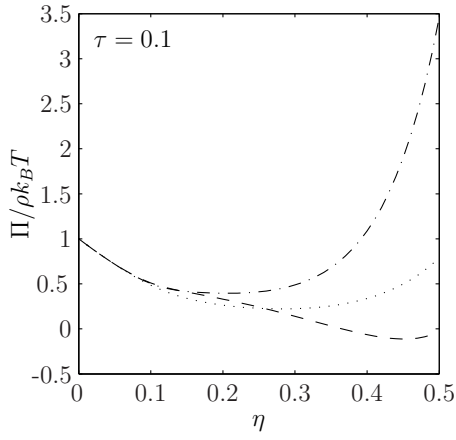
In Chapter 2, we set up the theoretical framework that describes how to deal with solutions of globular proteins that are to a good approximation spherical in shape, at a solution pH that is not too close to the isoelectric point of the protein. We first approximate the original system of proteins in water with added salt by a system of spherical particles that interact by a nontrivial isotropic potential consisting of a steric repulsion, a short range attraction and electrostatic repulsion. We then show how to replace this system by a system of particles that interact through the

relatively simple Baxter potential. We are able to choose the attractive strength of the Baxter potential to mimic the correct thermodynamic behavior of the original system. We name this the optimized Baxter model (OBM) for reasons which will become clear in Chapter 2.

In Chapter 2 we make two important approximations. First, we approximate the original solution by a system of spherical particles interacting isotropically. Then we approximate the latter by a solution of Baxter spheres. We then compare the theoretical results to experiments on the original protein system. Hence, the accuracy of the theoretical predictions gives information on how good the combination of both approximations is, but if there is a discrepancy, its cause will not be clear. Therefore, in Chapter 3, we test the OBM on a model system, that of hard particles with an attractive Yukawa interaction. The “measurements” in this case are computer simulations on this system.

In Chapter 4, we use the OBM to determine the thermodynamic properties of protein crystals that are present in a solution of proteins. We make use of the fact that there is chemical and mechanical equilibrium between a crystal and the surrounding fluid. In other words, the pressure and chemical potential of the crystal must be the same as the respective quantities in the fluid which we determine with the help of the OBM. We also develop an electrostatic model for protein crystals to rationalize the results.

In the final chapter we consider the collective diffusion of proteins. The collective diffusion coefficient describes how quickly a small gradient in the concentration of proteins will disappear. In Chapters 2 and 3, we use the Baxter potential to describe thermodynamic behavior. For a non-equilibrium quantity like the diffusion coefficient one cannot expect the Baxter potential to give an entirely correct prediction for the concentration dependence (in the real system there may be ionic friction, for instance). Nevertheless, in Chapter 5 we show that it does work, to a good approximation.



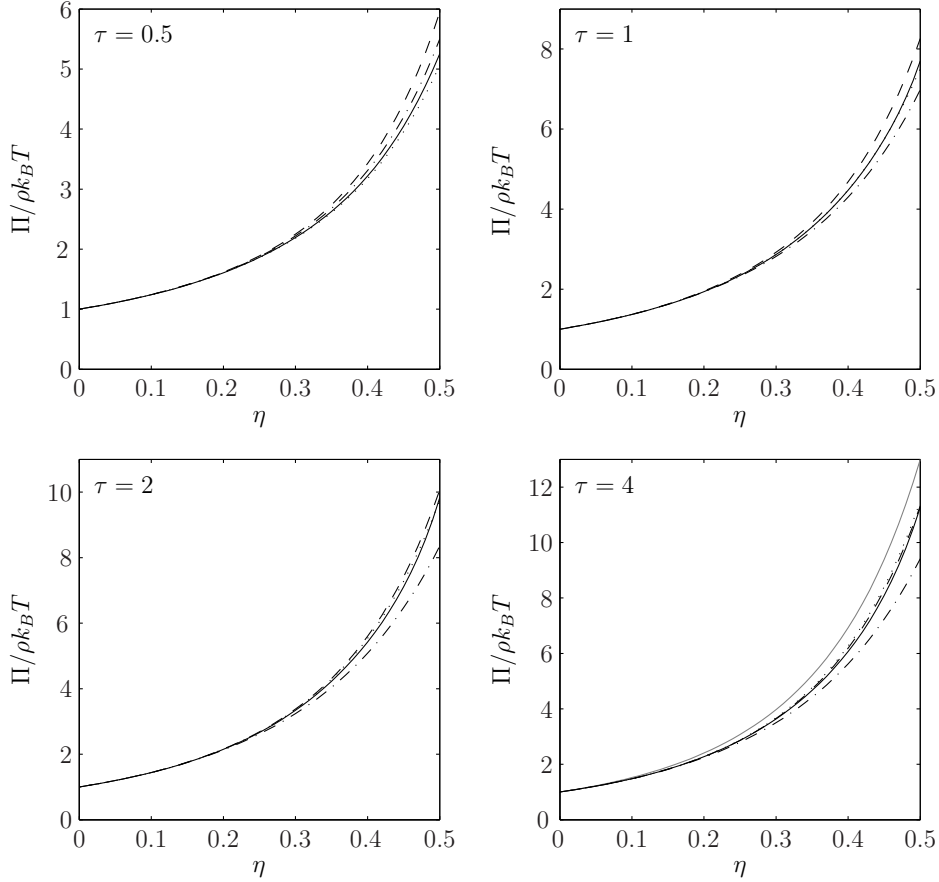
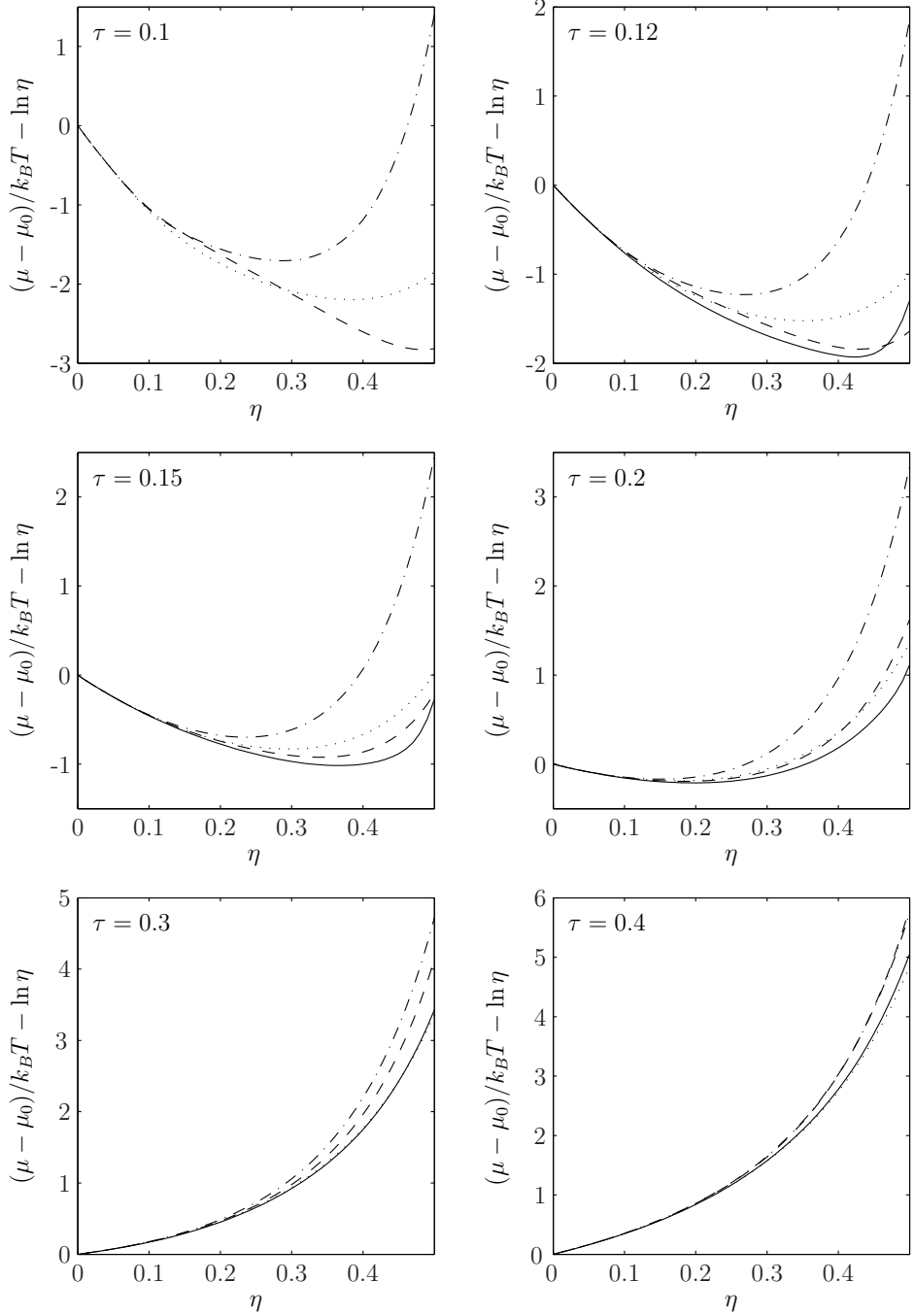


Figure 1.5: Pressure Π of the adhesive hard sphere system divided by the ideal contribution $\rho k_B T$ as a function of volume fraction of particles η for several values of the stickiness parameter τ . The black solid line denotes the results from simulations [28], the dash-dotted line, the dotted line and the dashed line denote the results from the solution of the Percus-Yevick approximation and respectively the compressibility equation (Eq. (1.49)), the virial equation (Eq. (1.55)) and the energy equation (Eq. (1.60)). In the last case we used the Carnahan-Starling equation [43], Eq. (1.62), for the pressure of the hard sphere system. The grey line in the last picture shows the result for the hard sphere case ($\tau \rightarrow \infty$) from the Carnahan-Starling equation.



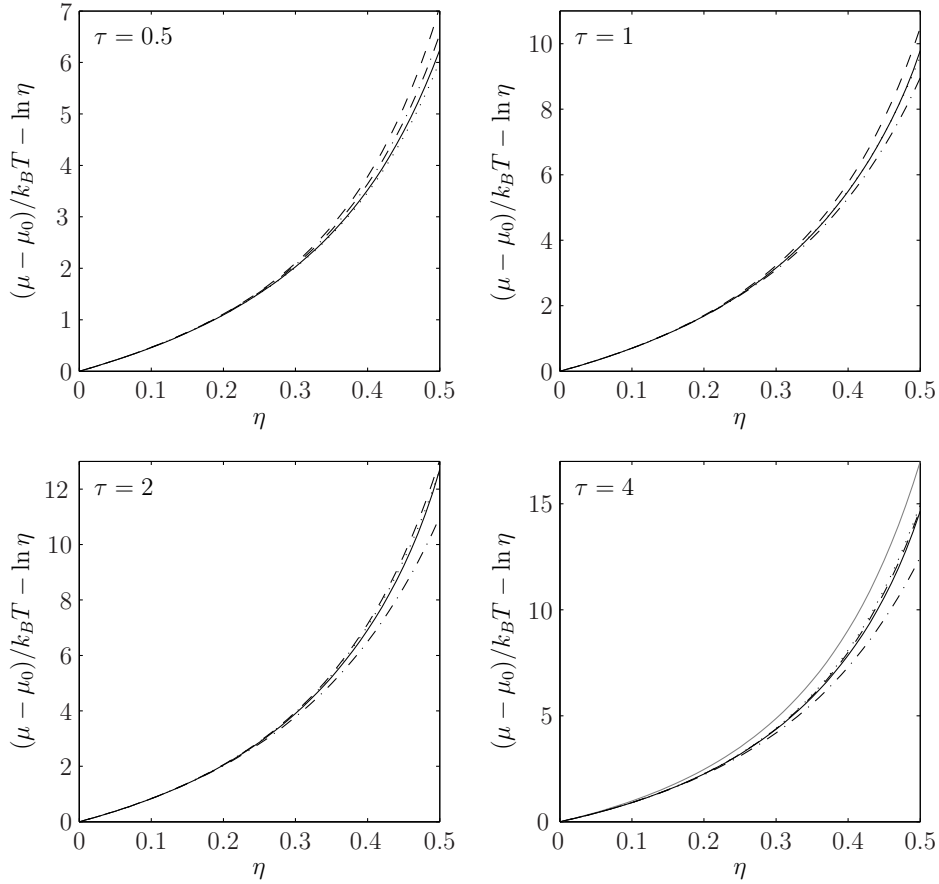


Figure 1.6: Dimensionless chemical potential $(\mu - \mu_0)/k_B T$ of the adhesive hard sphere system minus the density dependent part of the ideal contribution, $\ln \eta$, as a function of volume fraction of particles η for several values of the stickiness parameter τ . The black solid line denotes the results from simulations [28], the dash-dotted line, the dotted line and the dashed line denote the results from the solution of the Percus-Yevick approximation and respectively the compressibility equation (Eq. (1.51)), the virial equation (Eq. (1.59)) and the energy equation (Eq. (1.63)). In the last case we used the Carnahan-Starling result, Eq. (1.64), for the chemical potential of the hard sphere system. The grey line in the last picture shows the result for the hard sphere case ($\tau \rightarrow \infty$) from the Carnahan-Starling equation.

Optimized Baxter model of protein solutions: Electrostatics versus adhesion

Abstract A theory is set up of spherical proteins interacting by screened electrostatics and constant adhesion, in which the effective adhesion parameter is optimized by a variational principle for the free energy. An analytical approach to the second virial coefficient is first outlined by balancing the repulsive electrostatics against part of the bare adhesion. A theory similar in spirit is developed at nonzero concentrations by assuming an appropriate Baxter model as the reference state. The first-order term in a functional expansion of the free energy is set equal to zero which determines the effective adhesion as a function of salt and protein concentrations. The resulting theory is shown to have fairly good predictive power for the ionic-strength dependence of both the second virial coefficient and the osmotic pressure or compressibility of lysozyme up to about 0.2 volume fraction.

2.1 Introduction

It has been intimated that the solution properties of globular proteins may bear relation with their crystallization properties [44, 45]. Since the characterization of proteins commands ever more attention, such a contention is of considerable interest so much work has been carried out on this topic recently [46–51].

The difficulty of setting up a predictive theory of protein suspensions based on what is known about the interaction between two proteins, has been acknowledged for some time [52]. Best fitting of the osmotic pressure of, for instance, bovine serum albumin up to 100 g/l, leads to effective excluded volumes whose behavior as a function of salt is enigmatic [53].

In recent years, there has been a tendency to forget about all detail of the

protein interaction altogether—both attractive and repulsive—and to introduce a single adhesion parameter [23, 53–56]. Despite the electrostatic repulsion which is substantial, the data are often merely rationalized in terms of the bare protein diameter within the context of an adhesive sphere model and such an approach seems to have merit [23, 53–56]. This empiricism has prompted us to develop a theory of screened charged protein spheres that have a constant stickiness, but where the electrostatic interaction is compensated, in part, by the adhesive forces. Thus, we argue that, effectively, the spheres are assigned a hard diameter identical to the actual diameter provided the remnant adhesive interaction now depends on the electrolyte and protein concentrations in a manner to be determined variationally. Our primary aim is to formulate a new liquid state theory of protein solutions with the Baxter model as reference state. First, however, we analyze the second virial coefficient as such, for this will point toward a way of dealing with the osmotic pressure at nonzero concentrations. We focus on experiments with lysozyme, a protein which is reasonably spherical and has been well studied for a long time [57]. In particular, we show that there are enough measurements of the second virial of lysozyme to determine an adhesion parameter with some confidence.

2.2 Second virial coefficient

2.2.1 Theory

2.2.1.1 Second virial coefficient

The second virial coefficient B_2 describes the first order correction to Van 't Hoff's law

$$\frac{\Pi}{\rho k_B T} = 1 + B_2 \rho + O(\rho^2). \quad (2.1)$$

Here, Π is the osmotic pressure of the solution, ρ is the particle number density, k_B is Boltzmann's constant and T is the temperature. From statistical mechanics we know that, given the potential of mean force $U(\mathbf{r})$ between two spherical particles whose centers of mass are separated by the vector \mathbf{r} , one can calculate B_2 from

$$B_2 = -\frac{1}{2} \int_V d\mathbf{r} f(\mathbf{r}), \quad (2.2)$$

where $f(\mathbf{r}) = e^{-U(\mathbf{r})/k_B T} - 1$ is the Mayer function. In principle, the interaction $U(\mathbf{r})$ may be determined from experimental data on the second virial coefficient by suitable Laplace inversion. This has been done for atoms and spherically symmetric molecules [58, 59], for which the second virial coefficient has been measured over a broad enough range of temperatures. One might think of formulating a procedure similar in spirit and applicable to protein solutions, but with the ionic strength as independent variable instead of the temperature. However, to be able

to determine the interaction by inversion, the experimental data have to be known fairly accurately, which is not the case at hand, as will become clear further on. We are therefore forced to adduce presumptions about the interaction.

We assume the protein to be spherical with radius a , its charge being distributed uniformly on its surface. For convenience, all distances will be scaled by the radius a of the sphere and all energies will be in units of $k_B T$. Because monovalent ions (counterions and salt ions) are also present in solution, there will be a screened Coulomb repulsion between the proteins, here given by a far-field Debye-Hückel potential. We compute the effective charge qZ_{eff} in the Poisson-Boltzmann approximation where q is the elementary charge. For now, we let the attraction between two proteins be of short range, and we model it by a potential well of depth U_A and width $\delta \ll 1$. The total interaction $U_T(x)$ between two proteins is of the form

$$U_T(x) = \begin{cases} \infty & 0 \leq x < 2 \\ U_{DH}(x) - U_A & 2 \leq x < 2 + \delta \\ U_{DH}(x) & x \geq 2 + \delta \end{cases}, \quad (2.3)$$

$$x \equiv \frac{r}{a},$$

with Debye-Hückel potential [14]

$$U_{DH}(x) = 2\xi \frac{e^{-\omega(x-2)}}{x}. \quad (2.4)$$

Here, $\xi \equiv \frac{Q}{2a} \left(\frac{Z_{eff}}{1+\omega} \right)^2$, κ^{-1} is the Debye length defined by $\kappa^2 = 8\pi QI$, I is the ionic strength, $Q = q^2/\epsilon k_B T$ is the Bjerrum length, which equals 0.71 nm in water at 298 K, ϵ is the permittivity of water and $\omega \equiv \kappa a = 3.28a\sqrt{I}$, if a is given in nm and I in mol/l. We suppose 1-1 electrolyte has been added in excess so I is the concentration of added salt.

In order to evaluate B_2 analytically, we have found it expedient to split up B_2 into several terms:

$$B_2 = B_2^{HS} \left(1 + \frac{3}{8}J \right), \quad (2.5)$$

where $B_2^{HS} = 16\pi a^3/3$ is the second virial coefficient if the proteins were merely hard spheres and we introduce the following integrals to facilitate analytical computation

$$J \equiv \int_2^\infty dx x^2 \left(1 - e^{-U_T(x)} \right) \equiv J_1 - (e^{U_A} - 1) J_2, \quad (2.6)$$

$$J_1 \equiv \int_2^\infty dx x^2 \left(1 - e^{-U_{DH}(x)} \right), \quad (2.7)$$

$$J_2 \equiv \int_2^{2+\delta} dx x^2 e^{-U_{DH}(x)}. \quad (2.8)$$

Here, J_1 is the value of J in the absence of attraction and may be simplified by Taylor expanding the Boltzmann factor in the integrand for small values of U_{DH} to second order. However, to increase the accuracy of the expansion, we adjust the coefficient of the second order term so that the approximation to the integrand coincides with its actual value at $x = 2$, i.e., we approximate $x(1 - e^{-U_{DH}(x)}) \simeq 2\xi e^{-\omega(x-2)} - 2\alpha\xi^2 e^{-2\omega(x-2)}$, with $\alpha = \frac{e^{-\xi} - (1-\xi)}{\xi^2}$, resulting in

$$J_1 \simeq \frac{4(\omega + \frac{1}{2})\xi}{\omega^2} \left(1 - \frac{\alpha}{2}\xi\right), \quad (2.9)$$

where we have neglected the small term $\alpha\xi^2/2\omega^2$. For instance, in the case of lysozyme, the deviation of the approximation Eq. (2.9) from the exact result is smaller than about 3% for $I \geq 0.05$ M and smaller than about 1% for $I \geq 0.2$ M. Since $\delta \ll 1$, J_2 may be simplified by using the trapezoid approximation $\int_2^{2+\delta} dx g(x) \simeq \frac{1}{2}\delta [g(2) + g(2 + \delta)]$, which leads to

$$J_2 \simeq 2\delta \left[e^{-\xi} + \left(1 + \frac{\delta}{2}\right)^2 e^{-\frac{\xi}{1+\delta/2} e^{-\omega\delta}} \right]. \quad (2.10)$$

It is important to note that $\omega\delta$ may be greater than unity even if $\delta \ll 1$. Again, for lysozyme, this approximation deviates less than about 3% from the exact value for $I \geq 0.2$ M and $\delta \leq 0.5$ and less than about 1% for $I \geq 0.2$ M and $\delta \leq 0.15$.

2.2.1.2 Effective attractive well

We next present a discussion of B_2 in terms of equivalent interactions and their Mayer functions even though the analysis of the previous section is self-contained. Sections 2.2.1.2 and 2.2.1.3 may be viewed as preludes to the formulation of the liquid-state theory developed in Section 2.3. At large separations ($x > 2 + \delta$), the interaction between the particles is purely repulsive, leading to a positive contribution to the second virial coefficient. If, at a certain ionic strength, the second virial coefficient is smaller than the hard-core value ($B_2 < B_2^{HS}$), this positive contribution is necessarily cancelled by only part of the negative contribution of the attractive interaction at small separations, the part, say, between $x = 2 + \epsilon_0$ and $x = 2 + \delta$ (see Fig. 2.1).

The remaining potential, which we will call an effective attractive well, then consists of a hard-core repulsion plus a short-range attraction of range ϵ_0 . The value of ϵ_0 is determined by noting that the free energy of the suspension must remain invariant, which, in the asymptotic limit of low densities, leads to the identity

$$B_{2,\epsilon_0} = B_2, \quad (2.11)$$

where B_2 is the second virial coefficient of the previous section and B_{2,ϵ_0} is the second virial coefficient pertaining to the effective attractive well. Using Eq. (2.2),

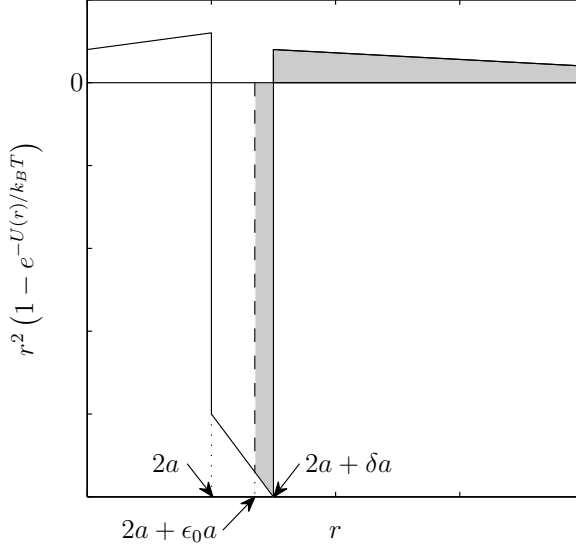


Figure 2.1: The integrand of Eq. (2.2) versus the distance r . As shown by the grey regions, the repulsive tail is compensated by part of the attractive interaction provided $B_2 < B_2^{HS}$.

we rewrite Eq. (2.11) as

$$\int_V d^3\mathbf{r} \Delta f = 0, \quad (2.12)$$

in terms of the difference in the respective Mayer functions

$$\Delta f \equiv f - f_{\epsilon_0}, \quad (2.13)$$

where f is the Mayer function of the original interaction and f_{ϵ_0} is the Mayer function of the effective attractive well. In dimensionless units, Eq. (2.12) is equivalent to the condition

$$\int_{2+\delta}^{\infty} dx x^2 (1 - e^{-U_{DH}(x)}) = \int_{2+\epsilon_0}^{2+\delta} dx x^2 (e^{U_A} e^{-U_{DH}(x)} - 1), \quad (2.14)$$

where, using the same approximation that led to Eq. (2.9), we write

$$\int_{2+\delta}^{\infty} dx x^2 (1 - e^{-U_{DH}(x)}) \simeq \frac{2\xi e^{-\omega\delta}}{\omega} \left(1 - \frac{\alpha}{2}\xi e^{-\omega\delta}\right) \left(2 + \delta + \frac{1}{\omega}\right) \quad (2.15)$$

and, using $\int_{2+\epsilon_0}^{2+\delta} dx x^2 \Delta f(x) \simeq 2(\delta - \epsilon_0) [\Delta f(2 + \delta) + \Delta f(2 + \epsilon_0)]$, we have

$$\int_{2+\epsilon_0}^{2+\delta} dx x^2 \left(e^{U_A} e^{-U_{DH}(x)} - 1 \right) \simeq 2(\delta - \epsilon_0) \left[-2 + e^{U_A} \left(e^{-\frac{\xi}{1+\delta/2}} e^{-\omega\delta} + e^{-\frac{\xi}{1+\epsilon_0/2}} e^{-\omega\epsilon_0} \right) \right]. \quad (2.16)$$

To leading order, we then find an explicit relation for ϵ_0

$$\delta - \epsilon_0 \simeq \frac{\xi e^{-\omega\delta}}{\omega e^{U_A}} e^{\xi e^{-\omega\delta}}, \quad (2.17)$$

which works well at high ionic strengths (i.e. at low values of ξ), e.g. whenever $I \geq 1$ M in the case of lysozyme at pH 4.5. A more accurate value of $\delta - \epsilon_0$ is obtained by equating Eqs. (2.15) and (2.16), and then iteratively updating the factor $(\delta - \epsilon_0)$, starting with the initial value $\epsilon_0 = \delta$.

Sometimes, it may be convenient to introduce an equivalent square well. The second virial coefficient pertaining to the original potential $U_T(x)$ (Eq. (2.3)) is now rewritten as

$$B_2 = B_{2,\epsilon_0} = B_2^{HS} \left(1 + \frac{3}{8} \int_2^{2+\epsilon_0} dx x^2 \left(1 - e^{U_A} e^{-U_{DH}(x)} \right) \right). \quad (2.18)$$

The depth $U_A - U_{DH}(x)$ does not vary strongly though, since $\epsilon_0 \ll 1$. To simplify things computationally, we approximate the interaction by a square well potential,

$$U_{SW}(x) = \begin{cases} \infty & 0 \leq x < 2 \\ -U_S & 2 \leq x < 2 + \epsilon_0 \\ 0 & x \geq 2 + \epsilon_0 \end{cases}. \quad (2.19)$$

We choose U_S in such a way that $B_2 = B_2^{SW}$ or, equivalently,

$$\int_2^{2+\epsilon_0} dx x^2 \left(e^{U_S} - e^{U_A} e^{-U_{DH}(x)} \right) = 0. \quad (2.20)$$

To leading order in ϵ_0 , we have

$$\int_2^{2+\epsilon_0} dx x^2 e^{U_S} \simeq 4\epsilon_0 e^{U_S}, \quad (2.21)$$

and, using the approximation $\int_2^{2+\epsilon_0} dx x^2 g(x) \simeq 2\epsilon_0 [g(2 + \epsilon_0) + g(2)]$, we write

$$\int_2^{2+\epsilon_0} dx x^2 e^{U_A} e^{-U_{DH}(x)} \simeq 2\epsilon_0 e^{U_A} \left[e^{-\xi} + e^{-\frac{\xi}{1+\epsilon_0/2}} e^{-\omega\epsilon_0} \right]. \quad (2.22)$$

The depth U_S of the potential is then given by

$$e^{U_S} \simeq \frac{1}{2} e^{U_A} \left(e^{-\xi} + e^{-\frac{\xi}{1+\epsilon_0/2}} e^{-\omega\epsilon_0} \right) \quad (2.23)$$

in terms of the original variables. Finally, we point out that the two attractive wells that we have introduced are physically meaningful only if $B_2 < B_2^{HS}$.

2.2.1.3 Attractive well in the Baxter limit

We have shown that one may simplify the statistical thermodynamics of the protein suspension at low densities considerably, by replacing the original interaction, consisting of an electrostatic repulsion and a short-range attraction, by a single attractive well of short range. The electrostatic interaction may be substantial but it is compensated by part of the original attractive well which is quite strong ($U_A > 1$). Another useful interaction expressing attractive forces of short range consists of a hard-sphere repulsion and an attraction of infinite strength and infinitesimal range, namely the adhesive hard sphere (AHS) potential of Baxter [27]

$$U_{AHS}(x) = \begin{cases} \infty & 0 \leq x < 2 \\ \ln \frac{12\tau\zeta}{2+\zeta} & 2 \leq x \leq 2 + \zeta \\ 0 & x > 2 + \zeta \end{cases}, \quad (2.24)$$

where τ is a constant and the limit $\zeta \downarrow 0$ has to be taken after formal integrations. The second virial coefficient remains finite

$$B_2^{AHS} = B_2^{HS} \left(1 - \frac{1}{4\tau} \right). \quad (2.25)$$

Because much is known about the statistical mechanics of the Baxter model, one often defines τ in terms of some B_2 and naively assumes there is a one-to-one correspondence between the original and Baxter models. For instance, in our case, $B_2^{AHS} = B_2 = B_{2,\varepsilon_0} = B_2^{SW}$. Since we have

$$\begin{aligned} B_2^{SW} &= B_2^{HS} \left(1 - (e^{U_S} - 1) \left[\left(1 + \frac{\epsilon_0}{2} \right)^3 - 1 \right] \right) \\ &\simeq B_2^{HS} \left(1 - \frac{3}{2} (e^{U_S} - 1) \epsilon_0 \right), \end{aligned} \quad (2.26)$$

we thus identify

$$\frac{1}{\tau_0} \simeq 6\epsilon_0 (e^{U_S} - 1), \quad (2.27)$$

where U_S is given by Eq. (2.23) and, for clarity, we use τ_0 to refer to the value of τ at low concentrations, when its value is determined by matching second virial coefficients. However, it is important to realize that this procedure is legitimate at small densities only. At finite concentrations, the optimal representation of the real suspension of proteins by a Baxter model has to be derived and we will show in Section 2.3 that the simple-minded identification of τ via $B_2^{AHS}(\tau_0) \equiv B_2$ no longer applies.

2.2.2 Application to lysozyme

2.2.2.1 Experimental Data

Lysozyme is, by far, the best studied protein with regard to solution properties. This is one of the reasons for using this protein to test theory, another being its moderate aspect ratio of about 1.5 so that it may be fairly well approximated by a sphere. Bovine Serum Albumin (BSA) has also been well studied, but is considerably more anisometric with an aspect ratio of about 3.5. Numerous measurements of the second virial coefficient of lysozyme have been published. In fact, there are quite a few sets of experiments pertinent to our analysis [17–26].

It turns out that there is appreciable scatter in the data if we plot all measurements of B_2 at a pH of about 4.5 as a function of ionic strength I (NaCl + small amount of Na acetate; we have set the ionic strength arising from the latter equal to $0.6 \times$ concentration [21]) (see Fig. 2.2).

Several sets of data [25, 26] appear to be way off the general curve within any reasonable margin of error. An important criterion is how well the θ point (i.e. when $B_2 = 0$) is established since then attractive forces—which we would like to understand—are well balanced against electrostatics—which we purportedly understand well. Experimentally speaking, it ought to be possible to monitor B_2 accurately about the θ point; large negative B_2 values at $I \gg I_\theta$ are more difficult to determine because the proteins may start to aggregate or nucleate, in principle. Various polynomial fits for all data close to the θ point yield $I_\theta = 0.20 \pm 0.01$ M. Hence, we have regarded data sets [25, 26] markedly disagreeing with this ionic strength as anomalous so we have not taken them into consideration. Fig. 2.3 displays all data we have taken into account.

Clearly, the composite curve yields a fairly reliable basis to test possible theories of the attractive force. On the other hand, it is unclear at present how the scatter in data in Fig. 2.3 translates into bounds for attractive interactions inferred by inverting Eq. (2.2).

2.2.2.2 Theory

Electrostatics

Next, it is important to ascertain the actual and effective charges of lysozyme under conditions relevant to the present work. Kuehner et al. [60] performed hydrogen-ion titrations on hen-egg-white lysozyme in KCl solutions. By interpolation, we obtain the actual charge Z of the protein as a function of the 1-1 electrolyte concentration I (see Tables 2.1 and 2.2).

Experiments on B_2 are usually carried out with NaCl (and some Na acetate) as the supporting monovalent electrolyte but we here assume KCl and NaCl behave identically in an electrostatic sense. We solve the Poisson-Boltzmann equation to get the effective charge Z_{eff} in the Debye-Hückel tail (for more detail, see Section 2.5.1). The dimensionless radius is set equal to $\omega = 3.28a\sqrt{I} = 5.58\sqrt{I}$

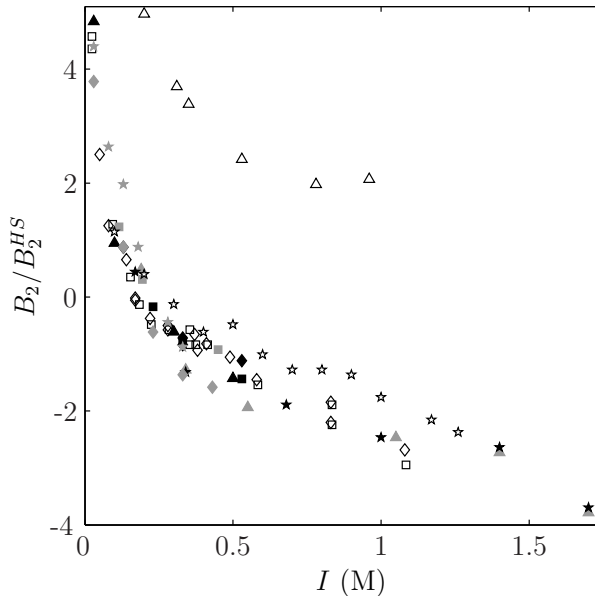


Figure 2.2: Experimental data of the second virial coefficient B_2 of lysozyme as a function of the ionic strength I at a pH of about 4.5. The second virial coefficient is scaled by the hard sphere value B_2^{HS} . Black squares: Bonneté et al. [17], pH 4.5, 20°C; grey triangles: Curtis et al. [18], pH 4.5, 20°C; grey squares: Muschol et al. [19], pH 4.7, 20°C; black stars: Curtis et al. [20], pH 4.5, 25°C; black diamonds: Bonneté et al. [17], pH 4.5, 25°C; black triangles: Velev et al. [21], pH 4.5, 25°C; white squares: Rosenbaum et al. [22], pH 4.6, 25°C; white diamonds: Rosenbaum et al. [23], pH 4.6, 25°C; grey stars: Bloustine et al. [24], pH 4.6, 25°C; white stars: Piazza et al. [25], pH 4.7, 25°C; white triangles: Behlke et al. [26], pH 4.5; grey diamonds: Bloustine et al. [24], pH 4.7. In all cases, the electrolyte is NaCl, often with a small amount of Na acetate added.

and Eq. (2.61) is used to compute the renormalized or effective charge. (Setting $a = 1.7$ nm for lysozyme as in Refs. [18] and [22]; the Bjerrum length $Q = 0.71$ nm for H_2O at room temperature). The other dimensionless parameter is given by $\xi = 0.209(\bar{Z}/(1 + \omega))^2$, where $\bar{Z} = Z_{eff} - 1$ (see below).

Attractive well

We have assumed U_A and δ to be independent of the ionic strength I . It is possible to show that this does not contradict the data displayed in Figs. 2.2 and 2.4.

In Section 2.5.2, we prove that if the interaction between the proteins is given by Eq. (2.3) but now $U_A = U_A(x)$ is a general attraction, then $dB_2/d\omega < 0$ and $d^2B_2/d\omega^2 > 0$, the last inequality being valid if $\xi < 1$. We recall that ω is

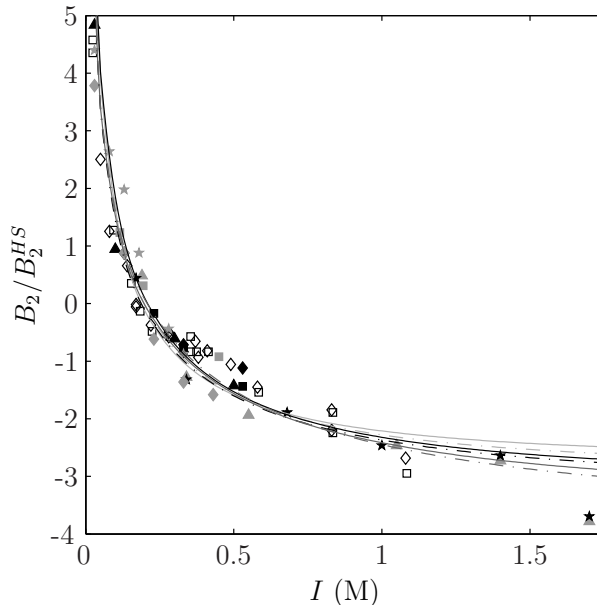


Figure 2.3: A fit of Eq. (2.5) to the experimental data of Fig. 2.2 (except for those of Refs. [25] and [26]). On the right-hand side of the figure, the upper solid line corresponds to $I_\theta = 0.19$, $\delta = 0.564$ and $U_A = 1.48$, the upper dash-dotted line to $I_\theta = 0.20$, $\delta = 0.468$ and $U_A = 1.70$ and the middle solid line to $I_\theta = 0.21$, $\delta = 0.379$ and $U_A = 1.95$, all at an effective charge Z_{eff} . The middle dash-dotted line corresponds to $I_\theta = 0.19$, $\delta = 0.25$ and $U_A = 2.4$, the lower solid one to $I_\theta = 0.20$, $\delta = 0.167$ and $U_A = 2.87$ and the lower dash-dotted one to $I_\theta = 0.21$, $\delta = 0.079$ and $U_A = 3.70$, all at a lowered effective charge \bar{Z} .

proportional to \sqrt{I} so that Figs. 2.3 and 2.4 indeed bear out these inequalities after due rearrangement.

Next, we determine the optimal values of U_A and δ yielding exact, numerical $B_2(I)$ curves given by Eq. (2.5) which are the best fits to the data of Fig. 2.3. We require that $I_\theta = 0.20 \pm 0.01$ M is predicted absolutely which fixes U_A , say, and δ is then determined by a nonlinear minimization procedure. We thus obtain $U_A = 1.70 \pm 0.25$ and $\delta = 0.468 \mp 0.097$ but we note that the quantity $\delta \exp U_A = 2.56 \pm 0.10$ is much more narrowly bounded. Now, it can be argued that the Debye-Hückel potential with effective charge Z_{eff} overestimates the real potential in magnitude so we have repeated this numerical procedure with a slightly lower effective charge, viz. $\bar{Z} = Z_{eff} - 1$ (see Tables 2.1 and 2.2). This yields the revised estimates $U_A = 2.87 \pm 0.65$, $\delta = 0.167 \mp 0.086$ and $\delta \exp U_A = 2.95 \pm 0.21$. The numerically computed curves are displayed in Fig. 2.3. We therefore conclude that the variables U_A and δ as such are difficult

I (M)	Z	Z_{eff}	\bar{Z}	ξ	ω	ϵ_0	U_S	τ_0
0.05	9.5	8.8	7.8	2.52	1.25			
0.10	9.8	9.2	8.2	1.84	1.76			
0.15	10.0	9.4	8.4	1.48	2.16	0.0208	2.26	0.933
0.20	10.1	9.6	8.6	1.27	2.50	0.0466	2.52	0.314
0.25	10.2	9.7	8.7	1.10	2.79	0.0585	2.70	0.205
0.30	10.2	9.8	8.8	0.984	3.06	0.0644	2.82	0.164
0.45	10.3	10.0	9.0	0.752	3.74	0.0720	3.05	0.115
1.0	10.4	10.2	9.2	0.409	5.58	0.0773	3.37	0.0767
1.5	10.4	10.3	9.3	0.295	6.83	0.0782	3.47	0.0684
2.0	10.4	10.3	9.3	0.229	7.89	0.0785	3.53	0.0642

Table 2.1: Values of the actual charge Z of hen-egg-white lysozyme (from [60]), the renormalized or effective charge Z_{eff} (from Eq. (2.61)), the lowered effective charge $\bar{Z} = Z_{eff} - 1$, and dimensionless interaction parameters ξ and ω , and ϵ_0 , U_S and τ_0 as a function of the ionic strength I . The pH equals 4.5 and ξ has been calculated using the lowered effective charge \bar{Z} . Values of U_S and τ_0 have been computed using Eqs. (2.23) and (2.27), respectively, and ϵ_0 has been calculated using the procedure described immediately after Eq. (2.17).

I (M)	Z	Z_{eff}	\bar{Z}	ξ	ω	ϵ_0	U_S	τ_0
0.05	6.9	6.6	5.6	1.30	1.25			
0.10	7.0	6.8	5.8	0.920	1.76	0.0493	2.83	0.212
0.15	7.1	6.9	5.9	0.728	2.16	0.0640	3.03	0.132
0.20	7.2	7.0	6.0	0.616	2.50	0.0695	3.14	0.108
0.25	7.2	7.0	6.0	0.524	2.79	0.0725	3.23	0.0943
0.30	7.3	7.1	6.1	0.473	3.06	0.0741	3.28	0.0877
0.45	7.3	7.2	6.2	0.357	3.74	0.0764	3.39	0.0758
1.0	7.1	7.0	6.0	0.174	5.58	0.0784	3.56	0.0623
1.5	6.9	6.9	5.9	0.119	6.83	0.0787	3.61	0.0590
2.0	6.8	6.8	5.8	0.0889	7.89	0.0788	3.63	0.0574

Table 2.2: Same as Table 2.1, but now with a pH equal to 7.5.

to ascertain unambiguously, though the variable $\delta \exp U_A$ is quite robust. This is also borne out if we use our approximations, Eqs. (2.9) and (2.10), instead of the

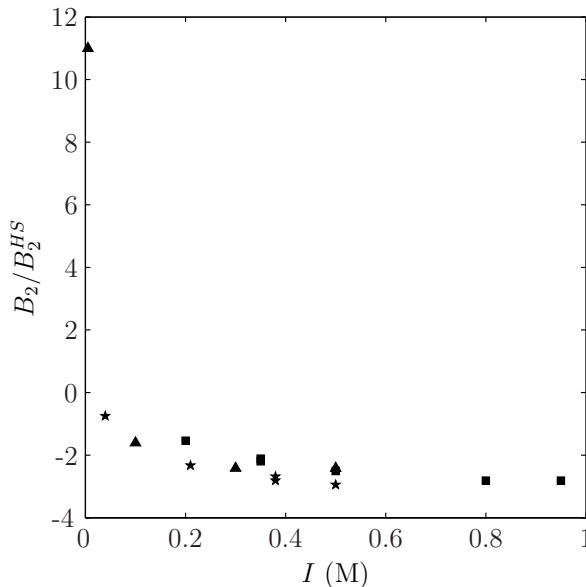


Figure 2.4: Experimental data of the second virial coefficient B_2 of lysozyme as a function of the ionic strength I at a pH of about 7.5. The second virial coefficient is scaled by the hard sphere value B_2^{HS} . Black stars: Rosenbaum et al. [22], pH 7.4, 25 °C; black triangles: Velev et al. [21], pH 7.5, 25 °C; black squares: Rosenbaum et al. [23], pH 7.8, 25 °C.

exact numerical computations. There are again wide variations in U_A and δ but the quantity $\delta \exp U_A$ is strictly bounded: $\delta \exp U_A = 2.70 \pm 0.11$ (effective charge = Z_{eff}) and $\delta \exp U_A = 3.02 \pm 0.21$ (effective charge = $Z_{eff} - 1$).

We now argue why $\delta \exp U_A$ is indeed a relevant quantity, to a good approximation. At the θ point we have $B_2 = 0$ so that $J_\theta = -8/3$ from Eq. (2.5). From Tables 2.1 and 2.2, we see that generally $\omega \gg 1$ and $\alpha\xi \ll 1$; hence, we have $J_1 \simeq 4\xi/\omega$ and $J_2 \simeq 4\delta \exp -\xi$ for often $\omega\delta > 1$. This would lead to $\delta \exp U_A \simeq 4.4$. On the other hand, at very high I , J_1 and ξ tend to zero and, because $U_A \gg 1$, the scaled virial coefficient B_2/B_2^{HS} reduces to $-\frac{3}{8}J_2 \exp U_A \simeq -\frac{3}{2}\delta \exp U_A$ leading to $\delta \exp U_A \simeq 3$ estimated from Fig. 2.3. Hence, the two estimates at the respective extremes are fairly consistent. To summarize, we may propose a crude approximation to the second virial coefficient which is a universal function of $\delta \exp U_A$

$$\frac{B_2}{B_2^{HS}} \simeq 1 + \frac{3\xi}{2\omega} - \frac{3}{2}e^{-\xi}\delta e^{U_A}. \quad (2.28)$$

The third term on the right is exact in the limit $\delta \rightarrow 0$, whereas the absolute error in the second term is smaller than 0.25 when $I \geq 0.1$ M. Using Eq. (2.28) to fit

the data leads to $\delta \exp U_A = 4.2$ when we use the effective charge Z_{eff} , whereas $\delta \exp U_A = 3.7$ when we use the lower effective charge \bar{Z} (see Fig. 2.5).

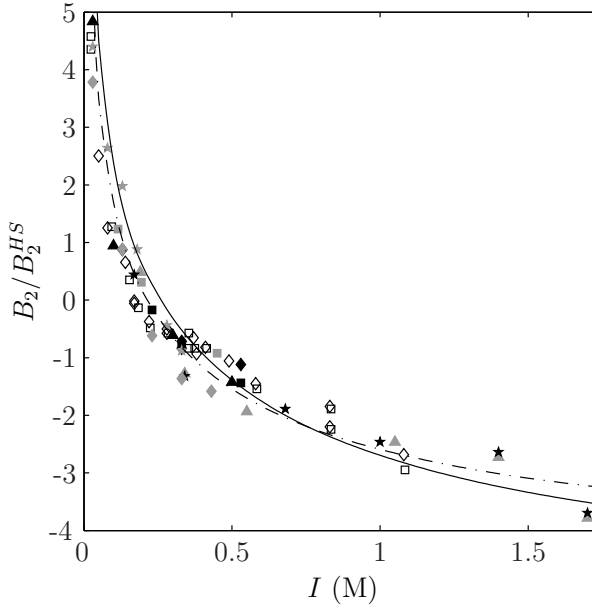


Figure 2.5: Fits of Eq. (2.28) to experimental data of Fig. 2.3. Full line (Z_{eff} and $\delta \exp U_A = 4.2$); Dash-dotted line (\bar{Z} and $\delta \exp U_A = 3.7$).

In Fig. 2.3 on page 38 we see that the curves at low values of δ fit the data at high ionic strengths better. In the remainder of this article, we therefore employ the values $\delta = 0.079$ and $U_A = 3.70$, corresponding to the lowered effective charge \bar{Z} and $I_\theta = 0.21$ M. In Fig. 2.6 we show a comparison between experimental data at a pH of about 7.5 and the theoretical curve computed numerically with the same parameters.

AHS potential

Values of ϵ_0 , U_S and τ_0 at several ionic strengths are given in Tables 2.1 and 2.2 on page 39. Fig. 2.7 on page 43 displays the ionic-strength dependence of the adhesion parameter τ_0 .

Near the θ point, τ_0 decreases quickly with increasing I . At high ionic strength, τ_0 approaches the limiting value of $(6\delta(e^{U_A} - 1))^{-1}$, which, upon the use of our choice $\delta = 0.079$ and $U_A = 3.7$, is equal to 0.0535. We note that at pH 4.5 and at ionic strengths $I = 0.05$ M and $I = 0.1$ M, the computed values of ϵ_0 , U_S and τ_0 become nonsensical. In that case, the attractive potential is simply not strong

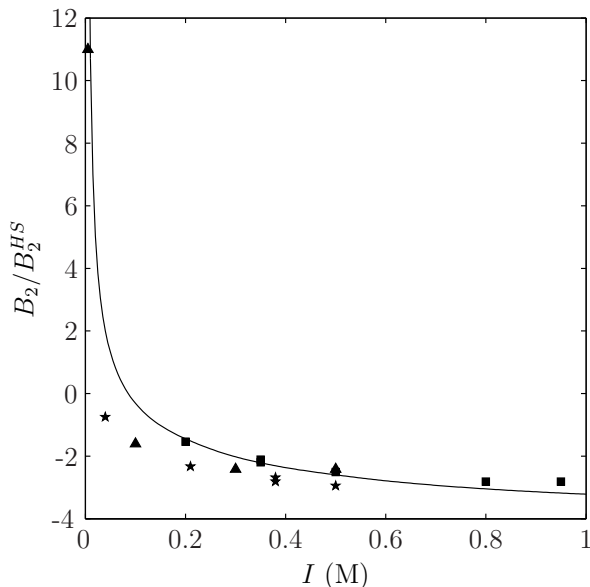


Figure 2.6: Comparison between the experimental data at pH 7.5 and full theory Eq. (2.5). Parameters as in the lower dash-dotted curve in Fig. 2.3 ($\delta = 0.079$ and $U_A = 3.70$).

enough to compensate the electrostatic repulsion completely so our analytical approach breaks down. This can also be seen in Fig. 2.3 on page 38, where we have $B_2 > B_2^{HS}$ for these two values of the ionic strength. The same effect occurs at pH 7.5 when $I = 0.05$ M.

2.3 Liquid state theory at higher densities

2.3.1 Theory

2.3.1.1 Density dependent attractive well in the Baxter limit

In Section 2.2, we introduced the AHS potential as a convenient first approximation to the interaction between proteins. We determined the adhesion parameter τ by matching values of the second virial coefficient which is methodologically correct only in the asymptotic limit of very low densities. In this section we propose a new procedure of choosing τ , which is valid at higher concentrations but τ now depends on the protein density. We extend a method originally proposed by Weeks, Chandler and Anderson [61, 62] for repulsive interactions. They variationally determined an effective hard sphere diameter for a soft, repulsive potential of

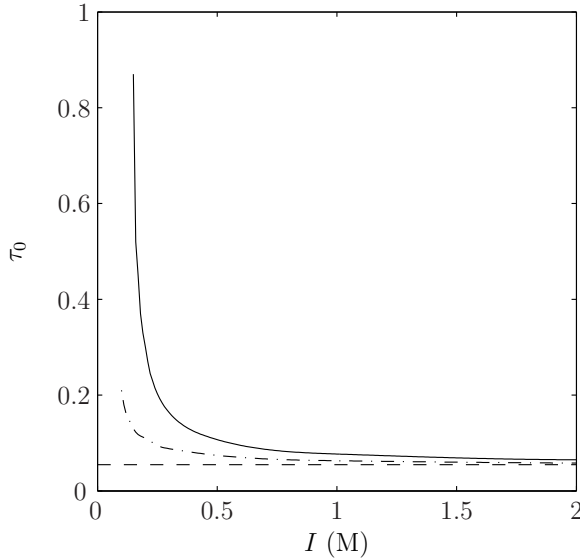


Figure 2.7: Ionic-strength dependence of AHS parameter τ_0 at pH 4.5 (solid line) and pH 7.5 (dash-dotted line). The dashed line denotes the limiting value of τ_0 as $I \rightarrow \infty$.

short-range, but we argue that their scheme is more generally applicable as long as the full interaction—attractive and repulsive—remains of short range, which is the case here.

We start by introducing a functional expansion of the excess Helmholtz free energy ΔA in terms of the Mayer function of the interaction U_T

$$\begin{aligned} \rho^{-1} \mathcal{A}(\rho, T; \varphi_s) &= \rho^{-1} \mathcal{A}(\rho, T; \varphi_{AHS}) + \frac{\eta}{2} \frac{3}{4\pi} \int d\mathbf{x} B_{AHS}(x) \\ &+ \frac{\eta^2}{2} \left(\frac{3}{4\pi} \right)^2 \frac{a^3}{V} \int d\mathbf{x}_1 d\mathbf{x}_2 d\mathbf{x}_3 B_{AHS}(x_{12}) B_{AHS}(x_{13}) J_{AHS}^{(3)}(\mathbf{x}_1, \mathbf{x}_2, \mathbf{x}_3) + \dots \end{aligned} \quad (2.29)$$

Here, V is the volume of the system, $\mathcal{A} = -\Delta A/V$, $\varphi_s(x) = e^{-U_T(x)}$, $\varphi_{AHS}(x) = e^{-U_{AHS}(x)}$, $\eta = 4\pi a^3 \rho/3$ is the volume fraction of particles, $J_{AHS}^{(3)}(\mathbf{x}_1, \mathbf{x}_2, \mathbf{x}_3)$ is a complicated function depending on two and three particle correlation functions (see Refs. [61] and [62]) and $\mathbf{x}_{12} = \mathbf{x}_1 - \mathbf{x}_2$ etc. We define the quantity

$$B_{AHS}(x) \equiv y_{AHS}(x) [\varphi_s(x) - \varphi_{AHS}(x)], \quad (2.30)$$

in terms of the so-called cavity function $y_{AHS}(x) \equiv g_{AHS}(x)/\varphi_{AHS}(x) = \frac{2}{\rho^2} \frac{\delta \mathcal{A}}{\delta \varphi(x)}$ and radial distribution function $g_{AHS}(x)$ pertaining to an appropriate AHS potential which is the reference state. Both these functions depend on ρ , T and the

effective adhesive parameter τ , the latter to be determined variationally. From now on, we omit the subscript *AHS* in $B_{AHS}(x)$, $g_{AHS}(x)$ etc. for the sake of brevity.

We next choose τ by requiring that the first-order correction to the excess free energy vanishes

$$\int d\mathbf{x} B(x) = 0. \quad (2.31)$$

This is the analogue of Eq. (2.12). Hence, in the spirit of the previous section, we split up this integral into two parts. The first indicates that the tail of the electrostatic interaction is compensated by part of the original square well attraction

$$\int_{2+\epsilon}^{\infty} dx x^2 B(x) = 0 \quad (2.32)$$

($0 < \epsilon \leq \delta$) and yields ϵ . The second determines the density dependent strength τ of the AHS interaction

$$\int_2^{2+\epsilon} dx x^2 B(x) = 0. \quad (2.33)$$

This expresses the fact that the reference potential has to compensate for the remaining part of the original interaction. We note that this scheme is only consistent if the attraction is sufficiently strong (τ may never be negative).

2.3.1.2 Approximate radial distribution function for the Baxter potential

In order to be able to determine τ from Eqs. (2.32) and (2.33), we need to know $g(x)$, the radial distribution function of the reference interaction, the AHS potential. In the Percus-Yevick approximation developed by Baxter, $g(x)$ has a singular contribution $g_\zeta(x)$ which, after the limit $\zeta \rightarrow 0$, acts like a delta function and results from the stickiness of the interaction at the surfaces of two touching spheres. We thus assume the functional expansion given by Eq. (2.29) exists after the limit $\zeta \rightarrow 0$. This is obviously very difficult to prove in general although we investigate the bilinear term in Section 2.5.3. We split $g(x)$ into $g_\zeta(x)$ and a regular term $\tilde{g}(x)$ [27]

$$g(x) = \tilde{g}(x) + g_\zeta(x) \quad (2.34)$$

with

$$g_\zeta(x) = \begin{cases} 0 & x < 2 \\ \frac{\lambda(2+\zeta)}{12\zeta} + O(1) & 2 \leq x \leq 2 + \zeta \\ 0 & x > 2 + \zeta \end{cases} \quad (2.35)$$

analogously to Eq. (2.24), where the amplitude λ is the smaller of the two solutions of

$$\tau = \frac{1 + \eta/2}{(1 - \eta)^2} \frac{1}{\lambda} - \frac{\eta}{1 - \eta} + \frac{\eta}{12} \lambda. \quad (2.36)$$

For $x < 2$, $\tilde{g}(x)$ equals zero owing to the hard-core repulsion, whereas $\tilde{g}(x)$ tends to unity for large x . For proteins, it turns out that $\varphi_s(x) - \varphi_{AHS}(x)$ is often appreciably nonzero only near the surface of the sphere so we approximate $\tilde{g}(x)$ in the interval $2 \leq x \leq 4$ by the first two terms of its Taylor expansion

$$\tilde{g}(x) \simeq \begin{cases} 0 & x < 2 \\ G(1 + H(x-2)) & 2 \leq x \leq 4 \\ 1 & x > 4 \end{cases} . \quad (2.37)$$

The constants G and H may be computed with the help of the auxiliary function $F(t)$ introduced by Bravo Yuste and Santos [63] (See their Eqs. (3.19) and (3.21); note that the first derivative we need in the Taylor expansion of $\tilde{g}(x)$ is taken after the limit $\zeta \rightarrow 0$). The Laplace transforms of the radial distribution and other functions which were computed by Baxter [27] (see his Eq. (30)), are related to $F(t)$ by their Eq. (3.12). Expansions at high t then lead to

$$G = \lambda\tau \quad (2.38)$$

and

$$H = \frac{\eta}{2\tau(1-\eta)} \left(\frac{\eta(1-\eta)}{12} \lambda^2 - \frac{1+11\eta}{12} \lambda + \frac{1+5\eta}{1-\eta} - \frac{9(1+\eta)}{2(1-\eta)^2} \frac{1}{\lambda} \right). \quad (2.39)$$

Numerical work [64] bears out that Eqs. (2.37), (2.38) and (2.39) are quite reasonable for $x-2 \ll 1$. In the case of proteins, the range of both attractive and electrostatic forces is much smaller than the diameter.

2.3.1.3 Determination of the effective adhesion

We next determine τ from Eq. (2.33), first using Eq. (2.32) to obtain ϵ . From Eqs. (2.24), (2.30) and (2.34), the function $B(x)$ can be shown to have the following form (repressing terms that ultimately disappear in the limit $\zeta \rightarrow 0$)

$$B(x) = \tilde{B}(x) - g_\zeta(x), \quad (2.40)$$

where the regular term is given by

$$\tilde{B}(x) = \begin{cases} 0 & 0 \leq x \leq 2 \\ (e^{-U_T(x)} - 1)\tilde{g}(x) & x > 2 \end{cases} . \quad (2.41)$$

Eq. (2.32) may be conveniently expressed as

$$\int_{2+\epsilon}^{\infty} dx x^2 B(x) = \int_{2+\epsilon}^{2+\delta} dx x^2 \tilde{B}(x) + \int_{2+\delta}^{\infty} dx x^2 \tilde{B}(x) = 0. \quad (2.42)$$

Using $\int_{2+\epsilon}^{2+\delta} dx f(x) \simeq \frac{1}{2}(\delta - \epsilon) [f(2 + \delta) + f(2 + \epsilon)]$ and neglecting terms of order δ^2 and ϵ^2 , we write the first integral as

$$\int_{2+\epsilon}^{2+\delta} dx x^2 B(x) \simeq G(\delta - \epsilon) K_1(\delta, \epsilon), \quad (2.43)$$

with

$$K_1(\delta, \epsilon) \equiv 2 \left(e^{U_A} e^{-\frac{\xi}{1+\delta/2} e^{-\omega\delta}} - 1 \right) (1 + (1 + H)\delta) \\ + 2 \left(e^{U_A} e^{-\frac{\xi}{1+\epsilon/2} e^{-\omega\epsilon}} - 1 \right) (1 + (1 + H)\epsilon). \quad (2.44)$$

Again, we stress that, although $\delta \ll 1$ and $\epsilon \ll 1$, $\omega\delta$ and $\omega\epsilon$ may be of order unity. Furthermore, we note that if we take the limit $\eta \downarrow 0$, then $\lambda \rightarrow \tau^{-1}$ and $G \rightarrow 1$, so we recover Eq. (2.16) if we neglect terms of order δ and ϵ . We tackle the second integral by adopting the approximation: $1 - \exp(-U_T(x)) = 1 - \exp(2\xi x^{-1} e^{-\omega(x-2)}) \simeq 2\xi x^{-1} e^{-\omega(x-2)} - 2\xi^2 x^{-2} e^{-2\omega(x-2)} + 2\xi^3 x^{-2} e^{-3\omega(x-2)}/3$ (note that in this Taylor expansion of the exponential we have replaced one factor x^{-1} by 2^{-1} in the last term). We then write

$$- \int_{2+\delta}^{\infty} dx x^2 B(x) \simeq G((1 + \delta H)P_1 + HP_2) \quad (2.45)$$

with

$$P_1 = \int_{2+\delta}^{\infty} dx x^2 (1 - e^{-U_T(x)}) \simeq \frac{8}{\omega^2} (1 + \omega\delta)M + \frac{16}{\omega} M \left(1 - M + \frac{8}{9} M^2 \right) \quad (2.46)$$

and

$$P_2 = \int_{2+\delta}^{\infty} dx x^2 (x - 2 - \delta) (1 - e^{-U_T(x)}) \\ \simeq \frac{8}{\omega^3} (2 + \omega\delta)M + \frac{16}{\omega^2} \left(M - \frac{1}{2} M^2 + \frac{8}{27} M^3 \right). \quad (2.47)$$

Here, $M \equiv \xi e^{-\omega\delta}/4$. Using the approximations $1 - M + 8M^2/9 \simeq (1 + M)^{-1}$ and $M - M^2/2 + 8M^3/27 \simeq \log(1 + M)$, we arrive at

$$P_1 \simeq \frac{8}{\omega^2} (1 + \omega\delta)M + \frac{16}{\omega} \frac{M}{1 + M} \quad (2.48)$$

and

$$P_2 \simeq \frac{8}{\omega^3} (2 + \omega\delta)M + \frac{16}{\omega^2} \ln(1 + M). \quad (2.49)$$

Hence, the variable ϵ , which depends on the density by virtue of the density dependence of H , is determined iteratively from

$$\delta - \epsilon_{new} = \frac{(1 + \delta H)P_1 + HP_2}{K_1(\delta, \epsilon_{old})}. \quad (2.50)$$

One starts with $\epsilon_{old} = \delta$ and iterates until a stationary ϵ_{new} is reached.

The next step is to calculate τ from Eq. (2.33), which, with the help of Eq. (2.40), is equivalent to the expression

$$\int_2^{2+\epsilon} dx x^2 \tilde{B}(x) = \frac{2\lambda}{3}. \quad (2.51)$$

We have taken the limit $\zeta \rightarrow 0$. Again using the approximation $\int_2^{2+\epsilon} dx f(x) \simeq \frac{1}{2}\epsilon [f(2+\epsilon) + f(2)]$, we write

$$\begin{aligned} \int_2^{2+\epsilon} dx x^2 \tilde{B}(x) \\ \simeq 2G\epsilon \left[\left(e^{U_A} e^{-\frac{\epsilon}{1+\epsilon/2}} e^{-\omega\epsilon} - 1 \right) (1 + (1+H)\epsilon) + (e^{U_A} e^{-\epsilon} - 1) \right]. \end{aligned} \quad (2.52)$$

Together with the expressions Eq. (2.51) and $G = \lambda\tau$ (Eq. (2.38)), this leads to

$$\frac{1}{\tau} \simeq 3\epsilon \left[\left(e^{U_A} e^{-\frac{\epsilon}{1+\epsilon/2}} e^{-\omega\epsilon} - 1 \right) (1 + (1+H)\epsilon) + (e^{U_A} e^{-\epsilon} - 1) \right]. \quad (2.53)$$

Accordingly, τ may be determined iteratively if we recall that both H and ϵ also depend on τ . A way of quickly determining τ and ϵ is choosing a starting value for both ($\epsilon = \delta$ and $\tau = 0.2$ say), and then alternately using Eqs. (2.50) and (2.53) until the iterates become stationary.

2.3.2 Application to lysozyme

We have already determined the interaction in Section 2.2.2.2 ($\delta = 0.079$ and $U_A = 3.70$). We next compute τ iteratively from Eqs. (2.39), (2.44), (2.48), (2.49), (2.50) and (2.53). They depend on both the density of protein and the ionic strength. (See Table 2.3).

Thermodynamic properties like the osmotic compressibility κ_T are then also simply obtained from τ . For instance, in the Percus-Yevick approximation, κ_T is given by [27]

$$(\rho k_B T \kappa_T)^{-1} \equiv \frac{1}{k_B T} \frac{\partial \Pi}{\partial \rho} = \frac{(1 + 2\eta - \lambda\eta(1 - \eta))^2}{(1 - \eta)^4}, \quad (2.54)$$

where λ is the smaller of the two solutions of Eq. (2.36). Fig. 2.8 on page 49 compares the predicted density dependence of the (scaled) inverse osmotic compressibility at various ionic strengths with experimental data from Refs. [23] and [56].

2.4 Discussion

One difficulty in comparing our computations with experiment has been the substantial margin of error in the osmotic measurements. By contrast, in the case

I (M)	$\eta = 0$		$\eta = 0.05$		$\eta = 0.10$		$\eta = 0.15$	
	τ	ϵ	τ	ϵ	τ	ϵ	τ	ϵ
0.15	0.829	0.0230	0.712	0.0266	0.620	0.0303	0.544	0.0342
0.20	0.295	0.0483	0.289	0.0492	0.283	0.0502	0.276	0.0514
0.25	0.194	0.0596	0.193	0.0600	0.192	0.0603	0.191	0.0607
0.30	0.156	0.0653	0.155	0.0655	0.155	0.0656	0.155	0.0657
0.45	0.110	0.0725	0.110	0.0725	0.110	0.0725	0.110	0.0724
1.0	0.0735	0.0775						
1.5	0.0656	0.0782						
2.0	0.0616	0.0786						

I (M)	$\eta = 0.20$		$\eta = 0.30$		$\eta = 0.40$	
	τ	ϵ	τ	ϵ	τ	ϵ
0.15	0.482	0.0383	0.380	0.0477	0.300	0.0600
0.20	0.268	0.0528	0.251	0.0563	0.228	0.0619
0.25	0.190	0.0611	0.186	0.0624	0.179	0.0651
0.30	0.155	0.0658	0.154	0.0663	0.152	0.0677
0.45	0.110	0.0723	0.110	0.0722	0.110	0.0724

Table 2.3: *The scaled range ϵ of the effective attractive well and the strength of the effective adhesive interaction τ at pH 4.5 as a function of the ionic strength I and volume fraction η . The values of ϵ and τ have been evaluated from Eqs. (2.50) and (2.53).*

of other biomacromolecules like rodlike DNA, it has been possible to obtain the second virial B_2 at better than 10% accuracy [65–67]. One possibility for the occurrence of discrepancies in B_2 is the variety of lysozyme types. Poznanski et al. [68] have established that popular commercial lysozyme preparations like Seikagaku and Sigma exhibit significant differences under dynamic light scattering. Nevertheless, the variation in B_2 at, say, about 0.5 M NaCl (see Fig. 2.3 on page 38), is so large that it needs to be explained. At nonzero concentrations, the difference between the osmotic data of Refs. [23] and [56] is also substantial.

The relatively large variation in the experimental measurements of B_2 makes it difficult to falsify stringently other models of attractive forces like that of van der Waals type, for instance. It proves feasible to get satisfactory agreement with the experimental data displayed in Fig. 2.3 if we let the dispersion interaction be given by the nonretarded Hamaker potential [14] for spheres of dimensions appropriate

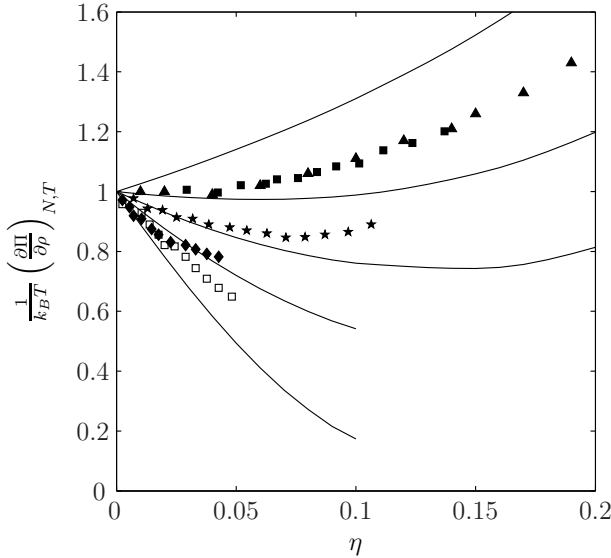


Figure 2.8: *Inverse osmotic compressibility as a function of the volume fraction η at various ionic strengths. Experimental data: black squares: $I = 0.18$ M; black triangles: $I = 0.23$ M; black stars: $I = 0.28$ M; black diamonds: $I = 0.33$ M; open squares: $I = 0.48$ M. All data from Rosenbaum et al. [23], except for those at $I = 0.23$ M (black triangles) (Piazza et al. [56]). Curves computed from Eq. (2.54) with $\delta = 0.079$, $U_A = 3.70$ and the lowered effective charge \bar{Z} ; τ has been determined from Eq. (2.53). From top to bottom: $I = 0.18$ M, $I = 0.23$ M, $I = 0.28$ M, $I = 0.33$ M and $I = 0.48$ M.*

for lysozyme, with an adjustable Hamaker constant of order $k_B T$ though with a very short cut-off at around $0.1 - 0.2$ nm. However, the necessity of such a cut-off, which is already beyond the limit of validity of continuum approximations, may be viewed as positing the equivalent of a short-range interaction like that of Eq. (2.3), in large part. It is well to note that the long-range dispersion interaction beyond some distance much smaller than the radius a , plays only a minor role.

Stell [69] has criticized the Baxter limit because divergences in the free energy appear at the level of the 12th virial. Therefore, the most straightforward way to interpret our liquid state theory is to stress that our zero-order theory describes the reference state only up to and including the 11th virial within the Percus-Yevick approximation. The analysis of phase transitions must be viewed with caution (for a comparison of recent simulations—taking the limit of zero polydispersity after the limit of vanishing well depth—with Percus-Yevick theory, see Ref. [70]). A second problem is here that, at large ionic strengths, a considerable electrostatic repulsion is balanced against a significant attraction (see Fig. 2.1 on page 33) and it is difficult to see how good such a compensatory scheme should

work at high concentrations near dense packing.

In summary, we have presented a fairly good theory of the ionic-strength dependence of the osmotic properties of lysozyme in terms of a sticky interaction which is independent of charge or salt concentration. This conclusion, by itself, is not new for it has been reached earlier by formulating numerical work incorporating short-range forces and screened electrostatics and comparing it with X-ray scattering [71, 72] and liquid-liquid phase separation [73–75]. The merit of the current analysis is its transparency because it is analytical and it is based on a nonperturbative variational principle for general short-range potentials so it may be readily generalized.

2.5 Appendix

2.5.1 Effective charge

For the repulsive tail of the two particle interaction, we use the Debye-Hückel potential, which is the far-field solution of the Poisson-Boltzmann equation. In our case, the (dimensionless) potential at the surface is often merely of order unity, so the Debye-Hückel potential slightly overestimates the solution to the Poisson-Boltzmann equation. To remedy this, we use a renormalized charge within the Debye-Hückel potential, chosen in such a way that, at large distances, the Debye-Hückel potential coincides with the tail of the solution of the Poisson-Boltzmann equation determined by the real charge [76]. This will result in an underestimation of the potential at small separations, but the form of the Debye-Hückel potential we use here (Eq. (2.4)) is in fact only accurate at large separations and overestimates the interaction at small separations appreciably i.e. when overlap of the two double layers occurs (by about 20%, see Ref. [14]). The two effects thus partly cancel, although the latter effect is larger than the former.

The Poisson-Boltzmann equation for the dimensionless potential $\psi(r) \equiv q\phi(r)/k_B T$ of a single sphere of radius a and total charge qZ , assumed positive for convenience, immersed in a solvent with Bjerrum length Q , at a concentration of ions leading to a Debye length κ , is written as

$$\frac{1}{r^2} \frac{d}{dr} r^2 \frac{d}{dr} \psi(r) = \kappa^2 \sinh \psi(r), \quad (2.55)$$

with boundary conditions

$$\left. \frac{d}{dr} \psi(r) \right|_{r=a} = \frac{ZQ}{a^2}; \quad \lim_{r \rightarrow \infty} \psi(r) = 0. \quad (2.56)$$

Linearizing Eq. (2.55) ($\psi \ll 1$), we find the Debye-Hückel solution

$$\psi_0 = \frac{ZQ}{1 + \omega} \frac{e^{-\kappa(r-a)}}{r}. \quad (2.57)$$

We next derive the first-order correction to this solution. Putting $\psi(r) = \psi_0(r) + \psi_1(r)$, with $|\psi_1(r)| \ll |\psi_0(r)|$, results in the following linear differential equation for ψ_1

$$\frac{1}{r^2} \frac{d}{dr} r^2 \frac{d}{dr} \psi_1(r) = \frac{1}{6} \kappa^2 \psi_0^3(r). \quad (2.58)$$

Keeping in mind that $\psi_1(r) = o(\psi_0(r))$, as $r \rightarrow \infty$, we integrate the differential equation once to obtain

$$\frac{d}{dr} \psi_1(r) = -\frac{\kappa^2}{6} \left(\frac{ZQe^\omega}{1+\omega} \right)^3 \frac{E_1(3\kappa r)}{r^2} \quad (2.59)$$

and a second time to derive

$$\psi_1(r) = -\frac{\kappa^3}{6} \left(\frac{ZQe^\omega}{1+\omega} \right)^3 \left(\frac{e^{-3\kappa r}}{\kappa r} - \left(3 + \frac{1}{\kappa r} \right) E_1(3\kappa r) \right), \quad (2.60)$$

where $E_1(x)$ is the exponential integral defined by $E_1(x) = \int_x^\infty dt t^{-1} e^{-t}$. Using the first of the two boundary conditions, we then determine the renormalized charge Z_{eff}

$$\begin{aligned} Z_{eff} &= \frac{a^2}{Q} \frac{d}{dr} \psi(r) \Big|_{r=a} = \frac{a^2}{Q} \frac{d}{dr} \psi_0(r) \Big|_{r=a} + \frac{a^2}{Q} \frac{d}{dr} \psi_1(r) \Big|_{r=a} \\ &= Z - \frac{\omega}{18} \left(\frac{Q}{a} \right)^2 \left(\frac{Z}{1+\omega} \right)^3 F(\omega), \end{aligned} \quad (2.61)$$

where

$$F(\omega) \equiv 3\omega e^{3\omega} E_1(3\omega) \sim 1 - \frac{1}{3\omega} + \frac{2}{9\omega^2} - \dots \quad (2.62)$$

Recapitulating, we have calculated, to leading order, the charge Z_{eff} which has to be inserted into the Debye-Hückel potential (Eq. (2.4)) so that this has the correct asymptotic behavior at large r , coinciding with the tail of the Poisson-Boltzmann solution.

2.5.2 Dependence of B_2 on ionic strength

Here, we prove some simple inequalities describing the behavior of the second virial coefficient as a function of the ionic strength for an interaction consisting of a Debye-Hückel repulsion $U_{DH}(x)$ and a general attractive potential $U_A(x)$, the latter not depending on the ionic strength. If we let $U(x) = U_{DH}(x) + U_A(x)$, then B_2 is given by Eq. (2.5) with

$$J = \int_2^\infty dx x^2 \left(1 - e^{-U(x)} \right). \quad (2.63)$$

Then, we have

$$\begin{aligned} \frac{dJ}{d\omega} &= \int_2^\infty dx x^2 \frac{dU_{DH}(x)}{d\omega} e^{-U(x)} \\ &= \int_2^\infty dx x^2 \left(\frac{d \ln \xi}{d\omega} - (x-2) \right) U_{DH}(x) e^{-U(x)}. \end{aligned} \quad (2.64)$$

In Fig. 2.9 we see that in the regime of interest $\frac{d \ln \xi}{d\omega} < 0$, so we conclude that

$$\frac{dB_2}{d\omega} = \frac{3}{8} B_2^{HS} \frac{dJ}{d\omega} < 0. \quad (2.65)$$

In the same way it is clear from the second derivative

$$\begin{aligned} \frac{d^2 J}{d\omega^2} &= \int_2^\infty dx x^2 \left(\frac{d^2 \ln \xi}{d\omega^2} + \left(\frac{d \ln \xi}{d\omega} - (x-2) \right)^2 (1 - U_{DH}(x)) \right) U_{DH}(x) e^{-U(x)} \end{aligned} \quad (2.66)$$

and the fact that $\frac{d^2 \ln \xi}{d\omega^2} \gtrsim 0$ in the regime of interest, that

$$\frac{d^2 B_2}{d\omega^2} = \frac{3}{8} B_2^{HS} \frac{d^2 J}{d\omega^2} > 0, \quad (2.67)$$

if $U_{DH}(2) < 1$, i.e. if $\xi < 1$ (a sufficient condition).

2.5.3 Corrections to the free energy

In Section 2.3, we viewed a suspension of proteins as a system of spheres with an AHS interaction and we chose the parameter τ of the AHS potential such that the first order correction in the functional expansion of the free energy (Eq. (2.29)) vanishes (see Eq. (2.31)). In an attempt to justify this approximation and explore its regime of applicability, we estimate the size of the second order correction to the free energy (from Eq. (2.29)) which is either positive or negative definite

$$\Delta \equiv \frac{\eta^2}{2} \left(\frac{3}{4\pi} \right)^2 a^3 V^{-1} \int d\mathbf{x}_1 d\mathbf{x}_2 d\mathbf{x}_3 B(x_{12})B(x_{13})h(x_{23}) = \frac{9}{4} \eta^2 Y. \quad (2.68)$$

It is convenient to rewrite the integral in such a way that the angular integration can be performed explicitly (see below).

$$\begin{aligned} Y &\equiv \int_0^\infty dt t^2 B(t) \int_0^\infty ds s^2 B(s) \int_0^\pi d\vartheta \sin \vartheta h(\sqrt{s^2 + t^2 - 2st \cos \vartheta}) \\ &= 2 \int_0^\infty dt t B(t) \int_t^\infty ds s B(s) \int_{s-t}^{s+t} du u h(u). \end{aligned} \quad (2.69)$$

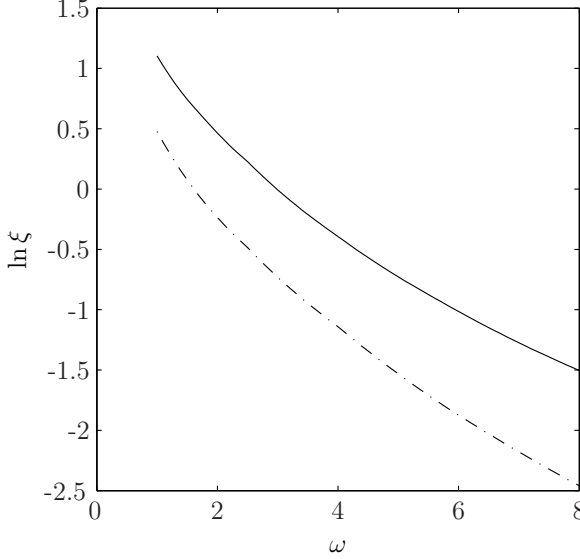


Figure 2.9: Dependence of $\ln \xi$ on ω at pH 4.5 (solid line) and pH 7.5 (dash-dotted line). In both cases $d \ln \xi / d\omega < 0$ and $d^2 \ln \xi / d\omega^2 \gtrsim 0$ if $1 \leq \omega \leq 8$.

Here we have used the Kirkwood superposition approximation $J_{BM}^{(3)}(\mathbf{x}_1, \mathbf{x}_2, \mathbf{x}_3) = h(x_{23})$ [61, 62], where $h(x) = g(x) - 1$ is the pair correlation function. We have employed the substitution $u^2 = s^2 + t^2 - 2st \cos \vartheta$, with ϑ the angle between \mathbf{x}_{12} and \mathbf{x}_{13} . Using the expression for $g(x)$ (Eq. (2.34)) and defining $\tilde{h}(x) = \tilde{g}(x) - 1$, we split Y into three parts

$$Y = Y_0 + Y_1 + Y_2 \quad (2.70)$$

where we have introduced the limit $\zeta \rightarrow 0$ and where

$$\begin{aligned} Y_0 &\equiv \frac{2\lambda}{3} \int_2^\infty dt t B(t) \int_t^{t+2} ds s B(s) \\ &\simeq \frac{2\lambda}{3} \int_2^\infty dt t B(t) \int_t^\infty ds s B(s) = \frac{\lambda}{3} \left[\int_2^\infty dt t B(t) \right]^2, \end{aligned} \quad (2.71)$$

$$Y_1 \equiv 2 \int_2^\infty dt t B(t) \int_t^{t+2} ds s B(s) \int_{s-t}^{s+t} du u \tilde{h}(u) \quad (2.72)$$

and

$$Y_2 \equiv 2 \int_2^\infty dt t B(t) \int_{t+2}^{t+4} ds s B(s) \int_{s-t}^{s+t} du u \tilde{h}(u) \ll Y_1. \quad (2.73)$$

To simplify Eq. (2.72), we substitute Eq. (2.37) and note that $s + t \geq 4$ and $0 \leq s - t \leq 2$. We then derive

$$\int_{s-t}^{s+t} du u \tilde{h}(u) = \frac{2}{3} (9G + 10GH - 12) + \frac{1}{2} (s-t)^2. \quad (2.74)$$

Next, using Eq. (2.31), we integrate the nonconstant term leading to a product of two integrals

$$\begin{aligned} \int_2^\infty dt t B(t) \int_t^{t+2} ds s B(s) (s-t)^2 &\simeq \int_2^\infty dt t B(t) \int_t^\infty ds s B(s) (s-t)^2 \\ &= \left[\int_2^\infty dt t B(t) \right] \left[\int_2^\infty ds s^3 B(s) \right]. \end{aligned} \quad (2.75)$$

Hence, Y_1 is written in terms of one-dimensional integrals

$$\begin{aligned} Y_1 &\simeq \frac{2}{3} (9G + 10GH - 12) \left[\int_2^\infty dt t B(t) \right]^2 \\ &\quad + \left[\int_2^\infty dt t B(t) \right] \left[\int_2^\infty ds s^3 B(s) \right], \end{aligned} \quad (2.76)$$

and this is also the case for Y

$$\begin{aligned} Y &\simeq \frac{2}{3} \left(9G + 10GH - 12 + \frac{\lambda}{2} \right) \left[\int_2^\infty dt t B(t) \right]^2 \\ &\quad + \left[\int_2^\infty dt t B(t) \right] \left[\int_2^\infty ds s^3 B(s) \right]. \end{aligned} \quad (2.77)$$

Our goal is to obtain explicit approximations for these integrals by expediently using Eqs. (2.32) and (2.33). First, we consider integrals on the interval $[2, 2 + \epsilon]$ which are dominated by the singular part of $B(x)$. We substitute Eq. (2.40) into (2.33) and let $\zeta \rightarrow 0$

$$\int_2^{2+\epsilon} dt t^2 \tilde{B}(t) = \frac{2\lambda}{3}. \quad (2.78)$$

We use this relation to rewrite part of one of the integrals in Eq. (2.77) in two ways, noting that $\epsilon \ll 1$.

$$\begin{aligned} \int_2^{2+\epsilon} dt t B(t) &= -\frac{\lambda}{3} + \int_2^{2+\epsilon} dt t \tilde{B}(t) = -\frac{1}{2} \int_2^{2+\epsilon} dt (t-2) t \tilde{B}(t) \\ &\simeq -\frac{\epsilon}{4} \int_2^{2+\epsilon} dt t \tilde{B}(t). \end{aligned} \quad (2.79)$$

We thus conclude that

$$\int_2^{2+\epsilon} dt t \tilde{B}(t) \simeq \left(1 - \frac{\epsilon}{4} \right) \frac{\lambda}{3} \quad (2.80)$$

so the first equality in Eq. (2.79) allows us to attain the explicit expression

$$\int_2^{2+\epsilon} dt tB(t) \simeq -\frac{\lambda\epsilon}{12}. \quad (2.81)$$

Similarly, we use Eqs. (2.40) and (2.78) to evaluate part of the other integral in Eq. (2.77).

$$\int_2^{2+\epsilon} dt t^3 B(t) = -\frac{4\lambda}{3} + \int_2^{2+\epsilon} dt t^3 \tilde{B}(t) = \int_2^{2+\epsilon} dt (t-2)t^2 \tilde{B}(t) \simeq \frac{\lambda\epsilon}{3}. \quad (2.82)$$

We note that both integrals in Eqs. (2.81) and (2.82) are $O(\epsilon)$ because the integral in Eq. (2.78) is independent of ϵ owing to the singular part of $B(x)$. If $B(x)$ had been completely regular, the integrals in Eqs. (2.81) and (2.82) would have been $O(\epsilon^2)$.

We next consider the remaining two integrals on the interval $[2+\epsilon, \infty)$. We start by splitting Eq. (2.32) into two parts since $2+\delta$ demarcates two different regimes

$$\int_{2+\epsilon}^{2+\delta} dt t^2 B(t) + \int_{2+\delta}^{\infty} dt t^2 B(t) = 0. \quad (2.83)$$

Using this equation and the approximation $B(t) \simeq -2\xi e^{-\omega(t-2)}/t$, we may simplify the two integrals, ultimately omitting $O(\delta)$ terms

$$\begin{aligned} \int_{2+\epsilon}^{\infty} dt tB(t) &= \int_{2+\epsilon}^{2+\delta} dt tB(t) + \int_{2+\delta}^{\infty} dt tB(t) \\ &\simeq \frac{1}{2} \left(1 - \frac{\delta}{2}\right) \int_{2+\epsilon}^{2+\delta} dt t^2 B(t) + \int_{2+\delta}^{\infty} dt tB(t) \\ &= \frac{\delta}{4} \int_{2+\delta}^{\infty} dt t^2 B(t) - \frac{1}{2} \int_{2+\delta}^{\infty} dt t(t-2)B(t) \simeq \frac{\xi}{\omega^2} e^{-\omega\delta} \end{aligned} \quad (2.84)$$

$$\begin{aligned} \int_{2+\epsilon}^{\infty} dt t^3 B(t) &= \int_{2+\epsilon}^{2+\delta} dt t^3 B(t) + \int_{2+\delta}^{\infty} dt t^3 B(t) \\ &\simeq (2+\delta) \int_{2+\epsilon}^{2+\delta} dt t^2 B(t) + \int_{2+\delta}^{\infty} dt t^3 B(t) \\ &= -\delta \int_{2+\delta}^{\infty} dt t^2 B(t) + \int_{2+\delta}^{\infty} dt t^2 (t-2)B(t) \simeq -4 \frac{\xi}{\omega^2} e^{-\omega\delta}. \end{aligned} \quad (2.85)$$

We remark that both expressions in Eqs. (2.84) and (2.85) are $O(\omega^{-2})$ because $B(t)$ is regular for $t \geq 2+\epsilon$. We then combine Eqs. (2.81) and (2.84), and Eqs. (2.82) and (2.85)

$$\int_2^{\infty} dt tB(t) \simeq -\frac{\lambda\epsilon}{12} + \frac{\xi}{\omega^2} e^{-\omega\delta} \simeq -\frac{1}{4} \int_2^{\infty} ds s^3 B(s). \quad (2.86)$$

Finally, using Eqs. (2.68), (2.77) and (2.86), we arrive at an approximation for the correction to the free energy

$$\Delta = \frac{9}{4}\eta^2 Y \simeq \frac{9}{2}\eta^2 \left(G + H - 6 + \frac{\lambda}{6} \right) \left[\frac{\xi}{\omega^2} e^{-\omega\delta} - \frac{\lambda\epsilon}{12} \right]^2. \quad (2.87)$$

Despite the variety of approximations used, this expression still retains its “definite” character (it turns out to be negative in the numerical calculations below). However, the numerical coefficients within the last quadratic factor are not exact. Furthermore, the status of the present theory differs from that of the Weeks-Chandler-Anderson theory [61, 62]. In the latter, Δ is of fourth order in the perturbation whereas it is basically quadratic here for the reason stated below Eq. (2.82).

I (M)	$\eta = 0.05$		$\eta = 0.10$		$\eta = 0.15$	
	$\Pi/\rho k_B T$	-2Δ	$\Pi/\rho k_B T$	-2Δ	$\Pi/\rho k_B T$	-2Δ
0.15	1.143	0.004	1.290	0.019	1.437	0.044
0.2	1.033	0.001	1.074	0.006	1.123	0.014
0.25	0.949	0.0004	0.915	0.002	0.898	0.004
0.3	0.889	0.0001	0.805	0.0005	0.749	0.001
0.45	0.763	0.000008	0.575	0.00002	0.448	0.00002

I (M)	$\eta = 0.20$		$\eta = 0.30$		$\eta = 0.40$	
	$\Pi/\rho k_B T$	-2Δ	$\Pi/\rho k_B T$	-2Δ	$\Pi/\rho k_B T$	-2Δ
0.15	1.583	0.085	1.866	0.228	2.17	0.488
0.2	1.183	0.026	1.361	0.068	1.659	0.143
0.25	0.904	0.008	0.988	0.022	1.231	0.046
0.3	0.721	0.003	0.753	0.008	0.960	0.016
0.45	0.375	0.000007	0.340	0.00002	0.470	0.0001

Table 2.4: *The osmotic pressure from Eq. (2.88) and its correction from Eq. (2.90) as a function of the ionic strength I and the packing fraction η .*

To estimate the importance of this correction, we first calculate the osmotic pressure resulting from the neglect of second and higher order terms in the functional expansion Eq. (2.29). This amounts to determining τ from Eqs. (2.36), (2.50) and (2.53) and then computing the osmotic pressure from Ref. [27] (see

also Eq. (1.49))

$$\frac{\Pi}{\rho k_B T} = \frac{1 + \eta + \eta^2}{(1 - \eta)^3} - \frac{\eta(1 + \eta/2)}{(1 - \eta)^2} \lambda + \frac{\eta^2}{36} \lambda^3. \quad (2.88)$$

Then, we evaluate the correction to the osmotic pressure due to the second order term in Eq. (2.29). The osmotic pressure is related to the free energy by

$$\frac{\Pi}{\rho k_B T} = -\eta \frac{\partial(\rho^{-1} \mathcal{A})}{\partial \eta}. \quad (2.89)$$

Because Y depends only weakly on η , we approximate the correction to the osmotic pressure by

$$-\eta \frac{\partial \Delta}{\partial \eta} \simeq -2\Delta. \quad (2.90)$$

We have compiled the pressure and its correction in Table 2.4 for the same sets of parameters as in Table 2.1 on page 39 (omitting the trivial case where $\eta = 0$).

Application of the optimized Baxter model to the hard-core attractive Yukawa system

Abstract We perform Monte Carlo simulations on the hard-core attractive Yukawa system to test the optimized Baxter model that was introduced in Chapter 2 to study a fluid phase of spherical particles interacting through a short-range pair potential. We compare the chemical potentials and pressures from the simulations with analytical predictions from the optimized Baxter model. We show that the model is accurate to within 10 percent over a range of volume fractions from 0.1 to 0.4, interaction strengths up to three times the thermal energy and interaction ranges from 6 to 20% of the particle diameter, and performs even better in most cases. We furthermore establish the consistency of the model by showing that the thermodynamic properties of the Yukawa fluid computed via simulations may be understood on the basis of one similarity variable, the stickiness parameter defined within the optimized Baxter model. Finally we show that the optimized Baxter model works significantly better than an often used, naive method determining the stickiness parameter by equating the respective second virial coefficients based on the attractive Yukawa and Baxter potentials.

3.1 Introduction

In Chapter 2 we devised a method to approximate systematically a system of spherical hard particles that interact through a short-range pair potential, by a system of particles interacting via an effective Baxter potential [27]. The latter consists of a hard-core repulsion and a sticky attraction at the surface of the particles which is computed by a variational principle for the free energy (hence the name “optimized Baxter model”, see Chapter 2). The original short-range potential was a sum of attractive and repulsive contributions (i.e. a square well

plus a Debye-Hückel interaction), but the variational method also applies to a purely attractive interaction provided its range is sufficiently smaller than the particle diameter. The advantage of approximating the original interaction by the Baxter potential is that the fluid phase of the Baxter model has been studied extensively, both theoretically [27, 41, 42, 69, 77–80] and in computer simulations [28, 64, 81, 82]. This means that, once the correspondence between the two systems has been established, all the analytical results of the Baxter model can be fruitfully used for the original system.

In the optimized Baxter model (OBM) (see Chapter 2), the free energy of the actual system is functionally expanded in terms of the Mayer function, where the reference state is a suspension of hard spheres interacting via an effective sticky potential. The stickiness parameter associated with the latter is determined by setting the first-order term in this expansion equal to zero. This constitutes a variational principle because the second-order term turns out to be either positive or negative definite. Nevertheless, the exact nature of the expansion is difficult to assess analytically. For instance, there may be mathematical problems arising from the limiting procedure in which the range of the effective adhesion goes to zero as its magnitude becomes infinitely large. Thus, a computational test of the OBM is important.

The model system we consider consists of hard-sphere particles with an attractive Yukawa interaction

$$\frac{U_Y(x)}{k_B T} = \begin{cases} \infty & 0 \leq x < 2 \\ -\beta \frac{e^{-\kappa(x/2-1)}}{x/2} & x \geq 2 \end{cases}. \quad (3.1)$$

Here, $x \equiv r/a$ is the dimensionless distance between the centers of mass of two spheres, a is their radius, k_B is Boltzmann's constant, T is the temperature, β is the dimensionless well depth and a/κ is a measure of the range of the attractive tail (if we wish to set the actual well depth \equiv unity, β may be viewed as identical with $1/k_B T$). Note that we scale distances by a here although often distances are scaled by the diameter $2a$ [46, 83].

The liquid-solid coexistence of this system has been studied before at various values of κ [46, 83]. These papers do not report the chemical potentials and pressures at coexistence however, which we need to test the validity of the OBM. We therefore perform new simulations to determine the volume fraction, chemical potential and pressure at various points along the phase boundaries. Moreover, we also determine the chemical potential and pressure within the fluid region of the phase diagram so as to gauge the accuracy of the OBM at lower concentrations.

We start by reviewing equations relevant to the OBM as applied to the Yukawa potential (Eq. (3.1)) in the next section. In Section 3.3 we describe the numerical simulations which, in Section 3.4, are compared with the theoretical predictions.

3.2 Theory

Here we give a short summary of the theory developed in Chapter 2. The relevant equations needed to determine the effective adhesion parameter τ and some of the thermodynamic properties of the system are presented here. For details of the derivation we refer to Chapter 2 and references mentioned there.

We consider a system of spherical particles of radius a . The interaction U between the particles is pairwise additive and consists of a hard-sphere repulsion plus a short-range interaction U_1 that is either purely attractive or consists of a combination of attractive and repulsive interactions (range $\ll a$). In the latter case, the attraction has to be strong enough to compensate for the repulsion—we come back to this issue later. For convenience, all distances are scaled by the radius a of the particles so we have

$$U(x) = \begin{cases} \infty & 0 \leq x < 2 \\ U_1(x) & x \geq 2 \end{cases}. \quad (3.2)$$

We wish to replace this system by a suspension of adhesive hard spheres with the same radius which is our reference state. The interaction of the latter is given by the adhesive hard sphere (AHS) potential of Baxter [27]

$$\frac{U_{AHS}(x)}{k_B T} = \begin{cases} \infty & 0 \leq x < 2 \\ \ln \frac{12\tau\zeta}{2+\zeta} & 2 \leq x \leq 2 + \zeta \\ 0 & x > 2 + \zeta \end{cases}. \quad (3.3)$$

Here, τ is the stickiness parameter whose magnitude we wish to determine and which signifies the strength of the effective adhesion. The limit $\zeta \downarrow 0$ has to be taken after formal integrations. The reason for approximating the original system by the AHS system is that the latter has been conveniently solved in the Percus-Yevick approximation [27]. This means that once the correspondence between the two systems has been established by appropriately choosing τ , other properties like, for example, the chemical potential, the pressure and the compressibility of the system can easily be computed analytically from the solution of the AHS system.

We next describe how to choose the stickiness parameter τ . In the limit of vanishing densities, this is done by equating second virial coefficients since we must equate the respective free energies of the two systems.

$$B_2 = 2\pi a^3 \int_0^\infty dx x^2 \left(1 - e^{-U(x)/k_B T}\right) \equiv B_2^{AHS} = B_2^{HS} \left(1 - \frac{1}{4\tau_0}\right). \quad (3.4)$$

This amounts to choosing

$$\tau_0 = \frac{2}{3 \int_2^\infty dx x^2 \left(e^{-U_1(x)/k_B T} - 1\right)}. \quad (3.5)$$

Here, $B_2^{HS} = 16\pi a^3/3$ is the second virial coefficient of a solution of hard spheres. At finite densities this procedure necessarily breaks down, however, because the higher virials come into play. The stickiness parameter τ , which depends on the density, has to be obtained by identifying the free energy of the actual system with that of the reference state as well as possible. In the functional expansion of the excess free energy in terms of the Mayer function [62], we then demand that the first order correction vanishes. This leads to the condition

$$\int_0^\infty dx x^2 (e^{-U(x)/k_B T} - 1) \tilde{g}(x) = \frac{2\lambda}{3}, \quad (3.6)$$

where $\tilde{g}(x)$ is the regular part of the pair correlation function $g(x)$ of the reference AHS system (which also has a singular term, see Chapter 2 and [27]) and

$$\lambda = \frac{6(\eta + (1 - \eta)\tau)}{\eta(1 - \eta)} \left(1 - \sqrt{1 - \frac{\eta(2 + \eta)}{6(\eta + (1 - \eta)\tau)^2}} \right) \quad (3.7)$$

with η the volume fraction of particles. For $x < 2$, $\tilde{g}(x)$ equals zero owing to the hard-core repulsion, whereas $\tilde{g}(x)$ tends to unity for large x . Since the interaction $U(x)$ is of short range, we approximate $\tilde{g}(x)$ in the interval $2 \leq x \leq 4$ by the first two terms of its Taylor expansion

$$\tilde{g}(x) \simeq \begin{cases} 0 & x < 2 \\ G(1 + H(x - 2)) & 2 \leq x \leq 4 \\ 1 & x > 4 \end{cases} . \quad (3.8)$$

Here, we define the functions

$$G = \lambda\tau \quad (3.9)$$

and

$$H = \frac{\eta}{2\tau(1 - \eta)} \left(\frac{\eta(1 - \eta)}{12} \lambda^2 - \frac{1 + 11\eta}{12} \lambda + \frac{1 + 5\eta}{1 - \eta} - \frac{9(1 + \eta)}{2(1 - \eta)^2} \frac{1}{\lambda} \right). \quad (3.10)$$

At a given volume fraction η , τ can then be determined iteratively from Eqs. (3.6)-(3.10). An iterative scheme, which converges fast, consists of choosing a starting value of τ , determining λ from Eq. (3.7), then τ from

$$\tau = \frac{2\lambda - 3 \int_4^\infty dx x^2 (e^{-U(x)/k_B T} - 1)}{3\lambda \int_2^4 dx x^2 (1 + H(x - 2))(e^{-U(x)/k_B T} - 1)}, \quad (3.11)$$

λ again from Eq. (3.7) and so on until convergence to the required accuracy is achieved.

There are two cases in which the above method does not yield meaningful results. The first occurs when the short-range interaction has both attractive and

repulsive components in the event that the repulsion is too strong in comparison with the attraction. The total interaction is then effectively repulsive in nature so it is clear that a suspension of particles interacting in such a way cannot be approximated by an AHS system. In this case, the iteration scheme described above leads to a τ which keeps on increasing and does not converge. If τ_0 is negative in the limit of vanishing density (Eq. (3.5)) implying a net repulsion, it is advisable not to compute τ in that case, even though τ could attain positive values at higher densities. Secondly, the attraction may be too strong. There exists a critical value of the stickiness parameter τ_c below which there is a range of densities for which there is no real solution of λ

$$\tau_c = \frac{2 - \sqrt{2}}{6}. \quad (3.12)$$

This means that if the attraction is strong enough (i.e. when τ is too small), there will not be a positive real solution to Eq. (3.11). In this case the iteration scheme would produce complex values of τ .

Finally, to compute the pressure P and the chemical potential μ we use the expressions derived via the compressibility route [27, 41], see Eqs. (1.49) and (1.51).

3.3 Simulations

We perform Monte Carlo simulations at constant volume V and temperature T on a system of $N = 256$ hard spheres with a short-range Yukawa attraction so we have (compare with Eq. (3.1))

$$\frac{U_1(x)}{k_B T} = -\beta \frac{e^{-\kappa(x/2-1)}}{x/2}. \quad (3.13)$$

We introduce a cutoff at $x = 4$, so that $U(x) = 0$ for $x > 4$. We determine the Helmholtz free energy per particle f_N at a chosen set of parameters of β , κ and η by thermodynamic integration at constant κ and η , starting from the known free energy per particle of the hard sphere system ($\beta = 0$) which is defined at the same volume fraction (see e.g. Ref. [84])

$$\frac{f_N(\eta, \beta) - f_N(\eta, 0)}{k_B T} = \int_0^\beta d\beta' \frac{1}{\beta'} \left\langle \frac{U_1}{k_B T} \right\rangle_N. \quad (3.14)$$

Here $\langle U_1 \rangle_N$ is the average energy per particle where the average is computed in the state with $\beta = \beta'$. From this we determine the equation of state $z_N(\eta, \beta)$

$$z_N(\eta, \beta) - z_N(\eta, 0) = \frac{P_N(\eta, \beta)}{\rho k_B T} - \frac{P_N(\eta, 0)}{\rho k_B T} = \eta \frac{\partial}{\partial \eta} \left[\frac{f_N(\eta, \beta) - f_N(\eta, 0)}{k_B T} \right], \quad (3.15)$$

where the particle density ρ is related to the volume fraction by $\rho v_0 = \eta$, and the chemical potential $\mu_N(\eta, \beta)$ is given by

$$\frac{\mu_N(\eta, \beta)}{k_B T} - \frac{\mu_N(\eta, 0)}{k_B T} \simeq \frac{\partial}{\partial \eta} \eta \left[\frac{f_N(\eta, \beta) - f_N(\eta, 0)}{k_B T} \right]. \quad (3.16)$$

The expression for the pressure is exact for a system consisting of a finite number of particles N , whereas that for the chemical potential has an error of order N^{-1} , because in the simulations we change only the volume V of the box leaving the number of particles invariant. (See Section 3.5.1 for details). For the equation of state of the pure hard-sphere system we have

$$z^l(\eta, 0) = 1 + \frac{4\eta + 1.216224\eta^2 + 1.246720\eta^3}{1 - 2.195944\eta + 1.210352\eta^2} \quad (3.17)$$

valid when the system is a fluid [85]. It is quadrature to determine the chemical potential

$$\frac{\mu^l(\eta, 0)}{k_B T} = \ln \eta - 1 + z^l(\eta, 0) + \int_0^\eta d\eta' \frac{z^l(\eta', 0) - 1}{\eta'}. \quad (3.18)$$

For the pressure of the hard sphere (fcc) solid we use [86]

$$z^s(\eta, 0) = \frac{3}{1 - \frac{6}{\pi\sqrt{2}}\eta} - \frac{0.5921 \left(\frac{6}{\pi\sqrt{2}}\eta - 0.7072 \right)}{\frac{6}{\pi\sqrt{2}}\eta - 0.601} \quad (3.19)$$

and for the chemical potential

$$\frac{\mu^s(\eta, 0)}{k_B T} = \ln \eta - 1 + z^s(\eta, 0) + \frac{f^s(\eta_0)}{k_B T} + \int_{\eta_0}^\eta d\eta' \frac{z^s(\eta', 0) - 1}{\eta'}, \quad (3.20)$$

where $f^s(\eta_0)/k_B T = 5.91889(4)$ is the free energy of the hard sphere solid in the thermodynamic limit $N \rightarrow \infty$ at volume fraction $\eta_0 = 0.5450$ [87]. We thus calculate the pressure and the chemical potential of the system in the thermodynamic limit using

$$\frac{P(\eta, \beta)v_0}{k_B T} \simeq \eta z^i(\eta, 0) + \eta^2 \frac{\partial}{\partial \eta} \int_0^\beta d\beta' \frac{1}{\beta'} \left\langle \frac{U_1}{k_B T} \right\rangle_N, \quad (3.21)$$

and

$$\frac{\mu(\eta, \beta)}{k_B T} \simeq \frac{\mu^i(\eta, 0)}{k_B T} + \frac{\partial}{\partial \eta} \eta \int_0^\beta d\beta' \frac{1}{\beta'} \left\langle \frac{U_1}{k_B T} \right\rangle_N \quad (3.22)$$

where $i = s, l$. These expressions are not exact but correct to order N^{-1} because the number of particles in the simulations is finite (see Section 3.5.1 for details).

To determine the average energy per particle $\langle U_1/k_B T \rangle_N$ we need to initiate the simulation by choosing a convenient starting configuration. In the case that

the system is a solid, we assume it is an fcc crystal at the appropriate density. For the liquid, a configuration at the required density is initiated by putting the particles in the box at random and then running the simulation until the particles no longer overlap. This is done at a low value of β and we then use this starting configuration for all values of β at the same density. The simulation is then run for 10,000 cycles (i.e. trial moves per particle) at the relevant value of β to determine the appropriate maximum displacement of a particle at an acceptance probability of a particle displacement of 0.40. The maximum displacement is then fixed and the simulation is run for another 10,000 cycles for the system to equilibrate. Finally, the average energy per particle is measured every 100 cycles during another 50,000 cycles.

To perform the integration in Eq. (3.14) we run simulations at values of β ranging from 0.1 until the appropriate value at intervals of 0.1. A simulation at $\beta = 0.02$ is also performed. We then fit the points to a curve and use this to perform the integration. To determine the density dependence of the free energy f_N about a certain density, we compute the free energy at about 10 values of the density close to it, at intervals of 0.1. We again fit these to a curve which is used in Eqs. (3.21) and (3.22) to determine the chemical potential and the pressure at the desired density.

3.4 Results and discussion

3.4.1 Phase equilibrium

We first test the optimized Baxter model with respect to the fluid phase of hard spheres with Yukawa attraction when it coexists with the solid phase. This coexistence has been studied before via computer simulations [46, 83] but these papers did not report the pressure and chemical potential, data we do need here.

At a given strength β and inverse range κ of the attraction, we compute the volume fractions of the coexisting fluid and solid phases by equating the pressures and the chemical potentials in the respective phases. This is done for $\kappa = 7$ and 9, and β running from 0 to 2 at intervals of 0.25 (see Tables 3.1 and 3.2).

Our phase boundaries at $\kappa = 7$ agree well with those computed earlier by Dijkstra [83] who used the same method, though with a smaller system of $N = 108$ particles. The deviation in volume fraction is at most 2% (we determined the phase boundaries from a plot presented in Ref. [83], so this may account for part of the difference). At low values of β , the agreement with the simulations of Hagen and Frenkel [46] is also good, but with increasing β the difference between their phase boundary on the fluid side and ours becomes appreciable until our prediction of the volume fraction is about 20% higher than theirs at $\beta = 2$. We note that in Ref. [46] a different method was used to determine the phase boundary. The phase boundaries on the solid side do agree within 3%. We regain essentially the same picture at $\kappa = 9$ though the difference in the phase boundaries at the fluid

β	η_l	η_s	τ (OBM)	τ_0 (B_2)
0	0.492	0.543	∞	∞
0.25	0.493	0.551	8.921	1.930
0.5	0.493	0.561	3.329	0.910
0.75	0.492	0.571	1.689	0.570
1	0.490	0.584	0.986	0.400
1.25	0.485	0.598	0.616	0.299
1.5	0.478	0.613	0.405	0.231
1.75	0.465	0.627	0.271	0.184
2	0.441	0.641	0.183	0.148

Table 3.1: Volume fraction of particles in the coexisting fluid and solid phases as a function of β at $\kappa = 7$ determined by the simulations. The stickiness parameter is computed via the optimized Baxter model (OBM) and the B_2 method (B_2).

β	η_l	η_s	τ (OBM)	τ_0 (B_2)
0	0.492	0.543	∞	∞
0.25	0.493	0.552	6.278	2.549
0.5	0.494	0.563	2.673	1.199
0.75	0.494	0.576	1.521	0.750
1	0.492	0.591	0.970	0.526
1.25	0.488	0.608	0.659	0.392
1.5	0.480	0.626	0.462	0.303
1.75	0.464	0.643	0.328	0.240
2	0.437	0.657	0.236	0.193

Table 3.2: Same as Table 3.1 but now for $\kappa = 9$.

side is less pronounced (about 14% at $\beta = 2$). The phase diagram at $\kappa = 9$ was not determined in Ref. [83].

Next, we use the OBM to determine the effective stickiness parameter τ (Eq. (3.11)) and the properties of the fluid at coexistence. By way of comparison, we also evaluate τ_0 by equating the respective second virial coefficients of the attractive Yukawa interaction and the Baxter potential (see Eq. (3.5)) and computing the properties of the resulting Baxter fluid. We will refer to this as the B_2 method which is strictly correct only at very low concentrations as we

stressed above. We employ Eqs. (1.49) and (1.51) to calculate the pressure and the chemical potential from the volume fractions and the respective values of τ from the two methods. These predictions are compared with the simulations in Figs. 3.1 and 3.2.

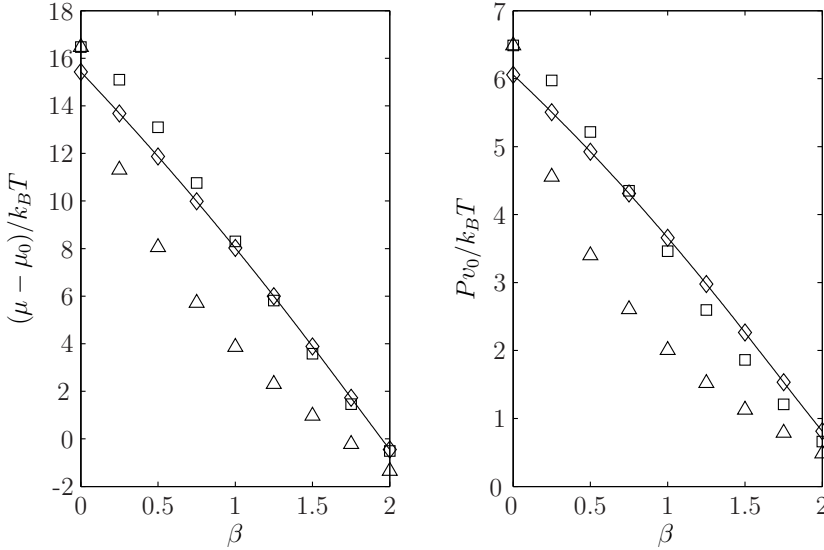


Figure 3.1: Dimensionless chemical potential and dimensionless pressure as a function of the strength β of the Yukawa potential for the coexisting fluid and solid phases. Here $\kappa = 7$. The diamonds and the fitted line are results from the simulations. The squares are predictions from the optimized Baxter model (at the same densities) and the triangles have been computed by the B_2 method.

It is clear from the figure that the predictions of the OBM are significantly better than those via the B_2 method along the whole phase boundary. The OBM is actually quite accurate to within a few percent. Recall that at $\beta = 0$, i.e. in the absence of attraction, the two volume fractions predicted by the two methods necessarily coincide simply because $\tau = \infty$ in both cases. However, this volume fraction does not agree with that from the simulations which is due to the fact that we use the accurate equation of state (Eq. (3.17)) in the latter. The analytical theory is, of course, approximate and overestimates the pressure and the chemical potential.

3.4.2 Consistency test in the fluid phase

The Baxter model itself has been solved in the Percus-Yevick approximation [27] and we here use the compressibility route to obtain the thermodynamic properties.

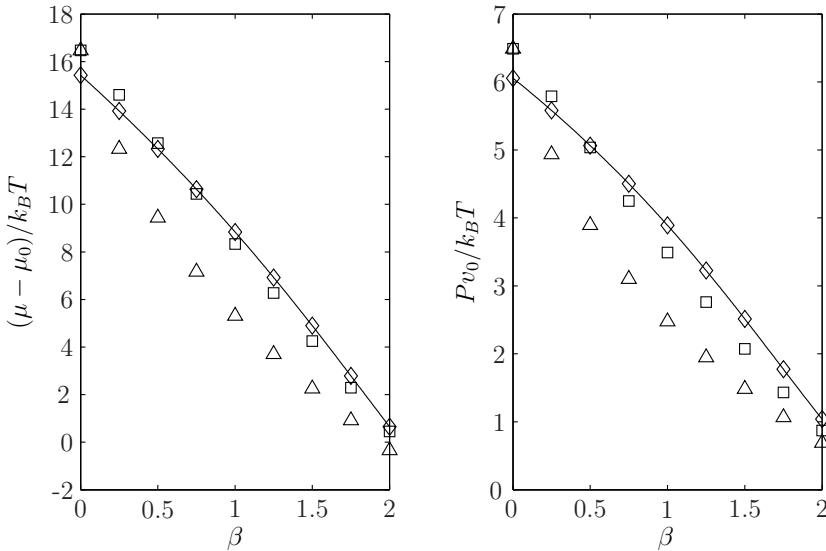


Figure 3.2: Same as Fig. 3.1 but now for $\kappa = 9$.

We know, however, that in the case of the hard sphere system, the analytical calculations carried out in this way are too high (e.g. at $\eta = 0.4$, both the pressure and the chemical potential are overestimated by 4%). We therefore seek to test the argumentation leading to the replacement of the actual fluid by the OBM in a way which is less sensitive to the Percus-Yevick approximation. For instance, we note that the stickiness parameter τ in the OBM merely depends on the properties of the distribution function \tilde{g} very close to the sphere (see Eq. (3.8)). Though this does depend on the Percus-Yevick approximation, it stands to reason that the functions G and H are more robust to approximation than the oscillatory behavior which \tilde{g} actually displays in full (and which is implicit in Eqs. (1.49) and (1.51)). Thus, in the following simulations for the fluid phase, we investigate whether mathematical similarity [88] is achieved with respect to the parameter τ as given by Eq. (3.11). This constitutes a reasonable consistency check with regard to the representation of the real fluid by the OBM.

Our procedure is as follows. We start at a given volume fraction. Next we choose a set of values of the inverse range of the Yukawa potential (i.e. $\kappa = 5, 7, 9, 11, 13$ and 15). We then fix a certain value of the stickiness parameter τ and compute the concomitant value β for each κ with the help of Eq. (3.11). If similarity [88] does apply, the thermodynamic properties should depend solely on τ and η i.e. they ought to be independent of κ at constant τ .

We have performed this test on simulations in a suitable range of volume fractions η and stickiness parameters τ with associated interaction parameters κ

and β as chosen above. (See Figs. 3.3 to 3.6).

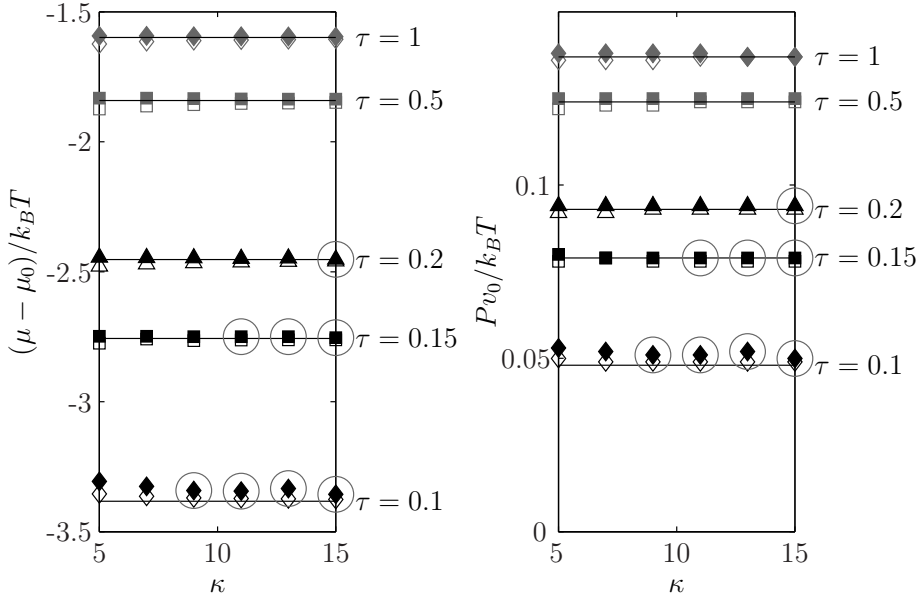


Figure 3.3: Dimensionless chemical potential and dimensionless pressure of the fluid phase as a function of the inverse range κ of the Yukawa potential at volume fraction $\eta = 0.1$. The solid symbols are results from the simulations, the horizontal lines are predictions from the optimized Baxter model at a variety of fixed values of τ . In the simulations the strength of the attraction β is chosen in such a way that the optimized Baxter model gives the appropriate value of τ : grey filled diamonds $\tau = 1$, grey filled squares $\tau = 0.5$, black filled triangles $\tau = 0.2$, black filled squares $\tau = 0.15$ and black filled diamonds $\tau = 0.1$. The corresponding open symbols have been computed by the B_2 method. Encircled points are metastable with regard to fluid-crystal coexistence.

In some cases the attraction is so strong in terms of β that the simulated fluid is actually in the metastable region with respect to fluid-crystal coexistence. In effect, if the system were macroscopic, phase separation into fluid and crystal phases would occur. We are aware of this on the basis of simulations performed by Hagen and Frenkel [46] and by Dijkstra [83]. In both these investigations, fluid-crystal coexistence was assessed quantitatively by positing the two phases a priori. We have not done this here because our main interest has been in testing the OBM for the fluid phase. From their data, we judge our simulations to be metastable in this sense for certain points encircled in Figs. 3.3-3.6. Despite the pre-emption of phase separation, we may still determine the pressure and chemical potential as if the phases were stable. The OBM pertains to the fluid phase and cannot address this type of metastability, though invariance of the pressures and

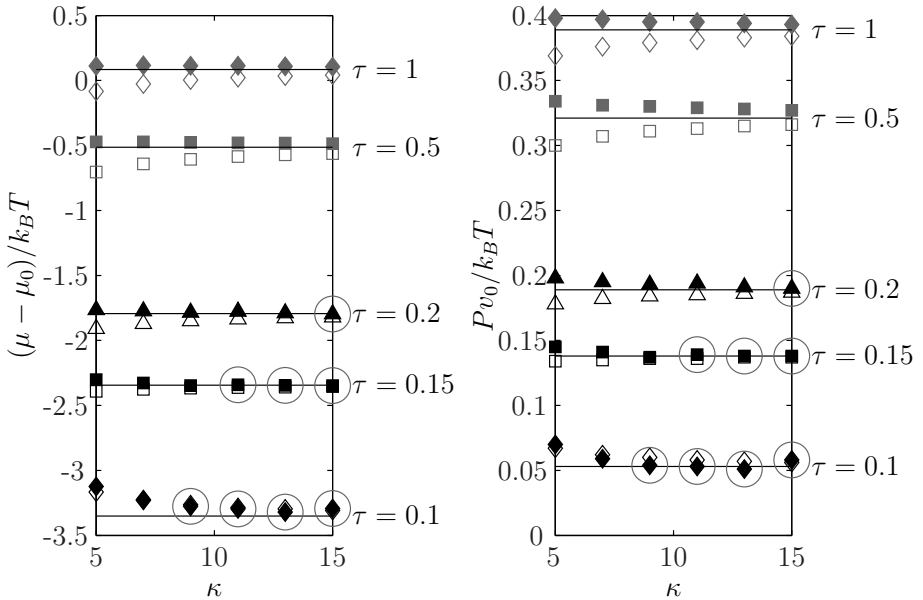


Figure 3.4: Same as Fig. 3.3 but now at volume fraction $\eta = 0.2$.

chemical potentials may be assumed in the two phases.

We first note that the simulated thermodynamic properties are generally quite independent of κ . (See the filled symbols in Figs. 3.3 to 3.6). This implies that τ is indeed a useful similarity variable and the OBM is a consistent approximation scheme. The variation in the pressures and chemical potentials computed by simulation is only a few percent with few exceptions. Sometimes, there are visible deviations from the horizontal at low values of κ , for instance, when the volume fraction is 0.4. By contrast, there are marked deviations from similarity when the attraction is strong ($\tau = 0.1$) at a volume fraction of $\eta = 0.4$ at $\kappa = 11$ and 13 (see Fig. 3.6 on page 72). Mere visual scrutiny of the simulation snapshots shows that gelation seems to be occurring—note that the attraction is so strong that we are now well beyond the percolation threshold [28]. This refers to a second type of metastability. It is beyond the scope of this paper to investigate this phenomenon further or the possibility of fluid-fluid coexistence.

Next, it is of interest to compare the magnitudes of the simulated thermodynamic properties with those computed with the help of the OBM (see the curves in Figs. 3.3 to 3.6 which are horizontal because τ was forced to be constant in each case). The analytical predictions are virtually quantitative, except at those densities at $\tau = 0.1$ where gelation seems to occur as discussed above and with regard to some of the pressures at higher concentrations. The latter are overestimated at

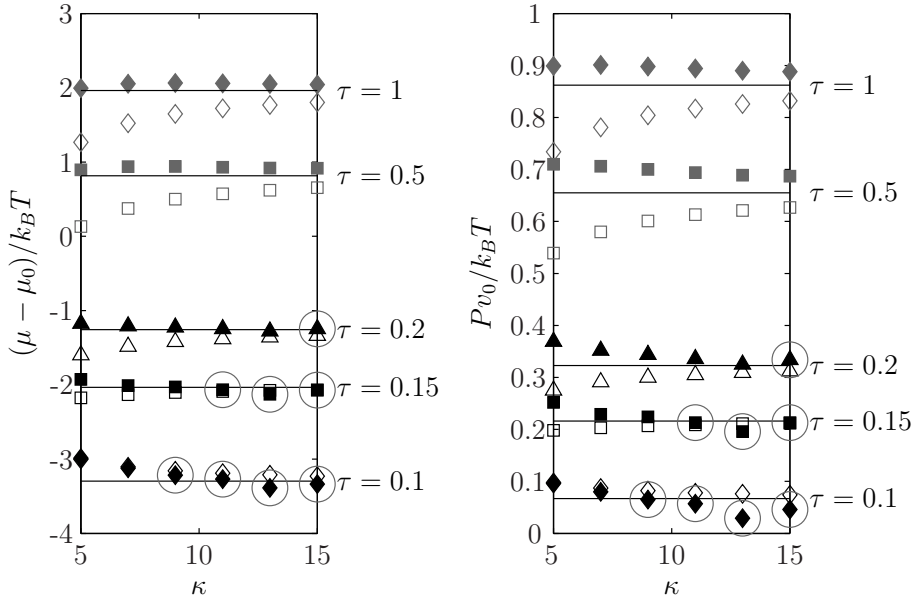


Figure 3.5: Same as Fig. 3.3 but now at volume fraction $\eta = 0.3$.

$\tau = 0.5$ and 1 in Figs. 3.5 and 3.6 which we attribute to deficiencies in the Baxter model itself (i.e. the Percus-Yevick approximation), since the simulational data are quite independent of κ as stressed above.

For the sake of comparison we have also displayed thermodynamic properties computed by the B_2 method. At a certain κ and β we evaluate τ_0 with the help of Eq. (3.5) using the Yukawa interaction Eq. (3.1) (thus τ_0 is not constant like τ) and then calculate the pressure and chemical potential within the Baxter model. The B_2 method works well at $\eta = 0.1$ (see Fig. 3.3 on page 69), which is not surprising since neglecting to variationally adjust virials higher than second is not so crucial in this case. However, the B_2 method worsens progressively as the concentration increases and ultimately becomes unreliable (see Figs. 3.4-3.6). This is of course expected: the B_2 method merely adjusts a single coefficient B_2 whereas the free energy itself is variationally optimized in the OBM.

We conclude that the optimized Baxter model is a convenient quantitative, analytical theory for computing the thermodynamic properties of a fluid of hard spheres interacting by an attraction of short range. Moreover, the variational scheme used in deriving the OBM is consistent, especially when the range of the potential is short i.e. less than approximately 10% of the particle diameter ($\kappa \gtrsim 10$). Overall, the OBM is accurate to within 10 percent, except under some conditions of very strong attraction at high volume fractions ($\tau = 0.1$, $\eta = 0.3$

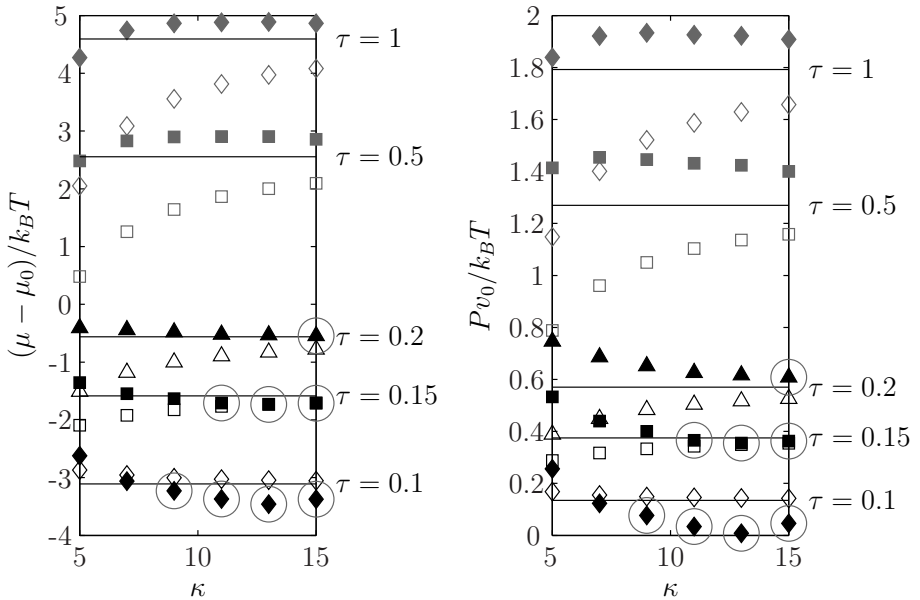


Figure 3.6: Same as Fig. 3.3 but now at volume fraction $\eta = 0.4$.

and 0.4), and it is actually much more precise in most cases.

3.5 Appendix

3.5.1 Finite size effects

Here we show that the error incurred in Eq. (3.16) for the chemical potential of the N -particle system is of order N^{-1} , whereas Eq. (3.15) for the equation of state is exact. We also prove that the error in the free energy of the system is of order N^{-1} .

Our simulations are carried out at a constant number of particles N . Hence, we modify the volume fraction η by altering the volume of the simulation box. The free energy difference per particle

$$\Delta f_N(\eta, \beta) \equiv f_N(\eta, \beta) - f_N(\eta, 0) = k_B T \int_0^\beta d\beta' \frac{1}{\beta'} \left\langle \frac{U_1}{k_B T} \right\rangle_N \quad (3.23)$$

is determined as a function of the volume fraction, so in effect it is a function of η (or ρ) and N (and of course β and κ). The exact equation of state $z_N(\eta, \beta)$ for

the N -particle system is then

$$z_N(\eta, \beta) \equiv -\frac{1}{\rho k_B T} \left(\frac{\partial F_N(\eta, \beta)}{\partial V} \right)_{N,T} = z_N(\eta, 0) + \eta \frac{\partial}{\partial \eta} \frac{\Delta f_N(\eta, \beta)}{k_B T}, \quad (3.24)$$

where $F_N(\eta, \beta) = N f_N(\eta, \beta)$ and the exact chemical potential is

$$\begin{aligned} \frac{\mu_N(\eta, \beta)}{k_B T} &\equiv \frac{1}{k_B T} \left(\frac{\partial F_N(\eta, \beta)}{\partial N} \right)_{V,T} \\ &= \frac{\mu_N(\eta, 0)}{k_B T} + \frac{\partial}{\partial \eta} \frac{\eta \Delta f_N(\eta, \beta)}{k_B T} - \frac{1}{N} \frac{\partial}{\partial N^{-1}} \frac{\Delta f_N(\eta, \beta)}{k_B T}. \end{aligned} \quad (3.25)$$

Here, and in the rest of the appendix, we have switched to the new independent variables η and N so that derivatives with respect to η are taken at constant N and derivatives with respect to N are taken at constant η . We see from Eqs. (3.24) and (3.25) that Eq. (3.16) has an error of order N^{-1} whereas Eq. (3.15) is exact.

We now assume that we may Taylor expand $\Delta f_N(\eta, \beta)$ for small values of N^{-1} at constant volume fraction. It's not obvious that this is allowed. In the case of a crystal for example, the first-order correction to the free energy per particle due to the fact that the number of particles is finite, is of order $N^{-1} \ln N$ [87, 89]. This correction is the same for systems of identical numbers of particles however, regardless of the interaction. Since our f_N is the difference in the free energies per particle pertaining to the two respective crystals (with different pair potentials), the $O(N^{-1} \ln N)$ corrections simply cancel. Moreover, from Ref. [87] we know that the leading higher order corrections to the free energy per particles are of order N^{-1} . These deliberations are confirmed in Figs. 3.7 and 3.8 which show that the leading corrections to the average dimensionless energy per particle $\langle U_1/k_B T \rangle_N$ are indeed of order N^{-1} at the representative values $\beta = 1$, $\kappa = 15$ and $\rho(2a)^3 = 0.4$ ($\eta = \pi/15 \simeq 0.20944$) for the fluid and $\rho(2a)^3 = 1.2$ ($\eta = \pi/5 \simeq 0.62832$) for the solid.

Therefore, we conclude that the free energy per particle in a system containing an infinite number of particles is given by

$$\Delta f_\infty(\eta, \beta) = \Delta f_N(\eta, \beta) + O\left(\frac{1}{N}\right). \quad (3.26)$$

In the same manner, the equation of state $z_\infty(\eta, \beta)$ is then

$$z_\infty(\eta, \beta) = z_\infty(\eta, 0) + \eta \frac{\partial}{\partial \eta} \frac{\Delta f_N(\eta, \beta)}{k_B T} + O\left(\frac{1}{N}\right), \quad (3.27)$$

and the chemical potential is expressed by

$$\frac{\mu_\infty(\eta, \beta)}{k_B T} = \frac{\mu_\infty(\eta, 0)}{k_B T} + \frac{\partial}{\partial \eta} \frac{\eta \Delta f_N(\eta, \beta)}{k_B T} + O\left(\frac{1}{N}\right). \quad (3.28)$$

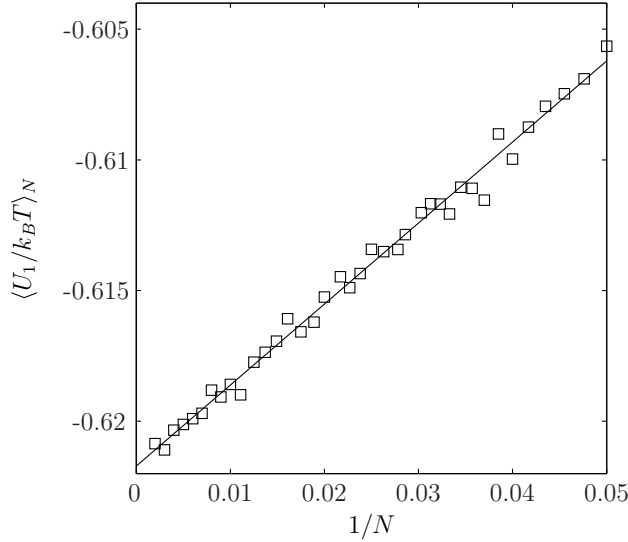


Figure 3.7: Example of the dependence of the average dimensionless energy per particle $\langle U_1/k_B T \rangle_N$ in the fluid on the size of the system. Here $\kappa = 9$, $\beta = 1$ and $\eta = \pi/15 \simeq 0.20944$ ($\rho(2a)^3 = 0.4$). N denotes the number of particles.

3.5.2 Second-order correction to the free energy

We estimate the second-order correction to the free energy (see Section 2.5.3)

$$\Delta = \frac{9}{4}\eta^2 Y. \tag{3.29}$$

This correction leads for instance to a correction to the dimensionless pressure $Pv_0/k_B T$ approximately equal to $-2\eta\Delta$. The first part of the analysis in Section 2.5.3 is also useful here and we again approximate Y by

$$Y \simeq \frac{2}{3} \left(9G + 10GH - 12 + \frac{\lambda}{2} \right) \left[\int_2^\infty dt t B(t) \right]^2 + \left[\int_2^\infty dt t B(t) \right] \left[\int_2^\infty ds s^3 B(s) \right], \tag{3.30}$$

where

$$B(x) \equiv g(x) \left[\exp \left(-\frac{U_Y(x)}{k_B T} + \frac{U_{AHS}(x)}{k_B T} \right) - 1 \right] \tag{3.31}$$

and λ , G and H are given by Eqs. (3.7), (3.9) and (3.10). We split the pair distribution function $g(x)$ in the reference state into $g_\zeta(x)$ and a regular part $\tilde{g}(x)$ given by Eq. (3.8) (see also Chapter 2):

$$g(x) = \tilde{g}(x) + g_\zeta(x) \tag{3.32}$$

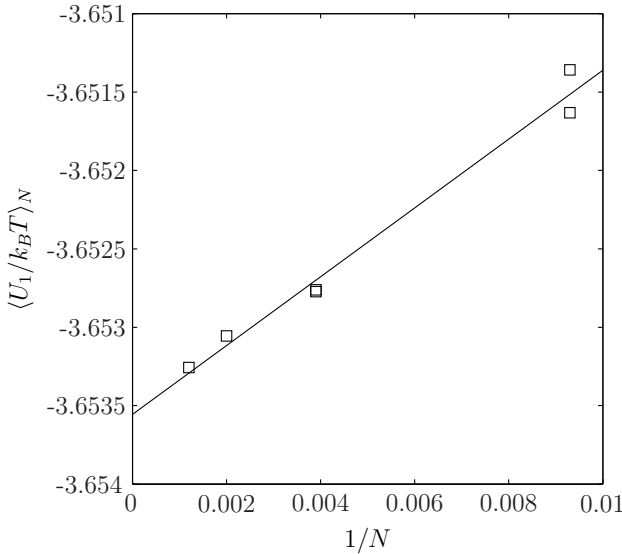


Figure 3.8: Same as Fig. 3.7 but now for the solid at $\eta = \pi/5 \simeq 0.62832$ ($\rho(2a)^3 = 1.2$).

with

$$g_\zeta(x) = \begin{cases} 0 & x < 2 \\ \frac{\lambda(2+\zeta)}{12\zeta} + O(1) & 2 \leq x \leq 2 + \zeta \\ 0 & x > 2 + \zeta \end{cases} . \quad (3.33)$$

We then insert the expressions for the potentials Eqs. (3.1) and (3.3) into Eq. (3.31) and derive in the limit $\zeta \rightarrow 0$

$$\begin{aligned} & \int_2^\infty dx x B(x) \\ &= -\frac{\lambda}{3} + G \int_2^\infty dx x (1 + H(x-2))(e^{-U_Y(x)/k_B T} - 1) + O(e^{-\kappa}) \end{aligned} \quad (3.34)$$

and

$$\begin{aligned} & \int_2^\infty dx x^3 B(x) \\ &= -\frac{4\lambda}{3} + G \int_2^\infty dx x^3 (1 + H(x-2))(e^{-U_Y(x)/k_B T} - 1) + O(e^{-\kappa}). \end{aligned} \quad (3.35)$$

In both cases the integration on the right hand side should run from $x = 2$ to $x = 4$, so extending the integrals to ∞ only introduces errors of order $e^{-\kappa}$. In the

OBM, τ is determined by the condition that the first-order correction to the free energy vanishes

$$\int_2^\infty dx x^2 B(x) = -\frac{2\lambda}{3} + G \int_2^\infty dx x^2 (1 + H(x-2)) (e^{-U_Y(x)/k_B T} - 1) + O(e^{-\kappa}) = 0. \quad (3.36)$$

This expression is used to rewrite Eqs. (3.34) and (3.35)

$$\int_2^\infty dx x B(x) = -\frac{1}{2} G \int_2^\infty dx x (x-2) (1 + H(x-2)) (e^{-U_Y(x)/k_B T} - 1) + O(e^{-\kappa}), \quad (3.37)$$

$$\int_2^\infty dx x^3 B(x) = G \int_2^\infty dx x^2 (x-2) (1 + H(x-2)) (e^{-U_Y(x)/k_B T} - 1) + O(e^{-\kappa}) \quad (3.38)$$

which are readily approximated. We substitute $y = \exp[-\kappa(x/2 - 1)]$ which ultimately leads to

$$\int_2^\infty dx x B(x) = \frac{4G}{\kappa^2} J_1(\beta) + O(\kappa^{-3}) \quad (3.39)$$

and

$$\int_2^\infty dx x^3 B(x) = -\frac{16G}{\kappa^2} J_1(\beta) + O(\kappa^{-3}). \quad (3.40)$$

Here we have introduced

$$J_1(\beta) \equiv - \int_0^1 dy \frac{e^{\beta y} - 1}{y} \ln y. \quad (3.41)$$

An approximation for $J_1(\beta)$ that is accurate to within 1.4% in the relevant range $0 \leq \beta \leq 3.52$ is given by

$$J_1(\beta) \simeq \begin{cases} \beta + \frac{1}{8}\beta^2 & 0 \leq \beta < 0.8 \\ 2.81 (e^{0.34\beta} - 1) & 0.8 \leq \beta \leq 3.52 \end{cases}. \quad (3.42)$$

Finally, we insert Eqs. (3.39) and (3.40) into Eq. (3.30). We thus obtain an approximation for the second-order correction to the free energy

$$\Delta \simeq \frac{24G^2}{\kappa^4} \left(9G + 10GH - 18 + \frac{\lambda}{2} \right) J_1^2(\beta) \eta^2. \quad (3.43)$$

In Table 3.3 we present typical values of Δ . The corrections to the pressure are very small (compare with Figs. 3.1 on page 67 and 3.2 on page 68).

κ	$\tau=0.10$		$\tau=0.15$		$\tau=0.20$		$\tau=0.50$		$\tau=1.0$	
	β	Δ	β	Δ	β	Δ	β	Δ	β	Δ
5	1.966	-0.1315	1.725	-0.2129	1.548	-0.2762	1.017	-0.4291	0.694	-0.4209
7	2.447	-0.0637	2.099	-0.0944	1.853	-0.1154	1.140	-0.1467	0.727	-0.1211
9	2.805	-0.0352	2.397	-0.0505	2.110	-0.0603	1.282	-0.0715	0.803	-0.0549
11	3.088	-0.0214	2.644	-0.0303	2.332	-0.0360	1.423	-0.0416	0.891	-0.0312
13	3.321	-0.0139	2.855	-0.0197	2.526	-0.0233	1.558	-0.0268	0.981	-0.0200
15	3.519	-0.0096	3.038	-0.0135	2.697	-0.0160	1.686	-0.0186	1.070	-0.0139

Table 3.3: Estimates of the second-order correction Δ to the free energy for $\eta = 0.4$ at various τ and κ . Δ is determined from Eq. (3.43) within the approximation given by Eq. (3.42).

Fluid-crystal coexistence for proteins and inorganic nanocolloids: Dependence on ionic strength

Abstract We investigate theoretically the fluid-crystal coexistence of solutions of globular charged nanoparticles like proteins and inorganic colloids. The thermodynamic properties of the fluid phase are computed via the optimized Baxter model. This is done specifically for lysozyme and silicotungstates for which the bare adhesion parameters are evaluated via the experimental second virial coefficients. The electrostatic free energy of the crystal is approximated by supposing the cavities in the interstitial phase between the particles are spherical in form. In the salt-free case a Poisson-Boltzmann equation is solved to calculate the effective charge on a particle and a Donnan approximation is used to derive the chemical potential and osmotic pressure in the presence of salt. The coexistence data of lysozyme and silicotungstates are analyzed within this scheme, especially with regard to the ionic-strength dependence of the chemical potentials. The latter agree within the two phases provided some upward adjustment of the effective charge is allowed for.

4.1 Introduction

One current view of protein crystallization centers on the second virial coefficient B_2 being a relevant quantity determining the onset of crystallization [44, 45, 48, 90]. There exists a crystallization slot of negative B_2 values which expresses a necessary range of solution conditions for adequate crystals to grow. A negative value of B_2 implies a Baxter stickiness parameter as it is conventionally defined via B_2 only and we here denote by τ_0 . Thus, in a similar vein, there have been

attempts to correlate τ_0 with the solubility of nanoparticles in explaining fluid-crystal coexistence curves [22, 47].

The free energy of a suspension of particles cannot, of course, depend on B_2 alone. In Chapter 2 we introduced a new analytical theory for protein solutions in which the real fluid is replaced by a suspension of spheres with an appropriately chosen adhesion of the Baxter type. The stickiness parameter τ is computed by a variational principle for the free energy instead of via B_2 . In our optimized Baxter model, τ is not at all identical to τ_0 ; τ depends not only on the ionic strength but also on the protein concentration. In Ref. [47], Rosenbaum et al. plotted τ_0 logarithmically as a function of the nanoparticle concentration which effectively coarse-grains the experimental data they show. If we zoom in on their curve, there is a lot of fine detail which we here argue to be related to the fact, in part, that τ is a better similarity parameter. In particular, we seek to understand the ionic-strength dependence of the fluid-crystal coexistence curves by going beyond theory based solely on τ_0 .

In Chapter 3 we have tested the optimized Baxter model on a system of spheres interacting via an attractive Yukawa potential analyzed by computer simulations. The stickiness parameter τ , evaluated by optimizing the free energy, is indeed a useful similarity variable for gaining insight into the pressures and chemical potentials from simulations of the fluid phase. The magnitudes of these quantities are also well predicted by the optimized Baxter model. However, τ is not a correct similarity variable to describe fluid-crystal coexistence as we show in Section 4.6.1, in view of the fact that the weighting of configurations is different in the respective phases.

Here, we will not focus on the variable τ and the fluid phase but rather on the coexistence itself. The systems we study are assumed to have a short enough range so that the coexistence between two fluid phases is apparently circumvented. An a priori theory is problematic because we would need a quantitative theory of the crystal phase in terms of postulated attractive forces which are currently unknown. Theoretical efforts exist in the literature [49, 50, 91] at the expense of introducing unknown parameters which we want to avoid here. We do not present conventional phase diagrams because we do not know the right thermodynamic variable to plot to get a universal diagram of states. The variable τ itself is not useful as we show in Section 4.6.1.

In practice, it may be very difficult to achieve ideal thermodynamic equilibrium between the liquid phase and some crystalline state. Equilibrium may not have been reached, the crystal could be heterogeneous and the formation of aggregates could complicate the attainment of equilibrium (see, for instance, the discussion by Cacioppo and Pusey on lysozyme [92]). Nevertheless, it may still be useful to assume equilibrium is ideally attained provided our goal is sufficiently modest. The balance of chemical potentials has been used before to acquire information about the crystal from the solubility in the fluid phase [90]. Our concern here will be to try to gain insight into the ionic-strength dependence of the thermodynamic properties of the crystal. We may argue that this dependence could

be approximated by a Donnan equilibrium so it would not be very sensitive to the precise crystal habit adopted. We therefore compute the protein chemical potential and osmotic pressure of the coexisting liquid phase at the experimentally determined solubility with the help of the optimized Baxter model. We then investigate whether their dependence on the electrolyte concentration agrees with that predicted by a simple crystal model. The theory is applied to a protein (lysozyme) and an inorganic nanocolloid (silicotungstate (STA)).

4.2 Optimized Baxter model

We first discuss how we obtain the bare adhesion parameters via the second virial coefficient, and then summarize the optimized Baxter model (see Chapter 2), which is an appropriate liquid state theory provided we use the right stickiness parameter τ as emphasized in the Introduction. We consider a system of charged nanometer-sized particles (e.g. proteins or nanocolloids) in water with added monovalent salt of ionic strength I . We suppose the particles are spherical with radius a . The charge is distributed uniformly on the particle's surface. For convenience, all distances in this section will be scaled by the radius a and all energies by $k_B T$, where k_B is Boltzmann's constant and T is the temperature. Because monovalent ions (counterions and salt ions) are present in solution, the Coulomb repulsion between the particles will be screened and it is here given by a far-field Debye-Hückel potential. The effective number Z_{eff} of charges on the sphere (taken to be positive) will here be computed in the Poisson-Boltzmann approximation. We let the attraction between two particles be of range much shorter than their radius, and we model it by a potential well of depth U_A and width $\delta \ll 1$. Actually, the attractive interactions are, of course, much more complicated than this simple form. Dispersion forces, in particular, have been reinvestigated for small particles recently [93, 94] although the continuum approximation certainly becomes rather poor at the nanolevel dealt with here. Also, arbitrary cut-offs need to be introduced (see Chapter 2); it turns out that a simple well is quite adequate to describe the experimental data on B_2 (see Section 4.3 below). The total interaction $U_T(x)$ between two particles whose centers of mass are separated by an actual distance r is thus of the form

$$U_T(x) = \begin{cases} \infty & 0 \leq x < 2 \\ U_{DH}(x) - U_A & 2 \leq x < 2 + \delta \\ U_{DH}(x) & x \geq 2 + \delta \end{cases}, \quad (4.1)$$

$$x \equiv \frac{r}{a},$$

with Debye-Hückel interaction

$$U_{DH}(x) = 2\xi \frac{e^{-\omega(x-2)}}{x}. \quad (4.2)$$

Here, $\xi \equiv \frac{Q}{2a} \left(\frac{Z_{eff}}{1+\omega} \right)^2$ and $\omega \equiv \kappa a$, which are given in terms of the Debye length κ^{-1} defined by $\kappa^2 = 8\pi QI$ and the Bjerrum length $Q = q^2/\epsilon k_B T$, which equals 0.71 nm in water at 298 K (ϵ is the permittivity of water, q is the elementary charge); $\omega = 3.28a\sqrt{I}$, if the radius a is given in nm and the ionic strength I in M. We suppose 1-1 electrolyte has been added in excess so I is the concentration of added salt. We have derived the effective charge qZ_{eff} in the Poisson-Boltzmann approximation (see Chapter 2)

$$Z_{eff} = Z - \frac{\omega^2}{6} \left(\frac{Q}{a} \right)^2 \left(\frac{Z}{1+\omega} \right)^3 e^{3\omega} E_1(3\omega). \quad (4.3)$$

Here $E_1(x)$ is the exponential integral defined by $E_1(x) = \int_x^\infty dt t^{-1} e^{-t}$ and qZ is the actual charge per particle. Eq. (4.3) is numerically consistent with a different form recently proposed by Aubouy et al. [95] which is also valid at large values of Z .

We suppose that the bare charge on the particles as a function of the ionic strength is known from experiment, so the only unknown parameters are U_A and δ which are chosen to be independent of I . The latter are determined by fitting preferably complete experimental data of the second virial coefficient B_2 as a function of the ionic strength I at constant pH to B_2 computed numerically with the help of the expression

$$B_2 = 2\pi a^3 \int_0^\infty dx x^2 \left(1 - e^{-U_T(x)} \right) \quad (4.4)$$

using Eq. (4.1). We have previously done this for a wide variety of B_2 data on lysozyme at two values of the pH (4.5 and 7.5) and we were able to obtain very good fits (see Chapter 2) (see e.g. Fig. 4.1 on page 85 which is discussed in Section 4.3.2).

It is important to stress that though there are two adjustable parameters δ and U_A , the actual fit in practice depends almost solely on adjusting the single combination $\delta \exp U_A$. This is because a convenient analytical approximation of the second virial turns out to have the form (see Chapter 2)

$$\frac{B_2}{B_2^{HS}} \simeq 1 + \frac{3\xi}{2\omega} - \frac{3}{2} e^{-\xi} \delta e^{U_A} \quad (4.5)$$

and is able to describe the experimental data on lysozyme quite well with an appropriate value of $\delta \exp U_A$. Here, B_2^{HS} is the second virial coefficient pertaining to hard spheres. The strong correlation of adjustable parameters is not unusual for it is well known in the theory of gases when one attempts to fit the temperature dependence of the second virial coefficient in terms of a Lennard-Jones interaction, for instance [96]. We note that Eq. (4.5) disagrees starkly with an approximation put forward earlier [97], both with regard to the pure electrostatic and the adhesive contributions. In particular, the third i.e. adhesion term in Eq. (4.5) is not at

all independent of the ionic strength but rather diminishes fast as the electrolyte concentration is lowered. Furthermore, the pure electrostatic term cannot be derived from a Donnan equilibrium as we point out in Section 4.4.

At high salt concentrations, the parameter ξ becomes small owing to screening so B_2 becomes lower than the hard sphere value as can be seen from Eq. (4.5). Nevertheless, the electrostatic repulsion still exerts itself, so an effective adhesion parameter we may wish to introduce would be smaller than the bare value. We therefore adopt a similar strategy to the liquid state at finite concentrations by first introducing a suitable reference state amenable to analytical computation (see Chapter 2). This is a solution of hard spheres whose radius is still a but with a Baxter adhesion potential whose strength is defined by a suitable stickiness parameter τ . The statistical properties of this suspension as a function of the volume fraction of spheres η ($= 4\pi a^3/3$ times number density) may be solved in the Percus-Yevick approximation [27]. The parameter τ is adjustable and is computed via a variational principle for the free energy. The latter may be written as a functional expansion in terms of the so-called blip function which is the difference in Mayer functions of the respective interactions (Eq. (4.1) and the Baxter interaction) (see Chapter 2 and Ref. [62]). We set the first-order deviation from the free energy pertaining to the reference state equal to zero. This determines τ which depends not only on the well parameters δ and U_A and electrostatic variables ω and ξ but also on the volume fraction of nanospheres. It is given by (see Chapter 2)

$$\frac{1}{\tau} = 3\epsilon \left[\left(e^{U_A} e^{-\frac{\xi}{1+\epsilon/2}} e^{-\omega\epsilon} - 1 \right) (1 + (1+H)\epsilon) + \left(e^{U_A} e^{-\xi} - 1 \right) \right], \quad (4.6)$$

where

$$\epsilon = \delta - K^{-1} [(1 + \delta H)P_1 + HP_2], \quad (4.7)$$

$$P_1 = \frac{8}{\omega^2} (1 + \omega\delta)M + \frac{16}{\omega} \left(\frac{M}{1+M} \right), \quad (4.8)$$

$$P_2 = \frac{8}{\omega^3} (2 + \omega\delta)M + \frac{16}{\omega^2} \ln(1+M), \quad (4.9)$$

$$M \equiv \xi e^{-\omega\delta}/4, \quad (4.10)$$

$$K = 2 \left(e^{U_A} e^{-\frac{\xi}{1+\delta/2}} e^{-\omega\delta} - 1 \right) (1 + (1+H)\delta) + 2 \left(e^{U_A} e^{-\frac{\xi}{1+\epsilon/2}} e^{-\omega\epsilon} - 1 \right) (1 + (1+H)\epsilon), \quad (4.11)$$

$$H = \frac{\eta}{2\tau(1-\eta)} \left(\frac{\eta(1-\eta)}{12} \lambda^2 - \frac{1+11\eta}{12} \lambda + \frac{1+5\eta}{1-\eta} - \frac{9(1+\eta)}{2(1-\eta)^2} \frac{1}{\lambda} \right) \quad (4.12)$$

and λ is given by

$$\tau = \frac{1+\eta/2}{(1-\eta)^2} \frac{1}{\lambda} - \frac{\eta}{1-\eta} + \frac{\eta}{12} \lambda. \quad (4.13)$$

Note that τ is readily obtained by iteration. One starts with initial values for τ and ϵ and then calculates λ , H and K from Eqs. (4.11)–(4.13). Then, a new value of ϵ at fixed H is computed iteratively with the help of Eqs. (4.7) and (4.11). Next, a new value of τ is given by Eq. (4.6) and then the cycle is repeated until the variables become stationary.

Having obtained the effective adhesion parameter τ , we simply calculate thermodynamic properties of the reference state within the Percus-Yevick approximation. The free energy of the actual system does deviate slightly from that of the reference state but we have shown that the deviations are very small (see Chapter 2). To compute the osmotic pressure and chemical potential we use the result from the compressibility route [27] (Eqs. (1.49) and (1.51)) which appears to be more in line with simulations [30], see Figs. 1.5 on page 25 and 1.6 on page 27.

4.3 Solubility curves: chemical potential of the fluid phases

4.3.1 Method

Since we suppose the crystal is in thermodynamic equilibrium with the fluid, the nanoparticle chemical potentials as well as the osmotic pressures in both phases are uniform. The chemical potential of the counter and co-ions must also be uniform but we will address this issue later within a Donnan equilibrium. Solubility data from experiment represent the particle concentration in the fluid phase as a function of the pH and the salt concentration. Thus we compute the chemical potential and the osmotic pressure of the solution with the help of the optimized Baxter model of the previous section. We have done this in two cases of nanoparticles where we have sufficient experimental data on the second virial coefficient to evaluate the well parameters U_A and δ with sufficient accuracy.

4.3.2 Lysozyme

The protein hen-egg-white lysozyme has been well characterized in aqueous solutions of simple electrolytes. We here choose the effective radius a such that the volume of the model sphere is equal to the volume of a lysozyme molecule in the tetragonal crystal state. The latter is determined from the water content of the tetragonal crystal (0.335 mass fraction [98]), the crystal volume per protein molecule (29.6 nm^3 , based on the dimensions $7.91 \times 7.91 \times 3.79 \text{ nm}^3$ of the unit cell containing 8 protein molecules [99]), the density of the crystal ($1.242 \cdot 10^3 \text{ kg m}^{-3}$ [98]) and the density of water ($0.998 \cdot 10^3 \text{ kg m}^{-3}$). Thus we have $a = 1.6 \text{ nm}$ and note that this is 0.1 nm less than the value of 1.7 nm we used previously in Chapter 2, which was based on approximating the protein by an ellipsoid of dimensions $4.5 \times 3.0 \times 3.0 \text{ nm}^3$ [100]. For the sake of consistency we here use the single value $a = 1.6 \text{ nm}$ in computations pertaining to both phases.

The experimental data for the second virial coefficient of lysozyme have been discussed by us at length in Chapter 2 and are presented in Fig. 4.1.

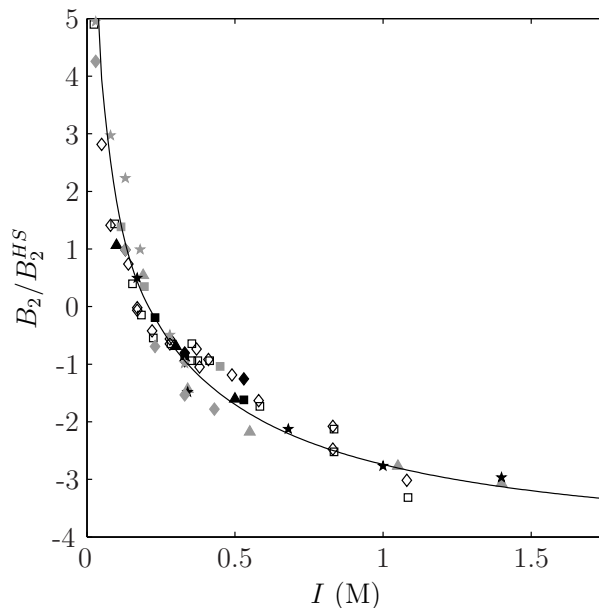


Figure 4.1: *The second virial coefficient of lysozyme as a function of the ionic strength. The second virial coefficient is scaled by the hard sphere value B_2^{HS} . The data are taken from a variety of experiments; see Chapter 2 for more details. The added salt is NaCl. The solid line is a fit to the data with $U_A = 2.90$ and $\delta = 0.183$.*

For details on determining the parameters U_A and δ of the attractive potential we also refer to Chapter 2. Since we are using a smaller effective radius here, we deduce the values $U_A = 2.90$ and $\delta = 0.183$ which are somewhat different from those derived earlier in Chapter 2. The values of the bare charge qZ of a lysozyme molecule as a function of the ionic strength are the same as those used in Chapter 2 i.e. they are determined by interpolation from hydrogen-ion titration data in KCl [60]. We assume that KCl and NaCl (see below) behave identically in an electrostatic sense. The effective charge does differ slightly because it is a function of a (see Eq. (4.3)). We again use the lowered effective charge $\bar{Z} = Z_{eff} - 1$ instead of the effective charge Z_{eff} in order to fit B_2 accurately at lower ionic strengths when it is dominated by electrostatics. We set U_A and δ to be independent of the pH.

Accurate data on the solubility S as a function of the NaCl concentration have been obtained by Cacioppo and Pusey [92] using column beds of tetragonal microcrystallites of lysozyme in a range of pH and temperatures. We here employ their data at 298 K and at three representative values of the pH. (See Table 4.1.)

The ionic strength I in M is determined from the ionic strength in %w/v by the

pH	I (%w/v)	I (M)	ω	Z	Z_{eff}	\bar{Z}	ξ	τ	S (g/l)	η	$(\mu - \mu_0)/k_B T$	$\Pi v_0/k_B T$
2.0	0.40	3.33	11.1	10.54	9.54	1.078	0.127	48.7	0.0354	-3.60	0.0308	
	0.57	3.97	11.2	10.74	9.74	0.851	0.096	14.0	0.0102	-4.72	0.0095	
	0.74	4.53	11.4	10.99	9.99	0.725	0.083	4.30	0.00313	-5.82	0.0030	
4.0	0.92	5.02	11.6	11.23	10.23	0.641	0.077	3.11	0.00226	-6.13	0.0022	
	1.26	5.89	11.7	11.40	10.40	0.506	0.068	1.36	0.00099	-6.94	0.0010	
4.5	0.40	3.33	10.2	9.76	8.76	0.909	0.107	30.1	0.0219	-4.05	0.0194	
	0.57	3.97	10.3	9.94	8.94	0.717	0.086	10.3	0.00750	-5.01	0.0071	
	0.74	4.53	10.3	10.00	9.00	0.588	0.075	5.22	0.00380	-5.64	0.0037	
5.0	0.92	5.02	10.4	10.13	9.13	0.510	0.070	3.43	0.00250	-6.04	0.0024	
	1.26	5.89	10.4	10.19	9.19	0.395	0.063	1.87	0.00136	-6.63	0.0013	
7.0	0.40	3.33	9.1	8.79	7.79	0.719	0.090	17.6	0.0128	-4.54	0.0117	
	0.57	3.97	9.1	8.85	7.85	0.553	0.075	7.38	0.00537	-5.33	0.0051	
	0.74	4.53	9.2	8.99	7.99	0.464	0.069	4.72	0.00344	-5.75	0.0033	
5.0	0.92	5.02	9.2	9.02	8.02	0.394	0.064	3.63	0.00264	-6.00	0.0026	
	1.26	5.89	9.1	8.96	7.96	0.297	0.059	2.46	0.00179	-6.37	0.0018	

Table 4.1: The change Z of hen-egg-white lysozyme (from Ref. [60]), the effective charge Z_{eff} (from Eq. (4.3)), the lowered effective charge $\bar{Z} = Z_{eff} - 1$, the dimensionless interaction parameters ω , ξ and τ , the solubility of lysozyme S , the volume fraction η , the dimensionless chemical potential $(\mu - \mu_0)/k_B T$ and the dimensionless pressure $\Pi v_0/k_B T$ as a function of the ionic strength I in the fluid phase. ξ has been calculated using the lowered effective charge \bar{Z} .

relation $I(M) = 0.06 + 0.171 I(\%w/v)$. Here, the value 0.06 accounts for the effective ionic strength of the 0.1 M sodium acetate buffer used and $0.171 = 10/M_{NaCl}$ where $M_{NaCl} = 58.44 \text{ g mol}^{-1}$ is the molar mass of NaCl. The dimensionless parameter ω is then given by $\omega = 5.25\sqrt{I}$, where I is given in M, and $\xi = 0.222(\bar{Z}/(1 + \omega))^2$.

The volume fraction η of protein in the liquid phase is given by $\eta = SN_A v_0/M$, where N_A is Avogadro's number, $v_0 = 4\pi a^3/3$ is the volume of a lysozyme molecule and $M = 14.3 \cdot 10^3 \text{ g mol}^{-1}$ [101] is the molar mass of lysozyme. The parameter τ describing the effective adhesion is determined as described in Section 4.2 (see Eqs. (4.6)–(4.13)), using the values $U_A = 2.90$ and $\delta = 0.183$. Then, the dimensionless chemical potential $(\mu - \mu_0)/k_B T$ and the dimensionless osmotic pressure $\Pi v_0/k_B T$ are determined from Eqs. (1.51) and (1.49) respectively. (See Table 4.1). Fig. 4.2 shows the chemical potential as a function of the ionic strength I at three different values of the pH.

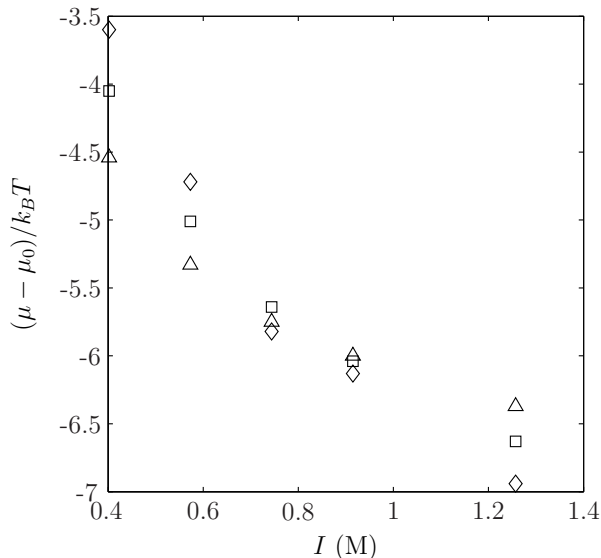


Figure 4.2: The dimensionless chemical potential of lysozyme in the fluid phase as a function of the ionic strength at pH 4.0 (diamonds), pH 4.5 (squares) and pH 5.4 (triangles). See also Table 4.1.

Fig. 4.3 shows the osmotic pressure under the same conditions.

4.3.3 Silicotungstates (STA)

The next system we consider is silicotungstate (STA) in water with three different kinds of added salt: NaCl, HCl and LiCl. STA molecules are spherical, more or

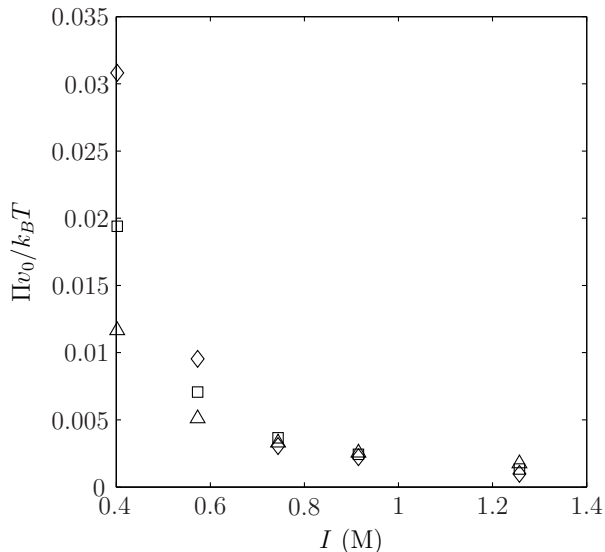


Figure 4.3: The dimensionless pressure of lysozyme in the fluid phase as a function of the ionic strength at pH 4.0 (diamonds), pH 4.5 (squares) and pH 5.4 (triangles). See also Table 4.1.

less, (see Fig. 2 in Ref. [102]) with an effective diameter of 1.1 nm [103, 104], so we set $a = 0.55$ nm. The structural formula for the polyanion $\text{SiW}_{12}\text{O}_{40}^{4-}$ implies a molar mass $M_{STA} = 2874.3 \text{ g mol}^{-1}$. We assume that the pH is low enough for the molecule to be fully dissociated, i.e. $Z = 4$.

We determine the well parameters U_A and δ for the attractive interaction by fitting experimental data of the second virial coefficient in the same way as was done for lysozyme in Chapter 2, except we now do not adjust Z_{eff} . The second virial coefficients for Li_4STA , H_4STA and Na_4STA are taken from Ref. [105] and plotted in Fig. 4.4.

In each case, the added salt is XCl , where X represents the counterion of the crystal. The values of the dimensionless parameters $\omega = 1.80\sqrt{I}$, $\xi = 0.645(Z_{eff}/(1 + \omega))^2$, Z and Z_{eff} pertaining to the data in Fig. 4.4 are given in Table 4.2.

We have set $\delta = 0.05$. A least-squares fit to the data represented in Fig. 4.4 then gives $U_A = 3.30$. In fact, there is a range of combinations of δ and U_A that yield almost the identical curve as long as $\delta \exp U_A \simeq 1.36$ and $\delta \ll 1$, so our choice of $\delta = 0.05$ is a bit arbitrary. This similarity with respect to the sole parameter $\delta \exp U_A$ is in accord with our approximation for B_2 give by Eq. (4.5).

The solubilities for Li_4STA , H_4STA and Na_4STA have been measured by Zukoski et al. [105], where the same electrolytes are used as in the measurements

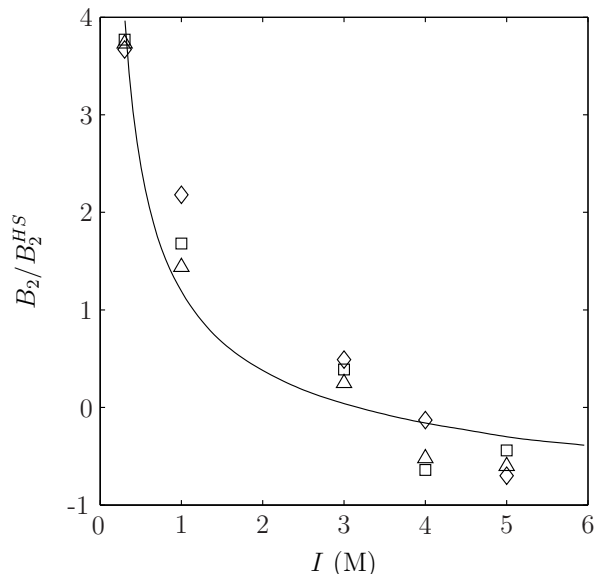


Figure 4.4: The second virial coefficient of STA as a function of the ionic strength. The second virial coefficient is scaled by the hard sphere value B_2^{HS} . The experimental data are taken from Zukoski et al. [105]. The added salt is LiCl (diamonds), HCl (squares) and NaCl (triangles) respectively and in all cases the counterion of STA is the same as that of the salt. The solid line is a fit to the experimental data with $U_A = 3.30$ and $\delta = 0.05$.

I (M)	ω	Z	Z_{eff}	ξ
0.3	0.99	4.0	3.42	1.905
1.0	1.80	4.0	3.58	1.054
3.0	3.13	4.0	3.76	0.536
4.0	3.61	4.0	3.80	0.439
5.0	4.03	4.0	3.83	0.373

Table 4.2: Values of the bare charge Z of STA, the effective charge Z_{eff} (from Eq. (4.3)) and the dimensionless interaction parameters $\omega = 1.80\sqrt{I}$ and $\xi = 0.645(Z_{eff}/(1+\omega))^2$ as a function of the ionic strength I . These entries apply to the data plotted in Fig. 4.4.

of B_2 . (See Table 4.3.)

The volume fraction η of STA is given by $\eta = SN_{A}v_0/M_{X_4STA}$, where S is the solubility of STA (note that here it is given in g/ml, whereas for lysozyme it

X	I (M)	ω	Z	Z_{eff}	ξ	τ	S (g/ml)	η	$(\mu - \mu_0)/k_B T$	$\Pi_{v0}/k_B T$
H	1.0	1.80	4.0	3.58	1.054	0.786	1.94	0.284	1.30	0.706
	2.0	2.55	4.0	3.70	0.700	0.358	1.67	0.243	-0.48	0.375
	3.0	3.13	4.0	3.76	0.536	0.255	1.36	0.198	-1.40	0.226
	4.0	3.61	4.0	3.80	0.439	0.215	1.11	0.162	-1.91	0.158
	5.0	4.03	4.0	3.83	0.373	0.193	0.57	0.0830	-2.65	0.077
	1.0	1.80	4.0	3.58	1.054	0.668	2.15	0.312	1.55	0.811
Li	2.0	2.55	4.0	3.70	0.700	0.352	1.85	0.267	-0.26	0.433
	3.0	3.13	4.0	3.76	0.536	0.255	1.36	0.197	-1.41	0.224
	4.0	3.61	4.0	3.80	0.439	0.215	0.81	0.118	-2.23	0.114
	5.0	4.03	4.0	3.83	0.373	0.193	0.32	0.0469	-3.16	0.045
	1.0	1.80	4.0	3.58	1.054	0.906	1.85	0.262	1.07	0.625
	2.0	2.55	4.0	3.70	0.700	0.359	1.67	0.236	-0.54	0.358
Na	3.0	3.13	4.0	3.76	0.536	0.255	1.36	0.192	-1.44	0.218
	4.0	3.61	4.0	3.80	0.439	0.215	0.74	0.104	-2.35	0.100
	5.0	4.03	4.0	3.83	0.373	0.193	0.46	0.0657	-2.86	0.062

Table 4.3: The charge Z of STA, the effective charge Z_{eff} (from Eq. (4.3)), the dimensionless interaction parameters ω , ξ and τ , the solubility S of X_3STA , the volume fraction η , the dimensionless chemical potential $(\mu - \mu_0)/k_B T$ and the dimensionless pressure $\Pi_{v0}/k_B T$ as a function of the ionic strength I in the fluid phase. Here the counterion is X^+ and the added salt is XCl . ξ has been calculated using the effective charge Z_{eff} .

was given in g/l), $v_0 = 4\pi a^3/3$ is the volume of an STA molecule and M_{X_4STA} is the molar mass, where X again represents the counterion in the respective cases. We have $M_{H_4STA} = 2878.3 \text{ g mol}^{-1}$, $M_{Li_4STA} = 2902.0 \text{ g mol}^{-1}$ and $M_{Na_4STA} = 2966.2 \text{ g mol}^{-1}$. The stickiness parameter τ is determined by the method described in Section 4.2 (see Eqs. (4.6)–(4.13)), using the values $U_A = 3.30$ and $\delta = 0.05$. The chemical potential and the osmotic pressure are again determined from Eqs. (1.51) and (1.49) respectively. (See Table 4.3). We display these thermodynamic variables as a function of the ionic strength in Figs. 4.5 and 4.6.

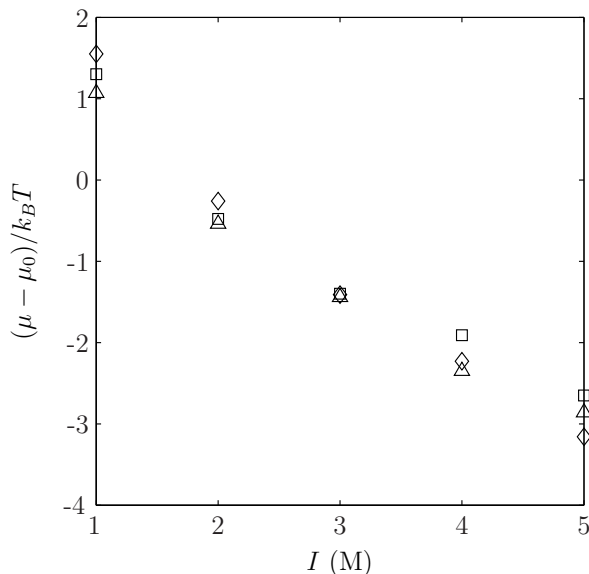


Figure 4.5: The dimensionless chemical potential of STA in the fluid phase as a function of the ionic strength. The added salt is LiCl (diamonds), HCl (squares) and NaCl (triangles) respectively and in all cases the counterion of STA is the same as that of the salt. See also Table 4.3.

4.4 Crystal model: Donnan effect

Having computed the thermodynamic properties of the fluid phases of lysozyme and STA, and hence those of the respective crystal phases under the assumption of equilibrium of the two phases, we now attempt to gain insight into them by introducing a simple model for the crystal. In the latter the spherical particles either touch or are very close. There are thus minute “surfaces of interaction” where the forces between two nearby spheres are predominantly attractive. It is therefore reasonable to write the thermodynamic potential Ω of a crystal of N spheres in

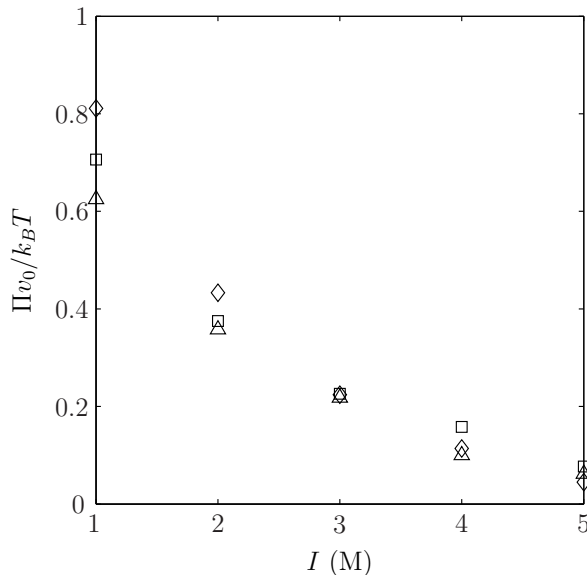


Figure 4.6: The dimensionless pressure of STA in the fluid phase as a function of the ionic strength. The added salt is LiCl (diamonds), HCl (squares) and NaCl (triangles) respectively and in all cases the counterion of STA is the same as that of the salt. See also Table 4.3.

a volume V as a superposition of attractive and electrostatic contributions to a first approximation

$$\Omega = \frac{1}{2} k(c) \frac{(V - V_0)^2}{V_0} + N f_{el}(c, I_c) + \Pi(S, I)V - \mu(S, I)N. \quad (4.14)$$

The crystal is immersed in a large reservoir at a constant osmotic pressure Π and chemical potential μ containing a saturated solution of nanospheres at a solubility S and ionic strength I (Π and μ are given by Eqs. (1.49) and (1.51) respectively). The crystal has elastic properties denoted by the modulus k which depends on the density $c = N/V$ and the crystal would have a volume V_0 in the absence of electrostatic forces ($|V - V_0| \ll V_0$). Actually, the form of the elastic energy is more complicated and depends on the precise crystal habit [106] but the simple harmonic form in Eq. (4.14) suffices for our purposes. There is a Donnan equilibrium (see below) which leads to a salt concentration I_c within the interstitial region in the crystal. We adopt a continuum approximation: the electrostatic free energy $N f_{el}$ is computed for a lattice of charged spheres embedded in a solvent of uniform permittivity ϵ and electrolyte concentration I_c .

At equilibrium, Ω must be minimized ($\partial\Omega/\partial V = 0$; $\partial\Omega/\partial N = 0$) so that

$$\Pi \simeq \Pi_{el} - k \left(\frac{V - V_0}{V_0} \right) + \frac{1}{2} c \frac{dk}{dc} \left(\frac{V - V_0}{V_0} \right)^2, \quad (4.15)$$

$$\mu \simeq \mu_{el} + \frac{1}{2} \frac{dk}{dc} \left(\frac{V - V_0}{V_0} \right)^2. \quad (4.16)$$

We have introduced the electrostatic counterparts of the osmotic pressure and the chemical potential of a charged sphere in the crystal phase on the right hand sides of Eqs. (4.15) and (4.16). In Eq. (4.15) the elastic term proportional to k may easily be of order Π_{el} but the quadratic form is negligible. In view of the fact that $\Pi_{el} = O(c\mu_{el})$, we then have $\mu \simeq \mu_{el}$ to a good approximation from Eq. (4.16). In effect, as we change the ionic strength of the fluid phase, the solubility S and the salt concentration I_c within the crystal readjust themselves whereas the volume V remains virtually constant. The chemical potential is modified only by virtue of the change in electrostatic shielding about a sphere in the lattice. But a substantial hydrostatic pressure may be exerted within the crystal as we decrease its volume a bit.

Next, we compute the electrostatic properties of the crystal. The colligative properties of salt-free polyelectrolytes are often addressed in terms of a cell model in which a test cylinder is surrounded by a boundary of similar symmetry on which the electric field vanishes [107]. The boundary effectively replaces the effect of the surrounding particles on the test particle. This picture is reasonable at low volume fractions but must break down at high concentrations when the electric field is highly heterogeneous. In the latter case, one of us has advocated focusing on the voidlike regions instead of on a test particle (see Ref. [108] which deals with a hexagonal lattice of DNA at very high concentrations). Thus, in a crystal of spheres we may distinguish very small regions between particles that almost touch which we view as thin boundary layers, and larger voids which we will simply approximate by spheres. (We are here concerned with spheres of high charge density which leads to counterions being “condensed”. At low charge densities, it is possible to give a more general analysis; see Section 4.6.2). Discrete charge effects should prevail when evaluating the electrostatics of the boundary layers. These energies are here assumed to be independent of the ionic strength since the relevant scales in the boundary layers are very small in crystals of nanoparticles.

We therefore first solve the Poisson-Boltzmann equation for a charged void or spherical cavity of radius b without salt and then discuss the effect of monovalent salt via a Donnan equilibrium. The charge density on the surface of the cavity is uniform and the total number of charges is Z . In view of electroneutrality there are Z counterions in the cavity, each bearing charge $-q$. Within a mean-field analysis, the counterion density $\rho(r)$ inside the cavity is given by a Boltzmann distribution in terms of the electrostatic potential $\Psi(r)$ at a distance r from its center

$$\rho(r) = \bar{\rho} e^{q\Psi/k_B T}. \quad (4.17)$$

We choose $\Psi = 0$ at the center of the cavity so that $\bar{\rho}$ is the actual charge density there. The charge density $-q\rho$ is also related to Ψ by Poisson's equation

$$\Delta\Psi = \frac{4\pi q\rho}{\epsilon} \quad (4.18)$$

leading to the Poisson-Boltzmann equation [107] which we conveniently express in the scaled form

$$\psi''(x) + \frac{2}{x}\psi'(x) = e^\psi. \quad (4.19)$$

Here, we have defined $\lambda^{-2} \equiv 4\pi Q\bar{\rho}$, $x \equiv r/\lambda$ and $\psi \equiv q\Psi/k_B T$ where λ may be interpreted as a screening length. The two additional boundary conditions are

$$\psi'(0) = 0 \quad (4.20)$$

owing to symmetry, and

$$\frac{b}{\lambda}\psi'\left(\frac{b}{\lambda}\right) = \Lambda \equiv \frac{QZ}{b} \quad (4.21)$$

signifying the relation between the electric field and the charge density at the surface of the cavity.

For small x , Eq. (4.19) admits a series expansion $\psi(x) = Ax^2 + Bx^4 + \dots$ with $A = 1/6$ and $B = O(1)$ independent of the value of the dimensionless variable Λ . As Λ tends to zero, Eq. (4.21) reduces to the condition of electroneutrality. Electrostatic screening vanishes in this limit and there are no counterions "condensed" on the surface of the sphere. It is straightforward to solve Eq. (4.19) numerically starting with $\psi(x) \rightarrow \frac{1}{6}x^2$ as $x \rightarrow 0$. We have fitted the solution to the convenient approximation

$$\psi(x) \simeq -2 \ln \left(1 - \frac{x^2}{12} - \frac{x^4}{1440} - \frac{x^6}{45330.3} \right), \quad (4.22)$$

which is accurate to within 0.6% for $0 \leq x \leq 3.273687$ ($\psi(x)$ diverges at $x \simeq 3.27368734$). This leads to an effective charge given by

$$Z_{eff} \equiv \frac{4\pi b^3 \bar{\rho}}{3} = \frac{Z}{3\Lambda} \left(\frac{b}{\lambda} \right)^2. \quad (4.23)$$

This is always less than the actual charge Z which one may interpret as a certain fraction of counterions being associated near the surface if $\Lambda > 0$. The effective charge Z_{eff} tends to Z as $\Lambda \rightarrow 0$ (for a general analysis of this limit, see Section 4.6.2).

We now wish to analyze the thermodynamic properties of the crystal in the presence of simple salt which we do within a Donnan approximation. At this stage it is well to recall the incorrectness of applying Donnan arguments to a fluid of charged colloidal particles. The probability of the double layers of two particles

interpenetrating is very small owing to Boltzmann weighting. Hence, only the Debye-Hückel tails in their interaction are important which represent effectively the potential of mean force between the particles. In the case of excess salt, we then use the McMillan-Mayer theory to calculate the statistical mechanical properties of the fluid as has been done in Section 4.2 (see Eq. (4.2); this line of argumentation goes back to Stigter [109]). The situation is decidedly different when the particles are positionally ordered as in a crystal. The double layers are forced to overlap in that case. A usual (Donnan) approximation is then to suppose those points at zero electric field are in equilibrium with the reservoir [107]. For the cavities in the crystal, this yields

$$I_c(\bar{\rho} + I_c) = I^2 \quad (4.24)$$

in view of the equality of the chemical potentials of the small ions in the respective phases. The osmotic pressure is given by the additivity rule as argued by Oosawa for polyions within conventional cell models [107]

$$\Pi = (\bar{\rho} + 2I_c - 2I)k_B T = \bar{\rho} k_B T \left[\sqrt{1 + w^2} - w \right], \quad (4.25)$$

$$w \equiv \frac{2I}{\bar{\rho}}.$$

The ions have been considered as ideal and the electrostatic stress is zero in Eq. (4.15). The chemical potential of the charged cavity, accurate to the same level of approximation, is readily computed from Eq. (4.25) (this is analogous to similar calculations for cell models of long charged rods [110])

$$\mu = \mu_{ref} + \frac{Z_{eff} k_B T}{2} \ln \left[\frac{\sqrt{1 + w^2} + 1}{\sqrt{1 + w^2} - 1} \right] \quad (4.26)$$

where μ_{ref} is a reference chemical potential independent of the concentration of salt, and not identical with μ_0 of Section 4.2. Because the number of particles in the crystal is equal to the number of cavities, Eq. (4.26) also represents the chemical potential of a charged sphere carrying Z charges but with a different μ_{ref} .

4.4.1 Comparison with experiment

4.4.1.1 Lysozyme crystal

The volume per lysozyme molecule in the tetragonal crystal is 29.6 nm^3 (see Section 4.3.2). The radius of the effective sphere is 1.60 nm so the volume of a cavity is 12.4 nm^3 and $b = 1.43 \text{ nm}$. In Table 4.4, we show values of Z as a function of the ionic strength I at three values of the pH.

From these we calculate the dimensionless quantities Λ , b/λ and Z_{eff} via the Poisson-Boltzmann equation. Then the pressure and the chemical potential are

pH	I (M)	Z	Λ	b/λ	Z_{eff}	w	$\mu/k_B T$	$\Pi v_0/k_B T$
4.0	0.40	11.1	5.51	2.52	4.27	1.41	2.83	1.92
	0.57	11.2	5.56	2.53	4.29	2.00	2.07	1.43
	0.74	11.4	5.66	2.54	4.32	2.57	1.64	1.14
	0.92	11.6	5.76	2.55	4.35	3.14	1.36	0.95
	1.26	11.7	5.81	2.55	4.37	4.30	1.01	0.71
4.5	0.40	10.2	5.06	2.48	4.13	1.45	2.66	1.81
	0.57	10.3	5.11	2.49	4.15	2.06	1.94	1.34
	0.74	10.3	5.11	2.49	4.15	2.68	1.52	1.06
	0.92	10.4	5.16	2.49	4.17	3.28	1.25	0.88
	1.26	10.4	5.16	2.49	4.17	4.51	0.92	0.64
5.4	0.40	9.1	4.52	2.42	3.94	1.53	2.42	1.66
	0.57	9.1	4.52	2.42	3.94	2.18	1.75	1.21
	0.74	9.2	4.57	2.43	3.95	2.81	1.38	0.96
	0.92	9.2	4.57	2.43	3.95	3.46	1.13	0.79
	1.26	9.1	4.52	2.42	3.94	4.77	0.82	0.58

Table 4.4: *The ionic strength I , the actual number of charges Z , the effective number Z_{eff} , the chemical potential μ and the osmotic pressure Π for a lysozyme crystal (the reference chemical potential has been set equal to zero).*

evaluated using Eqs. (4.25) and (4.26). (See Table 4.4). The curves in Fig. 4.7 represent the chemical potential computed in this manner together with the predictions from the theory of the liquid state as displayed in Fig. 4.2 on page 87.

The former have been shifted by an amount which is unknown in the present theory.

4.4.1.2 STA crystals

In order to compute the chemical potential we first need to discuss the crystal habits of STA. It is known that H_4STA is fully dissociated for a pH larger than 5 [111]. Zukoski et al. [47, 105, 112] fail to mention the pH at which their measurements were performed, though they did deduce that all forms of STA are dissociated in their experiments judging from the conductivities of their solutions.

4.4.1.3 $H_4STA \cdot 31H_2O$

This crystallizes at room temperature [113] in the tetragonal form (long axis = 1.856 nm, short axes = 1.301 nm [114]; there are 2 STA molecules per unit cell

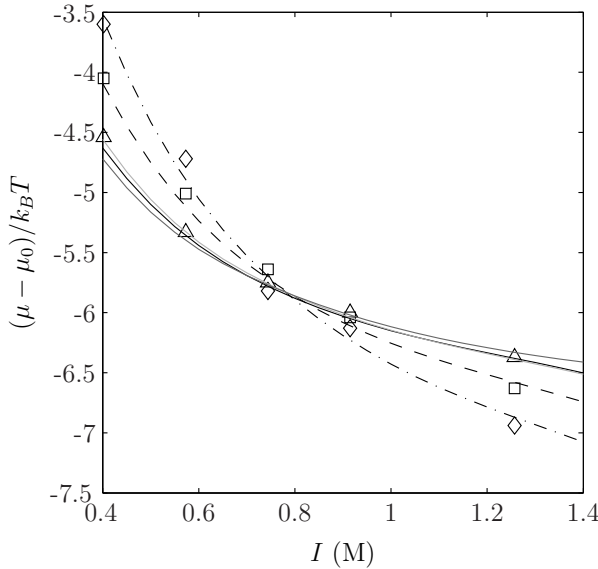


Figure 4.7: The chemical potential of lysozyme in the fluid phase as a function of the ionic strength at pH 4.0 (diamonds), pH 4.5 (squares) and pH 5.4 (triangles) (see Fig. 4.2 on page 87). The solid lines denote predictions from the theory of the crystalline state (Eq. (4.26)), with the effective charge from Table 4.4. The shift in chemical potential in units of $k_B T$ has been chosen to be 7.4 (light grey line, pH 4.0), 7.3 (black line, pH 4.5) and 7.15 (dark grey line, pH 5.4) respectively. Dashed line denotes the theory of the crystal for $Z_{eff} = 5.0$ (shift = 7.9) and the dash-dotted line for $Z_{eff} = 5.9$ (shift = 8.7).

of 3.142 nm^3). We have earlier set the radius of an STA ion equal to 0.55 nm (see Section 4.3.3) so the volume of H_2O per STA molecule is 0.874 nm^3 or $b = 0.593 \text{ nm}$. In Refs. [47] and [112] the water content of this crystal is given in terms of the molecular formula $\text{H}_4\text{STA} \cdot 31\text{H}_2\text{O}$.

4.4.1.4 $\text{Li}_4\text{STA} \cdot 24\text{H}_2\text{O} / \text{Li}_4\text{STA} \cdot 26\text{H}_2\text{O}$

Kraus describes two forms of Li_4STA with 24 H_2O and 26 H_2O molecules attached respectively [115]. Both crystals are rhombohedral (short axes in both cases = 1.559 nm , long axis = 3.898 nm in the former, long axis = 4.118 nm in the latter; the angle between the short axes = 120° [114]). Kraus also mentions that one Li ion should probably be replaced by one H ion. There are actually three different numbers quoted for the water content of $\text{Li}_4\text{STA} \cdot n\text{H}_2\text{O}$ in Refs. [47, 105, 112]: $n = 21, 24$ and 26 ! We have opted for $n = 25$, namely the average number for the crystal habits generally accepted. As there are 6 STA molecules per unit cell, the volume of crystal per STA molecule is 1.406 nm^3 and the radius of our effective

cavity is $b = 0.553$ nm.

4.4.1.5 $\text{Na}_4\text{STA.18H}_2\text{O}$

This crystallizes in the triclinic form within a narrow range around 308 K [113]. The absolute dimensions of the unit cell do not seem to be known. We thus estimate the amount of H_2O per STA molecule via the molecular formulas. The water content in $\text{Na}_4\text{STA.}n\text{H}_2\text{O}$ is stated to be $n = 18$ in Ref. [112] and $n = 14$ in Ref. [47]. The latter value seems too low and is possibly a misprint since n should be equal to 20 according to the usual citation [116]. Accordingly, we adopt $n = 18$ here to be used in the solubility studies [105]. A molecule of H_2O has a volume of 0.0285 nm^3 which is based on the amount of H_2O in the unit cells of $\text{H}_4\text{STA.31H}_2\text{O}$ and $\text{Li}_4\text{STA.26H}_2\text{O}$. Therefore, $\text{Na}_4\text{STA.18H}_2\text{O}$ has 0.513 nm^3 H_2O per STA molecule so we have $b = 0.496$ nm.

Overall, it is not clear how much H_2O is exactly present in the STA crystals. Fortunately, the chemical potential (Eq. (4.26)) depends only logarithmically on this quantity so the data compiled in Table 4.5 on page 100 are not so sensitive to this type of uncertainty. The predicted chemical potentials are depicted as curves in Fig. 4.8 together with the computations from our theory of the liquid state (Fig. 4.5 on page 91).

4.5 Discussion

Except for a slight downward adjustment of the effective charge of lysozyme in the fluid phase, there are essentially no adjustable parameters in our analysis. The adjustment is by one unit only which is insignificant compared with the approximations inherent in the standard electrostatic theory. The adhesion parameters are completely constrained by the second virial curves (Figs. 4.1 on page 85 and 4.4 on page 89). We predict that the chemical potentials in the fluid and solid phases should coincide apart from an unimportant shift in the vertical offset because the reference potential is not known exactly for the crystal. This appears to be almost the case for lysozyme (see Fig. 4.7) but there is an appreciable disparity between the respective curves in the case of the silicotungstates (see Fig. 4.8). Nevertheless, we note that the shapes of the curves are the same which implies that the logarithmic form in Eq. (4.26) appears to be confirmed i.e. the Donnan effect seems to apply to crystals of charged nanoparticles. This is borne out by adjusting Z_{eff} upward somewhat for both types of crystals. We then actually attain coincident curves (see Figs. 4.7 and 4.8). A further implication is that the precise crystal structure is unimportant with regard to the ionic-strength dependence of μ . Eq. (4.26) results from approximating the cavities within the crystals by spheres; the detailed electrostatics is independent of the salt concentration.

The coexistence equation for the osmotic pressure yields little information (see Eq. (4.15)) because it is unclear at present how to relate the adhesive forces be-

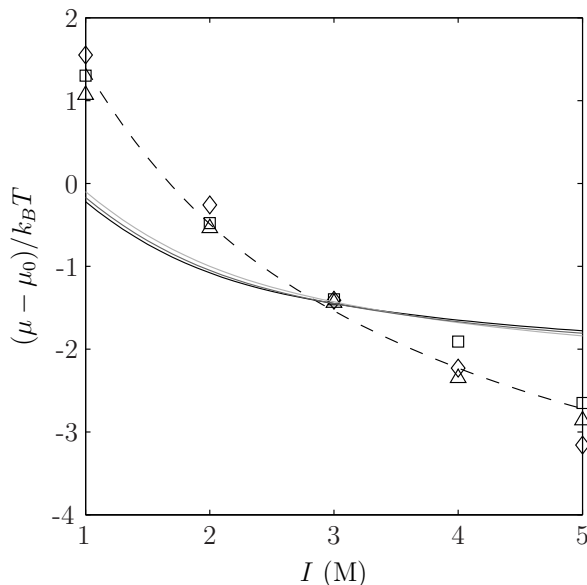


Figure 4.8: Chemical potential of STA in the fluid phase as a function of the ionic strength (see Fig. 4.5). Salt added: LiCl (diamonds); HCl (squares); NaCl (triangles) (counterion of STA is the same as that of the salt). Solid lines denote predictions from the theory of the crystalline state (Eq. (4.26)), with the effective charge from Table 4.5. The shift in chemical potential in units of $k_B T$ is 2.3 (black line, $H_4STA.31H_2O$), 2.4 (dark grey line, $Li_4STA.25H_2O$) and 2.55 (light grey line, $Na_4STA.18H_2O$) respectively. Dashed line denotes predictions from the theory of the crystal for $Z_{eff} = 2.8$ (shift = 5.5).

tween spheres to the elastic properties of the crystal. To compute the latter we need insight in the forces between the particles at the Ångström level which we do not have at present. Adhesive interactions appear to play a minor role in the STA crystals for the fluid and crystal pressures are quite close (compare Table 4.3 on page 90 with Table 4.5). By contrast, in lysozyme crystals the osmotic pressure due to electrostatic forces is largely balanced by sticky interactions between touching protein molecules. In a similar vein there is a marked difference between the two colloids with regard to their respective ionic strengths under theta conditions when B_2 equals zero (see Figs. 4.1 on page 85 and 4.4 on page 89). These salt concentrations may be estimated with the help of Eq. (4.5). Although $\delta \exp U_A = 1.36$ for STA is not substantially less than the respective value 3.33 for lysozyme, the concentrations differ appreciably because of the exponential screening term multiplying the attraction in Eq. (4.5).

It is wise to emphasize the shortcomings in the approximations introduced in the electrostatic interactions. Discrete charge effects have been disregarded en-

X	I (M)	Z	Λ	b/λ	Z_{eff}	w	$\mu/k_B T$	$\Pi v_0/k_B T$
H	0.60	4.0	4.789	2.452	1.67	0.629	2.08	0.738
	1.20	4.0	4.789	2.452	1.67	1.257	1.22	0.466
	1.81	4.0	4.789	2.452	1.67	1.886	0.85	0.332
	2.41	4.0	4.789	2.452	1.67	2.514	0.65	0.256
	3.01	4.0	4.789	2.452	1.67	3.143	0.52	0.207
Li	0.60	4.0	5.134	2.488	1.61	0.531	2.23	0.950
	1.20	4.0	5.134	2.488	1.61	1.062	1.35	0.626
	1.81	4.0	5.134	2.488	1.61	1.594	0.95	0.455
	2.41	4.0	5.134	2.488	1.61	2.125	0.73	0.353
	3.01	4.0	5.134	2.488	1.61	2.656	0.59	0.288
Na	0.60	4.0	5.721	2.542	1.51	0.410	2.45	1.374
	1.20	4.0	5.721	2.542	1.51	0.819	1.55	0.970
	1.81	4.0	5.721	2.542	1.51	1.229	1.12	0.728
	2.41	4.0	5.721	2.542	1.51	1.639	0.87	0.575
	3.01	4.0	5.721	2.542	1.51	2.049	0.71	0.473

Table 4.5: Same as Table 4.4 on page 96 but now for $X_4STA.nH_2O$. Here $n = 31$ when $X = H$, $n = 25$ when $X = Li$ and $n = 18$ when $X = Na$.

tirely. At the same level of approximation we have not addressed the electrostatics of the minutely thin boundary layers between almost touching spheres within the crystal phase. There are cavities at nanometer scales and these are assumed to give rise to the ionic-strength dependence of the free energy of the crystal. The Donnan approximation used suffers from the same drawback as always: the effective charge Z_{eff} is posited to be independent of the electrolyte in the crystal and thus the reservoir (the fluid phase in our case). It would be interesting to study the fluid-crystal coexistence of globular particles of low charge density. The counterions in the crystal would then be essentially free (see Section 4.6.2) and there would be less uncertainty about the magnitude of the electrostatic interactions.

There is another potential problem in the fluid phases of silicotungstates. At 1 M electrolyte, the solubilities of STA are remarkably high (see Table 4.3 on page 90). It would appear that the counterions arising from STA should contribute to the screening on a par with the salt ions. This is not borne out by the present analysis, however, since there is no levelling off of the chemical potentials in the crystal phases in Figs. 4.7 and 4.8. Nevertheless, a liquid state theory of concentrated charged nanoparticles needs to be developed in which the counterions are duly accounted for. We note that the interaction between the

particles is not pairwise additive in that case.

In summary, we have provided a semi-quantitative explanation for the ionic-strength dependence of the fluid-crystal coexistence of suspensions of charged nanoparticles. We believe this explanation is especially forceful because we have considered two rather disparate types of globular particles in detail. In particular, the solubility curves of lysozyme and silicotungstate differ markedly, yet the curves for the chemical potentials turn out to have the same form.

4.6 Appendix

4.6.1 Phase diagram of hard spheres interacting by attractive Yukawa forces

Dijkstra [83] performed computer simulations, more elaborate than those carried out by Hagen and Frenkel [46], on a system of hard spheres of diameter σ attracting each other by exponentially decaying forces (the Yukawa interaction). She varied both the amplitude β and the inverse range κ of the potential. The variable τ in the optimized Baxter model has been computed by us for the attractive Yukawa system in Chapter 3. At fluid-crystal coexistence in Dijkstra's simulations, we evaluate τ from κ , β and the volume fraction η of the fluid phase which is displayed as a function of η in Fig. 4.9.

It is immediately seen that $\tau(\eta)$ is not a single universal curve but depends markedly on the range of the interaction also. Of course, this is not surprising; although τ is a correct similarity variable for the fluid phase (see Chapter 3), it has nothing to do with the statistical properties of the crystal in which the configurations are weighted totally differently than those in the fluid.

4.6.2 Poisson-Boltzmann equation in a crystal or porous medium

Here, we present only a sketch of a general analysis of the Poisson-Boltzmann equation for the electrostatic potential $\Psi(\mathbf{r})$ at position \mathbf{r} within the aqueous interstitial space inside a crystal (which may be considered to be a porous medium), under appropriate conditions. The particles in the crystal are positively charged and simple salt is absent at first. The potential is again related to the counterion density $\rho(\mathbf{r})$ via the Poisson Eq. (4.18). Now it is possible to discern some point P in the void between several particles where the potential is a local minimum and where the density is $\bar{\rho}_P(0)$ (see Fig. 4.10).

Point P is chosen as the origin. If the potential is scaled analogously as in Section 4.4, we have $\rho(\mathbf{r}) = \bar{\rho}_P \exp \psi(\mathbf{r})$ (see Eq. (4.17)). Thus, the Poisson-Boltzmann equation may be written as

$$\Delta\psi = \lambda_P^{-2} e^\psi \quad (4.27)$$

where the screening length λ_P is given by $\lambda_P^{-2} = 4\pi Q\bar{\rho}_P$.

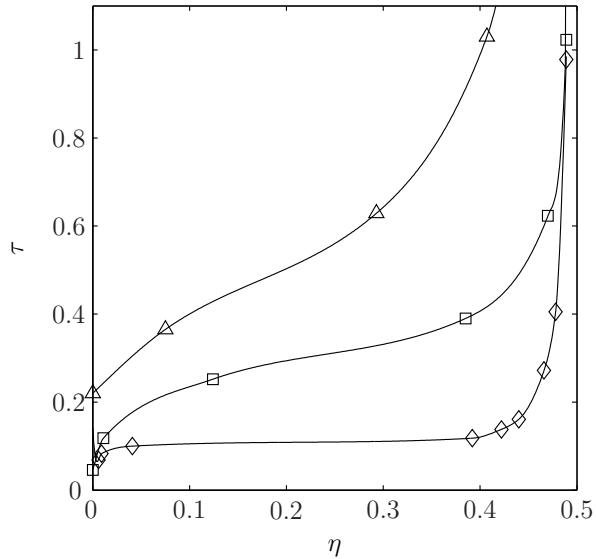


Figure 4.9: Fluid branches of the fluid-crystal coexistence computed by simulation for the Yukawa interaction for several values of the inverse range of the interaction $\kappa\sigma = 7$ (diamonds), $\kappa\sigma = 25$ (squares) and $\kappa\sigma = 100$ (triangles). The data were calculated using the theory from Chapters 2 and 3 and the simulations from Ref. [83]. The lines are a guide to the eye.

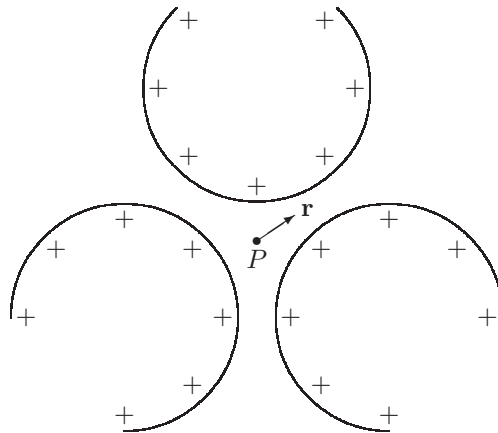


Figure 4.10: Point P in a void of the crystal.

In general, it is difficult to address Eq. (4.27) because λ_P is unknown. But it is possible to progress if we suppose $|\mathbf{d}| \lesssim \lambda_P$ where $|\mathbf{d}|$ is the largest vector distance between P and a point on the surface of the surrounding spheres (i.e. those belonging to a cluster enclosing the void centered on P). An inner solution of Eq. (4.27) must have the form $\psi_{in}(\mathbf{r}/\lambda_P)$ and may be written as a Taylor expansion to second order

$$\psi_{in}(\mathbf{r}) = \frac{1}{2} \mathbf{r} \mathbf{r} : \frac{\partial^2 \psi_{in}}{\partial \mathbf{r} \partial \mathbf{r}} \Big|_{\mathbf{r}=0} \quad (4.28)$$

if $|\mathbf{d}| \lesssim \lambda_P$. There is an outer solution ψ_{out} needed to accommodate for the complicated boundaries. Then, we have a boundary condition on the electric field at $\mathbf{r} = \mathbf{d}$ in terms of ψ_{out} which we rewrite in terms of ψ_{in}

$$\mathbf{n} \cdot \frac{\partial \psi_{in}}{\partial \mathbf{r}} \Big|_{\mathbf{r}=\mathbf{d}} = \mathbf{n} \mathbf{d} : \frac{\partial^2 \psi_{in}}{\partial \mathbf{r} \partial \mathbf{r}} \Big|_{\mathbf{r}=0} = 4\pi k_1 \sigma_b Q. \quad (4.29)$$

Here, σ_b is the uniform density of charge on a sphere and k_1 is a numerical coefficient of order unity associated with the matching of the inner and outer solutions. The effect of an internal permittivity is disregarded. The left-hand side of Eq. (4.29) scales as λ_P^{-2} implying that $\bar{\rho}_P$ must be proportional to σ_b . In view of electroneutrality we also require the average of $\rho(\mathbf{r})$ to be proportional to σ_b . Hence, the potential $\psi(\mathbf{r})$ must be very small, which is consistent with the initial Ansatz Eq. (4.28). We conclude that for small enough cavitylike voids, the density of counterions is approximately constant so that the effective charge density is virtually equal to the actual charge density. In that case, when the crystal is immersed in a reservoir containing monovalent electrolyte, Eqs. (4.25) and (4.26) are valid with $\bar{\rho}$ simply given by the concentration of counterions in the interstitial space between the spheres; $Z_{eff} = Z$ in Eq. (4.26). Because $|\mathbf{d}| = O(a)$, we ultimately require $ZQ/a \ll 1$ as a necessary and sufficient condition for this to hold true. In the spherical cavity approximation introduced in Section 4.4, we have $b = O(a)$ so $\Lambda \ll 1$ is effectively the same requirement (which led to $Z_{eff} = Z$).

Collective diffusion coefficient of proteins with hydrodynamic, electrostatic and adhesive interactions

Abstract A theory is presented for λ_C , the coefficient of the first-order correction in the density of the collective diffusion coefficient, for protein spheres interacting by electrostatic and adhesive forces. An extensive numerical analysis of the Stokesian hydrodynamics of two moving spheres is given so as to gauge the precise impact of lubrication forces. An effective stickiness is introduced and a simple formula for λ_C in terms of this variable is put forward. A precise though more elaborate approximation for λ_C is also developed. These and numerically exact expressions for λ_C are compared with experimental data on lysozyme at pH 4.5 and a range of ionic strengths between 0.05 M and 2 M.

5.1 Introduction

Fick's first law states that the particle flux is equal to minus the collective diffusion coefficient times the gradient of the particle concentration. For colloids or macromolecules in solution, this collective (also called cooperative or mutual) diffusion coefficient is often determined experimentally with the help of dynamic light scattering. If one extrapolates this coefficient to a vanishing concentration of particles, it reduces to the single-particle diffusion coefficient since the interactions between the particles are presumably negligible then. At non-zero volume fractions, particle interactions, such as those of electrostatic and hydrodynamic origin, influence the diffusion. At low enough concentrations, where three- and higher body interactions may be disregarded, the parameter λ_C characterizes the departure from the single-particle result.

The concentration dependence of the collective diffusion coefficient of proteins has been studied extensively in experiments, for example in the case of hemoglobin [117–121], bovine serum albumin [122–125], β -lactoglobulin [126], ovalbumin [127] and lysozyme [19, 128–137]. On the theoretical side, a fair number of papers [138–146] deal with the diffusion of interacting colloidal particles in solution. Apart from giving insight into the diffusion as such, the coefficient λ_C is also important because it could yield information about the complex pair interaction between protein molecules. Moreover, it has been argued that λ_C may be an alternative parameter useful in diagnosing under what conditions proteins would crystallize [132].

In Chapter 2 we approximated globular proteins in water with added monovalent salt by hard spherical particles that interact through a short-range attraction and a screened electrostatic repulsion. We appropriately replaced this system by one of spherical particles with sticky interactions only. At infinite dilution the effective stickiness is readily determined by equating the respective second virial coefficients of the two systems. In the effective stickiness, part of the bare adhesion is balanced against the electrostatic repulsion.

In the next section, we formulate a theory for the coefficient λ_C . We first introduce the interaction used previously to compute protein solution properties, see Chapter 2, and give expressions for the effective stickiness. We then outline the formal expression for λ_C due to Felderhof [138] in terms of the pair potential between two protein spheres and a hydrodynamic mobility function. Although the latter has been studied often in the past, we present a more extensive numerical analysis in order to gain more insight into the asymptotics of the lubrication regime for two moving spheres very close to each other. The coefficient λ_C is then computed in three ways: exactly via numerics and in terms of two convenient approximations. In Section 5.3, we compare these predictions for λ_C with experiment. A discussion of the results is given in the last section.

5.2 Theory

5.2.1 Effective interaction

We model the globular proteins as spherical particles of radius a with a total charge Zq per particle that is uniformly distributed over its surface. Here q is the elementary (proton) charge. For convenience, we scale all distances by the radius a and all energies by $k_B T$ where k_B is Boltzmann's constant and T is the temperature. We approximate the interaction between two proteins by a steric repulsion plus a short-range attraction of scaled range $\delta \ll 1$ and constant absolute magnitude U_A , and a far-field Debye-Hückel potential. The latter describes the Coulomb repulsion that is screened due to the presence of monovalent salt of ionic strength I . The effective number Z_{eff} of charges associated with the far field is computed in the Poisson-Boltzmann approximation. See Chapters 2 and

4 for further details. The total interaction $U_T(x)$ between the two particles with center-of-mass separation r is thus of the form

$$U_T(x) = \begin{cases} \infty & 0 \leq x < 2 \\ U_{DH}(x) - U_A & 2 \leq x < 2 + \delta \\ U_{DH}(x) & x \geq 2 + \delta \end{cases}, \quad (5.1)$$

$$x \equiv \frac{r}{a}. \quad (5.2)$$

Here, the Debye-Hückel interaction is given by

$$U_{DH}(x) = 2\xi \frac{e^{-\omega(x-2)}}{x} \quad (5.3)$$

where $\xi \equiv \frac{Q}{2a} \left(\frac{Z_{eff}}{1+\omega} \right)^2$ and $\omega \equiv \kappa a$. The Debye length κ^{-1} is defined by $\kappa^2 \equiv 8\pi QI$ and the Bjerrum length by $Q \equiv q^2/\epsilon k_B T$, which equals 0.71 nm in water at 298 K (ϵ is the permittivity of water); $\omega = 3.28a\sqrt{I}$, if the radius a is given in nm and the ionic strength I in M. We suppose 1-1 electrolyte has been added in excess so I is the concentration of added salt only. We have derived an exact perturbative expression for the effective charge qZ_{eff} in the Poisson-Boltzmann approximation (see Chapter 2)

$$Z_{eff} = Z - \frac{\omega^2}{6} \left(\frac{Q}{a} \right)^2 \left(\frac{Z}{1+\omega} \right)^3 e^{3\omega} E_1(3\omega). \quad (5.4)$$

Here, $E_1(x)$ is the exponential integral defined by $E_1(x) = \int_x^\infty dt t^{-1} e^{-t}$. It turns out that the first-order correction to the bare charge given by Eq. (5.4) is almost always small for proteins or nanocolloids so Eq. (5.4) is a convenient expression valid under a wide variety of conditions. However, Eq. (5.4) is not useful for highly charged particles of colloidal size because the correction term is not perturbative then.

Analysis of the Poisson-Boltzmann equation for a single sphere has a long history which we cannot discuss fully here. Mathematically rigorous work on the ‘‘condensation’’ of counterions on highly charged spheres was already presented some time ago [147–150]. A simple physical argument for condensation was advanced in Ref. [151]. Various approximations for the potential at large μ as a function of the distance have also been proposed [152–154] but the most complete solution appears to have been derived by Shkel et al. [155] using the method of multiple scales. It is straightforward to obtain Z_{eff} from the latter (see Ref. [95]). The resulting expression for the effective charge is quite accurate at all values of the bare charge provided $\mu \gtrsim 1$. In the case of proteins at large μ , it happens to be numerically very close to the expansion given by Eq. (5.4) but a small disparity remains because the original solution [155] is not expanded beyond $O(\mu^{-1})$.

We want to replace the system of particles interacting through the complicated interaction Eq. (5.1) by a system of particles interacting through a simpler potential, the adhesive hard sphere (AHS) potential of Baxter [27]

$$U_{AHS}(x) = \begin{cases} \infty & 0 \leq x < 2 \\ \ln \frac{12\tau\zeta}{2+\zeta} & 2 \leq x \leq 2 + \zeta \\ 0 & x > 2 + \zeta \end{cases} . \quad (5.5)$$

Here, τ is a positive constant which signifies the strength of the *effective* adhesion and the limit $\zeta \downarrow 0$ has to be taken appropriately after formal integrations. In order to replace the original system by this simpler system, we have to find the correspondence between the parameter τ in the AHS potential and the parameters ξ , ω , δ and U_A in the original interaction Eq. (5.1). In this case, we do this by matching the respective second virial coefficients, which ensures that the free energy of the two systems at small concentrations are identical, and we denote the value of the stickiness that is determined in this way by τ_0 . We emphasize that in the general case, at arbitrary concentrations, we have to match the complete free energies of the respective systems (see Chapters 2 and 4); it is then incorrect to focus on the second virials as has often been done in the past.

5.2.2 Stickiness parameter

We already determined the stickiness parameter τ_0 in Chapter 2. Here we reproduce the main results. The second virial coefficient B_2 is given by

$$B_2 = \frac{1}{2} \int_V d\mathbf{r} \left(1 - e^{-U(\mathbf{r})} \right), \quad (5.6)$$

where $U(\mathbf{r})$ is the pair potential scaled by $k_B T$, and \mathbf{r} is the unscaled position vector connecting the centers of mass of the two particles. For the pair interaction of Eq. (5.1), B_2 may be expressed by

$$B_2 = B_2^{HS} \left(1 + \frac{3}{8} J \right), \quad (5.7)$$

where we introduce the following integrals

$$J \equiv \int_2^\infty dx x^2 \left(1 - e^{-U_T(x)} \right) \equiv J_1 - (e^{U_A} - 1) J_2, \quad (5.8)$$

$$J_1 \equiv \int_2^\infty dx x^2 \left(1 - e^{-U_{DH}(x)} \right) \simeq \frac{4(\omega + \frac{1}{2})\xi}{\omega^2} \left(1 - \frac{\alpha}{2}\xi \right), \quad (5.9)$$

$$J_2 \equiv \int_2^{2+\delta} dx x^2 e^{-U_{DH}(x)} \simeq 2\delta \left[e^{-\xi} + \left(1 + \frac{\delta}{2} \right)^2 e^{-\frac{\xi}{1+\delta/2} e^{-\omega\delta}} \right]. \quad (5.10)$$

Here, $B_2^{HS} = 16\pi a^3/3$ is the value of B_2 if the proteins were solely hard spheres and $\alpha = \frac{e^{-\xi} - (1-\xi)}{\xi^2}$. We equate Eq. (5.7) with the second virial coefficient of the AHS model

$$B_2 = B_2^{HS} \left(1 - \frac{1}{4\tau}\right), \quad (5.11)$$

which results in a stickiness parameter τ_0 given by

$$\tau_0 = -\frac{2}{3J}. \quad (5.12)$$

From Eqs. (5.1) and (5.8) we see how part of the original attraction is compensated by repulsive electrostatics.

5.2.3 General expression for λ_C

For small volume fractions η of spherical particles, the collective diffusion coefficient D_C may be written as

$$D_C = D_0 (1 + \lambda_C \eta + O(\eta^2)), \quad (5.13)$$

where D_0 is the diffusion coefficient in the dilute limit. The linear coefficient λ_C may be split up into five contributions [138]

$$\lambda_C = \lambda_V + \lambda_O + \lambda_D + \lambda_S + \lambda_A. \quad (5.14)$$

These terms have been studied for some time [138–141]: there is a virial correction because a fluctuation in the osmotic pressure drives diffusion

$$\lambda_V = 3 \int_0^\infty dx x^2 (1 - e^{-U(x)}), \quad (5.15)$$

and four terms arising from the mutual friction between two hydrodynamically interacting spheres. An Oseen contribution

$$\lambda_O = 3 \int_0^\infty dx x (e^{-U(x)} - 1), \quad (5.16)$$

and a dipolar contribution

$$\lambda_D = 1, \quad (5.17)$$

express the long-range hydrodynamic interaction between two particles 1 and 2 whereas the short-range part of the hydrodynamic interaction comes into play in the term

$$\lambda_S = \int_2^\infty dx x^2 e^{-U(x)} \left(A_{12}^{tt}(x) + 2B_{12}^{tt}(x) - \frac{3}{x} \right). \quad (5.18)$$

Finally, the modification of the single-particle mobility is expressed by

$$\lambda_A = \int_2^\infty dx x^2 e^{-U(x)} (A_{11}^{tt}(x) + 2B_{11}^{tt}(x)). \quad (5.19)$$

Here, $A_{11}^{tt}(x)$, $A_{12}^{tt}(x)$, $B_{11}^{tt}(x)$ and $B_{12}^{tt}(x)$ are dimensionless hydrodynamic functions given in terms of the translational mobility matrix for two spheres centered at \mathbf{R}_1 and \mathbf{R}_2 ($\mathbf{r} = \mathbf{R}_1 - \mathbf{R}_2$) and acquiring velocities \mathbf{V}_1 and \mathbf{V}_2 as a result of the forces \mathbf{F}_1 and \mathbf{F}_2 acting on the spheres

$$\mathbf{V}_1 = \mu_{11}^{tt}(1, 2) \cdot \mathbf{F}_1 + \mu_{12}^{tt}(1, 2) \cdot \mathbf{F}_2 \quad (5.20)$$

$$\mathbf{V}_2 = \mu_{21}^{tt}(1, 2) \cdot \mathbf{F}_1 + \mu_{22}^{tt}(1, 2) \cdot \mathbf{F}_2. \quad (5.21)$$

In the notation of Cichocki and Felderhof [156], we have

$$\mu_{11}^{tt}(1, 2) = \frac{1}{6\pi\eta_0 a} \left[\mathbf{I} + A_{11}^{tt}(r) \frac{\mathbf{r}\mathbf{r}}{r^2} + B_{11}^{tt}(r) \left(\mathbf{I} - \frac{\mathbf{r}\mathbf{r}}{r^2} \right) \right] \quad (5.22)$$

$$\mu_{12}^{tt}(1, 2) = \frac{1}{6\pi\eta_0 a} \left[A_{12}^{tt}(r) \frac{\mathbf{r}\mathbf{r}}{r^2} + B_{12}^{tt}(r) \left(\mathbf{I} - \frac{\mathbf{r}\mathbf{r}}{r^2} \right) \right], \quad (5.23)$$

where η_0 is the viscosity of the solvent and \mathbf{I} is the unit tensor. The mobility tensors in Eq. (5.21) are given by interchanging the labels in Eqs. (5.22) and (5.23) while taking into account the symmetry relations

$$A_{12}^{tt}(r) = A_{21}^{tt}(r); \quad B_{12}^{tt}(r) = B_{21}^{tt}(r). \quad (5.24)$$

Recall that the particles have a hard-core interaction for $x < 2$ so $\exp -U(x)$ vanishes for $x < 2$. We then sum Eqs. (5.15)-(5.19) and conveniently rewrite λ_C as follows

$$\lambda_C = c_0 + c_1 \int_2^\infty dx x^2 \left(1 - e^{-U(x)} \right) + R. \quad (5.25)$$

The constant c_0 equals the value λ_C would adopt if the spheres were hard but without any other interaction

$$\begin{aligned} c_0 &\equiv 3 \int_0^2 dx x^2 - 3 \int_0^2 dx x + 1 + \int_2^\infty dx x^2 \left(h(x) - \frac{3}{x} \right) \\ &= 3 + \int_2^\infty dx x^2 \left(h(x) - \frac{3}{x} \right). \end{aligned} \quad (5.26)$$

Here, $h(x)$ is the sum of scalar mobility functions

$$h(x) \equiv A_{11}^{tt}(x) + A_{12}^{tt}(x) + 2B_{11}^{tt}(x) + 2B_{12}^{tt}(x). \quad (5.27)$$

The residual term R in Eq. (5.25) depends on the actual interaction

$$R \equiv \int_2^\infty dx x^2 \left(e^{-U(x)} - 1 \right) (h(x) - h(2)) \quad (5.28)$$

though it would vanish if the interaction U were adhesive and purely of the Baxter type (see Eq. (5.5)). The second term on the right hand side of Eq. (5.25) is proportional to the constant

$$c_1 \equiv 3 - h(2) \quad (5.29)$$

and the integral is related to the second virial coefficient B_2 by (see Eqs. (5.7) and (5.8))

$$\int_2^\infty dx x^2 \left(1 - e^{-U(x)}\right) = \frac{8}{3} \left(\frac{B_2}{B_2^{HS}} - 1\right). \quad (5.30)$$

The resulting expression for λ_C is

$$\lambda_C = c_0 + \frac{8c_1}{3} \left(\frac{B_2}{B_2^{HS}} - 1\right) + R \quad (5.31)$$

which we can evaluate once we know $h(x)$ given by Eq. (5.27).

5.2.4 Hydrodynamics

The function $h(x)$ was discussed by Batchelor [157] in his theory of the diffusion of hard spheres. The sum $A_{11}^{tt} + A_{12}^{tt}$ pertains to the mobility of a pair of spheres moving in the direction of their line of centers whereas $B_{11}^{tt} + B_{12}^{tt}$ is related to their mobility when they move perpendicular to that line. (Note that in Ref. [157] $A_{11} \equiv A_{11}^{tt} + 1$, $B_{11} \equiv B_{11}^{tt} + 1$, $A_{12} \equiv A_{12}^{tt}$ and $B_{12} \equiv B_{12}^{tt}$). In the latter case, because the spheres are couple-free, the spheres must rotate as the pair translates. At small separations ($x - 2 \ll 1$), lubrication forces with a logarithmic singularity $\ln^{-1}(x - 2)$ are then expected to develop on general grounds [158]. Goldman et al. [159] proposed a form for the singularity which we will test below.

Batchelor [157] computed $h(2) = 1.312$ on the basis of numerical work on the mobilities of touching spheres [160, 161]. Cichocki and Felderhof [156] evaluated $c_0 = 1.454$ (Eq. (5.26)) by numerically summing their series expansions of the hydrodynamic interactions while keeping track of a logarithmic singularity at close separations. Here we reanalyze $h(x)$ and go well beyond previous computations [156, 162] in order to gain more insight into the nature of the singularity and to calculate the residual R .

We assume the interaction $U(x)$ is of short range so we focus only on $h(x)$ for $x - 2 \lesssim 1$. First, we get an expression for $A_{11}^{tt} + A_{12}^{tt}$ as an infinite sum from the results of Stimson and Jeffery [163] who expressed the hydrodynamic problem in terms of bispherical coordinates. (Note that there is an error in their paper as pointed out in, for example, Ref. [164] in which one may find a similar expression for $A_{11}^{tt} - A_{12}^{tt}$ in case one needs A_{11}^{tt} and A_{12}^{tt} separately). Calculating B_{11}^{tt} and B_{12}^{tt} is more involved. We use the numerical scheme by O'Neill and Majumdar [165] which is similar to that of Goldman et al. [159]. (Note that there are a few typographical errors in Ref. [165]. In their Eq. (3.9) d should be d_1 , the expression for v in Eq. (4.1) should have a minus sign, ξ , ϕ and ψ in Eqs. (4.3)-(4.5) should be replaced by $c\xi$, $c\phi$ and $c\psi$ respectively, and $\sinh^2|\beta|$ in Eq. (5.10) should be $\sinh^3|\beta|$). Also, to obtain $D_2(A_n, B_n)$ (Eq. (3.29)) from $D_1(A_n, B_n)$ (Eq. (3.28)) the signs of δ_{n-1} , δ_n and δ_{n+1} should be reversed as well (we only checked the case of spheres of equal size). Their Table I is correct, however, for spheres of

equal size, apart from the value for $g_{12}(1, 0.1)$ which should read -0.1017 instead of -1.1017).

In order to investigate the regime of lubrication for a pair of spheres moving under the action of applied forces normal to their line of centers, we performed the numerical analysis down to $r/a - 2 = 10^{-10}$ which implies two million terms in the series expansions are needed. We attempted to speed up the iteration by adapting the recurrence relationships introduced more recently by O'Neill and Bhatt [166] for a sphere moving near a wall to the case of two spheres. However, this did not turn out to be useful as it is for the wall configuration [167]. One way of circumventing series expansions could be to elaborate on the trial functions initially used by Fixman in his variational theorem for the mobility matrix [168] but we did not investigate this.

Goldman et al. [159] were the first to give a comprehensive analysis of the mobility of a pair of identical spheres of arbitrary orientation. They numerically solved the Stokes and continuity equations using expansions in terms of bipolar coordinates to high order. For moving spheres whose line of centers is perpendicular to the applied force, the force consists not only of a term arising from pure translation but also a term stemming from pure rotation of the spheres. The latter involves a torque on one sphere diverging as [159]

$$T_r \sim \frac{3 \ln(x - 2)}{160\pi\eta_0\Omega a^3} \quad (5.32)$$

at very small separations where Ω is its angular velocity. Eq. (5.32) was derived by extending the nontrivial lubrication theory of Ref. [169] in which inner and outer regions have to be matched. Eq. (5.32) ultimately leads to the following analytical expression for $h(x)$ valid at small separations

$$h(x) = h(2) - \frac{0.47666}{\ln(x - 2) + c_2} + O(x - 2). \quad (5.33)$$

The coefficient 0.47666 is computed from the numerical tables presented in Ref. [159]. We have added a constant c_2 to the logarithm because we expect the next higher order term in Eq. (5.32) to be a constant judging by the earlier analysis of the sphere-wall problem [169]. In Fig. 5.1 we have fitted Eq. (5.33) to the numerical results discussed above, letting $h(2)$ and c_2 be adjustable. The intercept $h(2) = 1.30993$ turns out to be close to the value 1.312 quoted above for touching spheres which lends credence to the validity of the asymptotic expression that we propose. Moreover, the resulting coefficient $c_2 = -4.694$ and the concomitant shift in Eq. (5.32) are consistent with the numerical values of the torque T_r at small separations as presented in Table 3 of Ref. [159].

Next, we derive an expression for the residual term given by Eq. (5.28). First, we propose an initial estimate $h_0(x)$ for $h(x)$. We have plotted the numerical values of $h(x)$ as a function of x in Fig. 5.2. As a result of the lubrication regime, h has a maximum as displayed in the inset. However, $h(x)$ is only a strongly

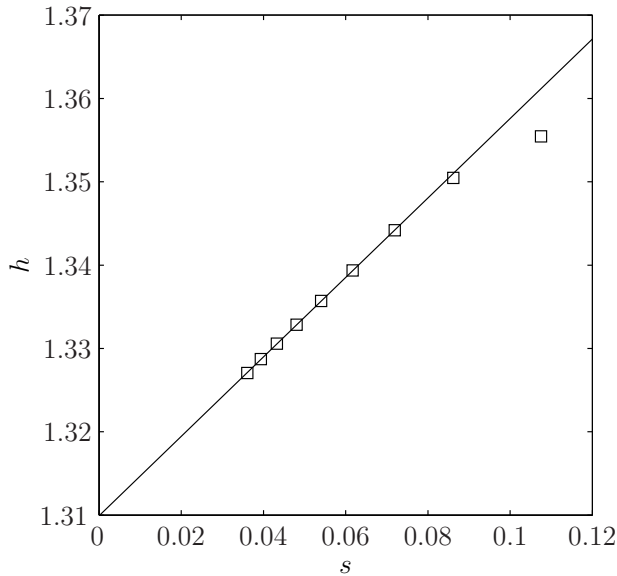


Figure 5.1: The hydrodynamic function h plotted in terms of the variable $s = -1/(\ln(x-2)-4.694)$. Squares denote results from the numerical analysis to the accuracy as explained in the text. The straight line signifies the function $h = 0.47666s + 1.30993$.

varying function for $x < 2.04$. We therefore simply force a linear fit to the data for h at $x = 2.1, 2.2$ and 2.3

$$h_0(x) \simeq 1.3670 - 0.4745(x - 2). \quad (5.34)$$

We then insert this estimate into Eq. (5.28) and add a correction term so as to derive an expression for R accurate enough for our purposes.

$$R \simeq -0.147 \left(\frac{B_2}{B_2^{HS}} - 1 \right) + 0.4745 \int_2^\infty dx x^2 (x - 2) (1 - e^{-U(x)}) + 9 \times 10^{-4} (1 - e^{-U(2)}). \quad (5.35)$$

The first term on the right comes from the fact that the linear interpolation gives $h_0(2) = 1.3670$ whereas the real value is $h(2) = 1.312$. Since the interaction usually does not change appreciably for $2 < x < 2.04$, it is straightforward to write an estimate for the error—the third term—owing to the deviation of Eq. (5.34) from the exact function $h(x)$ (see inset Fig. 5.2). In our case the error term turns out to be an order of magnitude smaller than the first two terms.

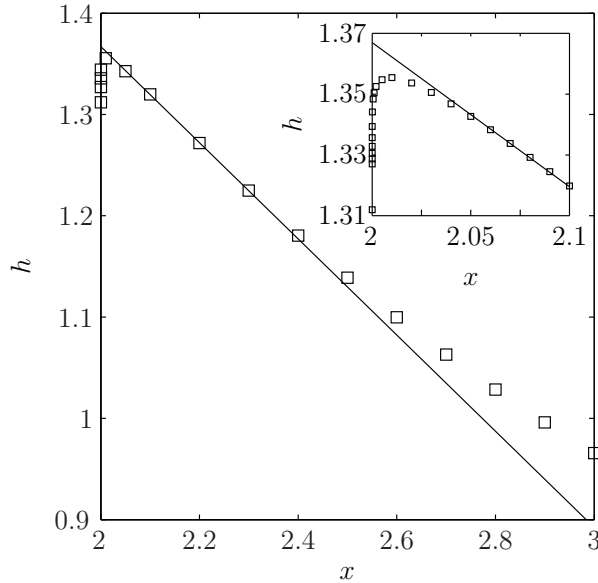


Figure 5.2: The hydrodynamic function $h(x)$ as a function of the dimensionless separation $x \equiv r/a$ between the centers of two spheres. The straight line signifies $h_0(x)$ given by Eq. (5.34).

5.2.5 Determination of λ_C

It is clear from Eq. (5.28) that R would vanish if the actual interaction were a pure AHS potential. If we then insert Eq. (5.11) into Eq. (5.31), we obtain [141]

$$\lambda_C = c_0 - \frac{2c_1}{3\tau_0}. \quad (5.36)$$

Inspection of the various terms in Eq. (5.35) reveals that R is often much smaller than unity when the interaction is given by Eq. (5.1). Hence, a possibly convenient approximation to the coefficient λ_C is from Eq. (5.12)

$$\lambda_C = c_0 + c_1 J = c_0 + \frac{8c_1}{3} \left(\frac{B_2}{B_2^{HS}} - 1 \right) \quad (5.37)$$

where J may be evaluated numerically or approximately with the help of Eqs. (5.8)-(5.10).

The full expression for the dynamical coefficient is written as

$$\lambda_C = c_0 + c_1 J + R, \quad (5.38)$$

using Eqs. (5.7) and (5.31). Now R from Eq. (5.35) is reexpressed as

$$R \simeq -0.055J + 0.4745K - 9 \times 10^{-4} (e^{U_A - \xi} - 1). \quad (5.39)$$

in view of Eqs. (5.1) and (5.3). Here we have introduced the function K for which we derive a convenient approximation.

$$K \equiv \int_2^\infty dx x^2 (x-2) \left(1 - e^{-U_T(x)}\right) \equiv K_1 - (e^{U_A} - 1) K_2, \quad (5.40)$$

where

$$K_1 \equiv \int_2^\infty dx x^2 (x-2) \left(1 - e^{-U_{DH}(x)}\right) \quad (5.41)$$

and

$$K_2 \equiv \int_2^{2+\delta} dx x^2 (x-2) e^{-U_{DH}(x)}. \quad (5.42)$$

In the same spirit as in Chapter 2, we approximate $x(1 - e^{-U_{DH}(x)}) \simeq 2\xi e^{-\omega(x-2)} - 2\alpha\xi^2 e^{-2\omega(x-2)}$, with $\alpha = \frac{e^{-\xi} - (1-\xi)}{\xi^2}$. We then have

$$K_1 \simeq \frac{\xi(\omega+1)(4-\alpha\xi)}{\omega^3}, \quad (5.43)$$

where we have neglected the small term $\alpha\xi^2/2\omega^3$. In the case of lysozyme at pH 4.5, the deviation of Eq. (5.43) from the exact result is smaller than about 3% for $I \geq 0.05$ M and smaller than about 1% for $I \geq 0.3$ M. For the second integral we use the trapezoid approximation $\int_2^{2+\delta} dx g(x) \simeq \frac{1}{2}\delta [g(2) + g(2+\delta)]$ ($\delta \ll 1$) and we neglect a factor $(1 + \delta/2)^2$

$$K_2 \simeq 2\delta^2 \exp\left[-\frac{\xi e^{-\omega\delta}}{1 + \delta/2}\right]. \quad (5.44)$$

For lysozyme at pH 4.5 with $\delta = 0.079$ (see below), this approximation deviates less than about 5% from the exact value for $I \geq 0.05$ M and less than about 3% for $I \geq 0.2$ M.

5.3 Comparison with experiment

We compare our predictions of λ_C as a function of the ionic strength I with experimental results for lysozyme at room temperature and at a pH of about 4.5. The added salt is NaCl and in most cases a small amount of Na acetate has been added as buffer. The reason for choosing lysozyme under these conditions is that we have previously evaluated the range and strength of the short-range attraction (see Chapter 2) and a lot of experimental data on the collective diffusion coefficient are available in the literature (see Fig. 5.3).

Lysozyme has a moderate aspect ratio of about 1.5 and we approximate it by a sphere of radius $a = 1.7$ nm [100]. The dimensionless parameter ω is then given by $\omega = 5.58\sqrt{I}$, where the ionic strength I is given in M, and $\xi = 0.209(\bar{Z}/(1+\omega))^2$.

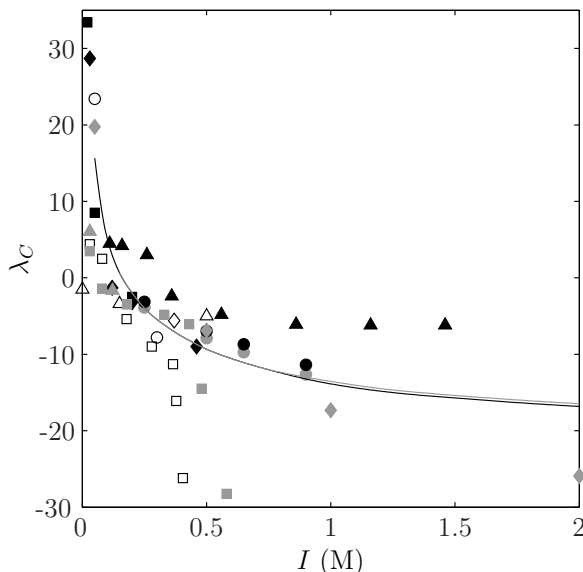


Figure 5.3: Experimental data and theoretical predictions of λ_C for lysozyme as a function of the ionic strength I at a pH of about 4.5. Data: black squares: Nyström et al. [128], pH 4.0, 25 °C; grey squares: Mirarefi et al. [129], pH 4.6; white squares: Mirarefi et al. [129], pH 4.6; black diamonds: Muschol et al. [19], pH 4.7, 20 °C; grey diamonds: Zhang et al. [130], pH 4.5, 20 °C; white diamonds: Skouri et al. [131], pH 4.6, 20 °C; black triangles: Eberstein et al. [132], pH 4.2, 20 °C; grey triangles: Leggio et al. [133], pH 4.75, 25 °C; white triangles: Price et al. [134], pH 4.6, 25 °C; black circles: Annunziata et al. [135], pH 4.5, 25 °C; grey circles: Annunziata et al. [135], pH 4.5, 25 °C; white circles: Retailleau et al. [136], pH 4.0. In all cases, the supporting electrolyte is NaCl, often with a small amount of Na acetate added. The grey line denotes the theoretical curve setting $R \equiv 0$ i.e. Eq. (5.36) with τ_0 given by Eq. (5.12), and the black line is the curve given by Eq. (5.38). The functions J and K have been approximated as outlined in the text.

Here we follow our discussion in Chapter 2 and use the adjusted charge on the lysozyme sphere $\bar{Z} = Z_{eff} - 1$ instead of the effective charge Z_{eff} . Values of Z , Z_{eff} and \bar{Z} as a function of ionic strength can be found in Table 5.1 as well as the corresponding quantities ω and ξ . For the range δ and strength U_A of the attraction we use $\delta = 0.079$ and $U_A = 3.70$ which were computed on the basis of a wide variety of data on the second virial coefficient (see Chapter 2).

We next employ three methods to predict λ_C theoretically. In the first, we compute τ_0 by equating the respective second virial coefficients of Section 5.2.2 (see Eqs. (5.8) and (5.12)). We then calculate λ_C from Eq. (5.36) using $c_0 = 1.454$ and $c_1 = 1.688$. In the second method we use Eq. (5.38) to determine λ_C , where

I (M)	Z	Z_{eff}	\bar{Z}	ξ	ω	R	τ_0	λ_C		
								via τ_0	direct	exact
0.05	9.5	8.8	7.8	2.52	1.25	4.267		16.63	15.66	
0.10	9.8	9.2	8.2	1.84	1.76	1.382		5.30	5.14	
0.15	10.0	9.4	8.4	1.48	2.16	0.744	0.742	-0.06	0.68	0.65
0.20	10.1	9.6	8.6	1.27	2.50	0.514	0.286	-2.48	-1.97	-1.96
0.25	10.2	9.7	8.7	1.10	2.79	0.408	0.193	-4.38	-3.97	-3.95
0.30	10.2	9.8	8.8	0.984	3.06	0.354	0.155	-5.81	-5.46	-5.45
0.45	10.3	10.0	9.0	0.752	3.74	0.302	0.109	-8.82	-8.53	-8.51
1.0	10.4	10.2	9.2	0.409	5.58	0.323	0.0734	-13.87	-13.55	-13.58
1.5	10.4	10.3	9.3	0.295	6.83	0.349	0.0655	-15.72	-15.38	-15.43
2.0	10.4	10.3	9.3	0.229	7.89	0.367	0.0616	-16.82	-16.46	-16.52

Table 5.1: Values of the actual charge Z of hen-egg-white lysozyme (from Ref. [60]), the effective charge Z_{eff} (see Eq. (5.4)), the lowered effective charge $\bar{Z} = Z_{eff} - 1$, and dimensionless interaction parameters ξ and ω as a function of the ionic strength I . The pH equals 4.5 and ξ has been calculated using the lowered effective charge \bar{Z} . R has been calculated from Eq. (5.39), τ_0 from Eq. (5.12), λ_C (via τ_0) from Eq. (5.36) and λ_C (direct) from Eq. (5.38). In all cases approximations for J and K given by Eqs. (5.8)-(5.10) and (5.40), (5.43), (5.44) were used. The computation of the numerically exact λ_C is explained in the text.

R is evaluated with the help of Eq. (5.39). In both cases the approximations for J and K given by Eqs. (5.8)-(5.10) and Eqs. (5.40), (5.43) and (5.44) were used (see Table 5.1 and Fig. 5.3). Note that there are no free parameters so the curves in Fig. 5.3 are predictions not fits. For comparison, we also calculate λ_C from Eq. (5.14) exactly, that is by performing the integrals in Eqs. (5.15)-(5.19) numerically with the help of a highly accurate interpolation formula for $h(x)$ (see Table 5.1). Finally, in Fig. 5.3 we have also plotted data of λ_C measured by several experimental groups.

5.4 Discussion

In Section 5.2.5 we have outlined two approximate methods to calculate λ_C . As one can see from Table 5.1, both the direct method incorporating an approximation for the residual R and the method relying solely on the stickiness τ_0 via the second virial yield results that are often close to the exact numerical computations. The direct method is, of course, somewhat more accurate. The τ_0 method breaks down below 0.2 M. Note that in the important regime $I > 0.2$ M pertaining to protein crystallization, R is much smaller than the absolute magnitude of λ_C . This may explain why λ_C is a useful parameter to characterize the onset of crystallization [132].

We also note in Fig. 5.3 that λ_C decreases monotonically with increasing ionic strength or effective attraction. The friction per particle becomes less as the chance of two spheres clustering together is enhanced, yet this is offset by the decrease in the osmotic pressure driving the diffusion, for numerical reasons (see Eqs. (5.25) and (5.29); the residual R is merely a perturbation).

In Fig. 5.3, it is clear that there is a large degree of scatter which may be attributed to the systematic variation in sets of data from the various groups, especially at large ionic strengths ($I > 0.4$ M). We do not know what is the cause of this. In one experiment [129], we do observe there is considerable scatter in a plot of the diffusion coefficient versus the protein solubility which might explain the extreme downturn of several data in Fig. 5.3 at about 0.5 M. Fig. 5.3 also shows that our predicted curves lie fairly neatly in the midst of the swarm of data. We emphasize again that we have no adjustable parameters in our calculations except for a slight downward adjustment of the effective charge (see also the discussion in Chapters 2 and 4). The model is thus not inconsistent with the experimental data though we will have to await more experiments under conditions which are better controlled before one may reach a more definitive conclusion. In a similar vein, it is not possible to claim that the neglect of electrolyte friction assumed here is entirely warranted.

In summary, we have approximated proteins by spherical particles interacting by a hard-core and electrostatic repulsion together with a short-range attraction. An analysis of the two-particle statistics and hydrodynamics leads to a reasonable prediction of the ionic-strength dependence of the linear coefficient λ_C . At high

ionic strengths, when B_2 is negative, the residual R is relatively small so there is then an interesting direct relationship between λ_C and B_2 (Eq. (5.37)) which could be tested experimentally.



Bibliography

- [1] B. ALBERTS, A. JOHNSON, J. LEWIS, M. RAFF, K. ROBERTS AND P. WALTER. *Molecular Biology of the Cell*, 4th ed. Garland Science, New York, NY, U.S.A., 2002.
- [2] G. D. FASMAN (ED.). *Practical Handbook of Biochemistry and Molecular Biology*. CRC Press, Boca Raton, FL, U.S.A., 1989.
- [3] D. R. LIDE (ED. IN CHIEF). *Handbook of Chemistry and Physics*, 85th ed. CRC Press, Boca Raton, FL, U.S.A., 2004.
- [4] H. LODISH, A. BERK, S. L. ZIPURKSY, P. MATSUDAIRA, D. BALTIMORE AND J. DARNELL. *Molecular Cell Biology*, 4th ed. W. H. Freeman and Company, New York, NY, U.S.A., 2000.
- [5] A. B. FULTON AND W. B. ISAACS. Titin, a huge, elastic sarcomeric protein with a probable role in morphogenesis. *Bioessays* **13**, 157 (1991).
- [6] M. C. VANEY, S. MAIGNAN, M. RIÈS-KAUTT AND A. DUCRUIX. High-resolution structure (1.33 Å) of a HEW lysozyme tetragonal crystal grown in the APCF apparatus. Data and structural comparison with a crystal grown under microgravity from SpaceHab-01 mission. *Acta Crystallogr. D* **52**, 505 (1996).
- [7] H. M. BERMAN, J. WESTBROOK, Z. FENG, G. GILLILAND, T. N. BHAT, H. WEISSIG, I. N. SHINDYALOV AND P. E. BOURNE. The Protein Data Bank. *Nucleic Acids Res.* **28**, 235 (2000).
- [8] M. L. CONNOLLY. Solvent-accessible surfaces of proteins and nucleic-acids. *Science* **221**, 709 (1983); M. L. CONNOLLY. Analytical molecular surface calculation. *J. Appl. Crystallogr.* **16**, 548 (1983).

- [9] A. E. FERENTZ. in *Protein Structure: Determination, Analysis, and Applications for Drug Discovery*, ed. by D. I. Chasman. Marcel Dekker, Inc., New York, NY, U.S.A., 2003.
- [10] A. MCPHERSON. *Crystallization of Biological Macromolecules*. Cold Spring Harbor Laboratory Press, Cold Spring Harbor, NY, U.S.A., 1999.
- [11] A. KILARA AND V. R. HARWALKAR. in *Food Proteins: Properties and Characterization*, ed. by S. Nakai and H. W. Modler. VCH Publishers, Inc., New York, NY, U.S.A., 1996.
- [12] P. W. ATKINS. *Physical Chemistry*. Oxford University Press, Oxford, U.K., 1998.
- [13] C. A. HAYNES, K. TAMURA, H. R. KÖRFER, H. W. BLANCH AND J. M. PRAUSNITZ. Thermodynamic properties of aqueous α -chymotrypsin solutions from membrane osmometry measurements. *J. Phys. Chem.* **96**, 905 (1992).
- [14] E. J. W. VERWEY AND J. TH. G. OVERBEEK. *Theory of the Stability of Lyophobic Colloids*. Dover Publications, Inc., New York, NY, U.S.A., 1999.
- [15] T. L. HILL. *An Introduction to Statistical Thermodynamics*. Dover Publications, Inc., New York, NY, U.S.A., 1986.
- [16] C. S. JOHNSON, JR. AND D. A. GABRIEL. *Laser Light Scattering*. Dover Publications, Inc., New York, NY, U.S.A., 1994.
- [17] F. BONNETÉ, S. FINET AND A. TARDIEU. Second virial coefficient: variations with lysozyme crystallization conditions. *J. Cryst. Growth* **196**, 403 (1999).
- [18] R. A. CURTIS, J. M. PRAUSNITZ AND H. W. BLANCH. Protein-protein and protein-salt interactions in aqueous protein solutions containing concentrated electrolytes. *Biotechnol. Bioeng.* **57**, 11 (1998).
- [19] M. MUSCHOL AND F. ROSENBERGER. Interactions in undersaturated and supersaturated lysozyme solutions: Static and dynamic light scattering results. *J. Chem. Phys.* **103**, 10424 (1995).
- [20] R. A. CURTIS, J. ULRICH, A. MONTASER, J. M. PRAUSNITZ AND H. W. BLANCH. Protein-protein interactions in concentrated electrolyte solutions. Hofmeister-series effects. *Biotechnol. Bioeng.* **79**, 367 (2002).
- [21] O. D. VELEV, E. W. KALER AND A. M. LENHOFF. Protein interactions in solution characterized by light and neutron scattering: comparison of lysozyme and chymotrypsinogen. *Biophys. J.* **75**, 2682 (1998).
- [22] D. F. ROSENBAUM AND C. F. ZUKOSKI. Protein interactions and crystallization. *J. Cryst. Growth* **169**, 752 (1996).

- [23] D. F. ROSENBAUM, A. KULKARNI, S. RAMAKRISHNAN AND C. F. ZUKOSKI. Protein interactions and phase behavior: Sensitivity to the form of the pair potential. *J. Chem. Phys.* **111**, 9882 (1999).
- [24] J. BLOUSTINE, V. BEREJNOV AND S. FRADEN. Measurement of protein-protein interactions by size exclusion chromatography. *Biophys. J.* **85**, 2619 (2003).
- [25] R. PIAZZA AND M. PIERNO. Protein interactions near crystallization: a microscopic approach to the Hofmeister series. *J. Phys.: Condens. Matter* **12**, A443 (2000).
- [26] J. BEHLKE AND O. RISTAU. Analysis of the thermodynamic non-ideality of proteins by sedimentation equilibrium experiments. *Biophys. Chem.* **76**, 13 (1999).
- [27] R. J. BAXTER. Percus-Yevick equation for hard spheres with surface adhesion. *J. Chem. Phys.* **49**, 2770 (1968).
- [28] M. A. MILLER AND D. FRENKEL. Phase diagram of the adhesive hard sphere fluid. *J. Chem. Phys.* **121**, 535 (2004).
- [29] T. L. HILL. *Statistical Mechanics: Principles and Selected Applications*. Dover Publications, Inc., New York, NY, U.S.A., 1977.
- [30] J. P. HANSEN AND I. R. McDONALD. *Theory of Simple Liquids*. Academic Press, London, U.K., 1976.
- [31] J. K. PERCUS AND G. J. YEVICK. Analysis of classical statistical mechanics by means of collective coordinates. *Phys. Rev.* **110**, 1 (1958).
- [32] E. THIELE. Equation of state for hard spheres. *J. Chem. Phys.* **39**, 474 (1963); M. S. WERTHEIM. Exact solution of the Percus-Yevick integral equation for hard spheres. *Phys. Rev. Lett.* **10**, 321 (1963); M. S. WERTHEIM. Analytic solution of the Percus-Yevick equation. *J. Math. Phys.* **5**, 643 (1964).
- [33] E. J. COHN AND J. T. EDSALL. *Proteins, Amino Acids and Peptides as Ions and Dipolar Ions*. Reinhold Publishing Corporation, New York, NY, U.S.A., 1943.
- [34] J. N. ISRAELACHVILI. *Intermolecular and Surface Forces*, 2nd ed. Academic Press, London, U.K., 1991.
- [35] W. G. McMILLAN AND J. E. MAYER. The statistical thermodynamics of multicomponent systems. *J. Chem. Phys.* **13**, 276 (1945).
- [36] J. E. MAYER AND M. G. MAYER. *Statistical Mechanics*, 2nd ed. John Wiley & Sons, New York, NY, U.S.A., 1977.

- [37] J. G. KIRKWOOD. Statistical mechanics of fluid mixtures. *J. Chem. Phys.* **3**, 300 (1935).
- [38] J. K. PERCUS. Approximation methods in classical statistical mechanics. *Phys. Rev. Lett.* **8**, 462 (1962); J. K. PERCUS. in *The Equilibrium Theory of Classical Fluids*, ed. by H. L. Frisch and J. L. Lebowitz. W. A. Benjamin, Inc., New York, NY, U.S.A., 1964.
- [39] L. S. ORNSTEIN AND F. ZERNIKE. Accidental deviations of density and opalescence at the critical point of a single substance. *Proc. Akad. Sci. (Amsterdam)* **17**, 793 (1914).
- [40] J. M. J. VAN LEEUWEN, J. GROENEVELD AND J. DE BOER. New method for the calculation of the pair correlation function. I. *Physica* **25**, 792 (1959); E. MEERON. Nodal expansions. III. Exact integral equations for particle correlation functions. *J. Math. Phys.* **1**, 192 (1960); T. MORITA. Theory of classical fluids: hyper-netted chain approximation. III. A new integral equation for the pair distribution function. *Prog. Theor. Phys.* **23**, 829 (1960); G. S. RUSHBROOKE. On the hyper-chain approximation in the theory of classical fluids. *Physica* **26**, 259 (1960); L. VERLET. On the theory of classical fluids. *Nuovo Cimento* **18**, 77 (1960).
- [41] B. BARBOY. On a representation of the equation of state of fluids in terms of the adhesive hard-sphere model. *J. Chem. Phys.* **61**, 3194 (1974).
- [42] R. O. WATTS, D. HENDERSON AND R. J. BAXTER. Hard spheres with surface adhesion: the Percus-Yevick approximation and the energy equation. *Adv. Chem. Phys.* **21**, 421 (1971).
- [43] N. F. CARNAHAN AND K. E. STARLING. Equation of state for nonattracting rigid spheres. *J. Chem. Phys.* **51**, 635 (1969).
- [44] A. GEORGE AND W. W. WILSON. Predicting protein crystallization from a dilute solution property. *Acta Crystallogr. D* **50**, 361 (1994).
- [45] A. GEORGE, Y. CHIANG, B. GUO, A. ARABSHAHI, Z. CAI AND W. W. WILSON. Second virial coefficient as predictor in protein crystal growth. *Methods Enzymol.* **276**, 100 (1997).
- [46] M. H. J. HAGEN AND D. FRENKEL. Determination of phase diagrams for the hard-core attractive Yukawa system. *J. Chem. Phys.* **101**, 4093 (1994).
- [47] D. ROSENBAUM, P. C. ZAMORA AND C. F. ZUKOSKI. Phase behavior of small attractive colloidal particles. *Phys. Rev. Lett.* **76**, 150 (1996).
- [48] C. HAAS AND J. DRENTH. The protein-water phase diagram and the growth of protein crystals from aqueous solution. *J. Phys. Chem. B* **102**, 4226 (1998).

- [49] C. HAAS, J. DRENTH AND W. W. WILSON. Relation between the solubility of proteins in aqueous solutions and the second virial coefficient of the solution. *J. Phys. Chem. B* **103**, 2808 (1999).
- [50] C. HAAS AND J. DRENTH. Understanding protein crystallization on the basis of the phase diagram. *J. Cryst. Growth* **196**, 388 (1999).
- [51] B. L. NEAL, D. ASTHAGIRI, O. D. VELEV, A. M. LENHOFF AND E. W. KALER. Why is the osmotic second virial coefficient related to protein crystallization? *J. Cryst. Growth* **196**, 377 (1999).
- [52] V. L. VILKER, C. K. COLTON AND K. A. SMITH. The osmotic pressure of concentrated protein solutions: effect of concentration and pH in saline solutions of bovine serum albumin. *J. Coll. Int. Sci.* **79**, 548 (1981).
- [53] A. P. MINTON. A molecular model for the dependence of the osmotic pressure of bovine serum albumin upon concentration and pH. *Biophys. Chem.* **57**, 65 (1995).
- [54] B. M. FINE, A. LOMAKIN, O. O. OGUN AND G. B. BENEDEK. Static structure factor and collective diffusion of globular proteins in concentrated aqueous solution. *J. Chem. Phys.* **104**, 326 (1996).
- [55] A. LOMAKIN, N. ASHERIE AND G. B. BENEDEK. Monte Carlo study of phase separation in aqueous protein solutions. *J. Chem. Phys.* **104**, 1646 (1996).
- [56] R. PIAZZA, V. PEYRE AND V. DEGIORGIO. "Sticky hard spheres" model of proteins near crystallization: A test based on the osmotic compressibility of lysozyme solutions. *Phys. Rev. E* **58**, R2733 (1998).
- [57] A. J. SOPHIANOPOULOS, C. K. RHODES, D. N. HOLCOMB AND K. E. VAN HOLDE. Physical studies of lysozyme. I. Characterization. *J. Biol. Chem.* **237**, 1107 (1962).
- [58] J. B. KELLER AND B. ZUMINO. Determination of intermolecular potentials from thermodynamic data and the law of corresponding states. *J. Chem. Phys.* **30**, 1351 (1959).
- [59] G. C. MAITLAND, V. VESOVIC AND W. A. WAKEHAM. The inversion of thermophysical properties. I. Spherical systems revisited. *Mol. Phys.* **54**, 287 (1985).
- [60] D. E. KUEHNER, J. ENGMANN, F. FERGG, M. WERNICK, H. W. BLANCH AND J. M. PRAUSNITZ. Lysozyme net charge and ion binding in concentrated aqueous electrolyte solutions. *J. Phys. Chem. B* **103**, 1368 (1999).

- [61] J. D. WEEKS, D. CHANDLER AND H. C. ANDERSEN. Role of repulsive forces in determining the equilibrium structure of simple liquids. *J. Chem. Phys.* **54**, 5237 (1971); H. C. ANDERSEN, D. CHANDLER AND J. D. WEEKS. Roles of repulsive and attractive forces in liquids: the optimized random phase approximation. *J. Chem. Phys.* **56**, 3812 (1972).
- [62] H. C. ANDERSEN, J. D. WEEKS AND D. CHANDLER. Relationship between the hard-sphere fluid and fluids with realistic repulsive forces. *Phys. Rev. A* **4**, 1597 (1971).
- [63] S. BRAVO YUSTE AND A. SANTOS. Radial distribution function for sticky hard-core fluids. *J. Stat. Phys.* **72**, 703 (1993).
- [64] W. G. T. KRANENDONK AND D. FRENKEL. Simulation of the adhesive-hard-sphere model. *Mol. Phys.* **64**, 403 (1988).
- [65] T. NICOLAI AND M. MANDEL. Ionic strength dependence of the second virial coefficient of low molar mass DNA fragments in aqueous solutions. *Macromolecules* **22**, 438 (1989).
- [66] M. E. FERRARI AND V. A. BLOOMFIELD. Scattering and diffusion of mononucleosomal DNA: effects of counterion valence and salt and DNA concentration. *Macromolecules* **25**, 5266 (1992).
- [67] P. WISSEBURG, T. ODIJK, P. CIRKEL AND M. MANDEL. Multimolecular aggregation of mononucleosomal DNA in concentrated isotropic solutions. *Macromolecules* **28**, 2315 (1995).
- [68] J. POZNANSKI, Y. GEORGALIS, L. WEHR, W. SAENGER AND P. ZIELENKIEWICZ. Comparison of two different lysozyme types under native and crystallization conditions using two-dimensional NMR and dynamic light scattering. *Biophys. Chem.* **104**, 605 (2003).
- [69] G. STELL. Sticky spheres and related systems. *J. Stat. Phys.* **63**, 1203 (1991).
- [70] M. A. MILLER AND D. FRENKEL. Competition of percolation and phase separation in a fluid of adhesive hard spheres. *Phys. Rev. Lett.* **90**, 135702 (2003).
- [71] M. MALFOIS, F. BONNETÉ, L. BELLONI AND A. TARDIEU. A model of attractive interactions to account for fluid-fluid phase separation of protein solutions. *J. Chem. Phys.* **105**, 3290 (1996).
- [72] A. TARDIEU, A. LE VERGE, M. MALFOIS, F. BONNETÉ, S. FINET, M. RIÈS-KAUTT AND L. BELLONI. Proteins in solution: from X-ray scattering intensities to interaction potentials. *J. Cryst. Growth* **196**, 193 (1999).

- [73] V. VLACHY, H. W. BLANCH AND J. M. PRAUSNITZ. Liquid-liquid phase separations in aqueous solutions of globular proteins. *AIChE J.* **39**, 215 (1993).
- [74] J. J. GRIGSBY, H. W. BLANCH AND J. M. PRAUSNITZ. Cloud-point temperatures for lysozyme in electrolyte solutions: effect of salt type, salt concentration and pH. *Biophys. Chem.* **91**, 231 (2001).
- [75] D. N. PETSEV, X. WU, O. GALKIN AND P. G. VEKILOV. Thermodynamic functions of concentrated protein solutions from phase equilibria. *J. Phys. Chem. B* **107**, 3921 (2003).
- [76] T. H. GRONWALL, V. K. LA MER AND K. SANDVED. Über den Einfluß der sogenannten höheren Glieder in der Debye-Hückelschen Theorie der Lösungen starker Elektrolyte. *Physik. Z.* **29**, 358 (1928).
- [77] P. T. CUMMINGS, J. W. PERRAM AND E. R. SMITH. Percus-Yevick theory of correlation functions and nucleation effects in the sticky hard-sphere model. *Mol. Phys.* **31**, 535 (1976).
- [78] B. BARBOY AND R. TENNE. Distribution functions and equations of state of sticky hard sphere fluids in the Percus-Yevick approximation. *Chem. Phys.* **38**, 369 (1979).
- [79] A. J. POST AND E. D. GLANDT. Cluster concentrations and virial coefficients for adhesive particles. *J. Chem. Phys.* **84**, 4585 (1986).
- [80] D. GAZZILLO AND A. GIACOMETTI. Analytical solutions for Baxter's model of sticky hard sphere fluids within closures different from the Percus-Yevick approximation. *J. Chem. Phys.* **120**, 4742 (2004).
- [81] N. A. SEATON AND E. D. GLANDT. Monte Carlo simulation of adhesive spheres. *J. Chem. Phys.* **87**, 1785 (1987).
- [82] M. A. MILLER AND D. FRENKEL. Simulating colloids with Baxter's adhesive hard sphere model. *J. Phys.: Condens. Matter* **16**, S4901 (2004).
- [83] M. DIJKSTRA. Phase behavior of hard spheres with a short-range Yukawa attraction. *Phys. Rev. E* **66**, 021402 (2002).
- [84] D. FRENKEL AND B. SMIT. *Understanding Molecular Simulation: from Algorithms to Applications*. Academic Press, San Diego, CA, U.S.A., 2002.
- [85] R. J. SPEEDY. Pressure of the metastable hard-sphere fluid. *J. Phys.: Condens. Matter* **9**, 8591 (1997).
- [86] R. J. SPEEDY. Pressure and entropy of hard-sphere crystals. *J. Phys.: Condens. Matter* **10**, 4387 (1998).

- [87] J. M. POLSON, E. TRIZAC, S. PRONK AND D. FRENKEL. Finite-size corrections to the free energies of crystalline solids. *J. Chem. Phys.* **112**, 5339 (2000).
- [88] The concept of “mathematical similarity” or “similarity” is well explained in: G.I. BARENBLATT. *Similarity, Self-similarity, and Intermediate Asymptotics*. Consultants Bureau, New York, NY, U.S.A., 1979. For instance, in our case, the pressure which was originally some function of η , β and κ , is proposed to be a function of η and τ only, via argumentation based on the optimized Baxter model. Hence, a system defined by η_1 , β_1 and κ_1 is mathematically *similar* to that defined by η_1 , β_2 and κ_2 if $\tau(\beta_1, \kappa_1) = \tau(\beta_2, \kappa_2)$.
- [89] W. G. HOOVER. Entropy for small classical crystals. *J. Chem. Phys.* **49**, 1981 (1968).
- [90] B. GUO, S. KAO, H. McDONALD, A. ASANOV, L. L. COMBS AND W. W. WILSON. Correlation of second virial coefficients and solubilities useful in protein crystal growth. *J. Cryst. Growth* **196**, 424 (1999).
- [91] R. A. CURTIS, H. W. BLANCH AND J. M. PRAUSNITZ. Calculation of phase diagrams for aqueous protein solutions. *J. Phys. Chem. B* **105**, 2445 (2001).
- [92] E. CACIOPPO AND M. L. PUSEY. The solubility of the tetragonal form of hen egg white lysozyme from pH 4.0 to 5.4. *J. Cryst. Growth* **114**, 286 (1991).
- [93] M. BOSTRÖM, D. R. M. WILLIAMS AND B. W. NINHAM. Surface tension of electrolytes: specific ion effects explained by dispersion forces. *Langmuir* **17**, 4475 (2001).
- [94] F. W. TAVARES, D. BRATKO, H. W. BLANCH AND J. M. PRAUSNITZ. Ion-specific effects in the colloid-colloid or protein-protein potential of mean force: role of salt-macroion van der Waals interactions. *J. Phys. Chem. B* **108**, 9228 (2004).
- [95] M. AUBOUY, E. TRIZAC AND L. BOCQUET. Effective charge versus bare charge: an analytical estimate for colloids in the infinite dilution limit. *J. Phys. A* **36**, 5835 (2003).
- [96] R. FOWLER AND E. A. GUGGENHEIM. *Statistical Thermodynamics*. Cambridge University Press, Cambridge, U.K., 1956.
- [97] W. C. K. POON, S. U. EGELHAAF, P. A. BEALES, A. SALONEN AND L. SAWYER. Protein crystallization: scaling of charge and salt concentration in lysozyme solutions. *J. Phys.: Condens. Matter* **12**, L569 (2000); P. B. WARREN. Simple models for charge and salt effects in protein crystallization. *J. Phys.: Condens. Matter* **14**, 7617 (2002).

- [98] L. K. STEINRAUF. Preliminary X-ray data for some new crystalline forms of β -lactoglobulin and hen egg-white lysozyme. *Acta Crystallogr.* **12**, 77 (1959).
- [99] A. NADARAJAH AND M. L. PUSEY. Growth mechanism and morphology of tetragonal lysozyme crystals. *Acta Crystallogr. D* **52**, 983 (1996).
- [100] V. MIKOL, E. HIRSCH AND R. GIEGÉ. Diagnostic of precipitant for biomacromolecule crystallization by quasi-elastic light-scattering. *J. Mol. Biol.* **213**, 187 (1990).
- [101] M. RIÈS-KAUTT, A. DUCRUIX AND A. VAN DORSSELAER. Crystallization of previously desalted lysozyme in the presence of sulfate ions. *Acta Crystallogr. D* **50**, 366 (1994).
- [102] M. GE, A. A. GEWIRTH, W. G. KLEMPERER AND C. G. WALL. A structural model for silicotungstate (α -SiW₁₂O₄₀⁴⁻) monolayers on silver (111). *Pure & Appl. Chem.* **69**, 2175 (1997).
- [103] M. C. BAKER, P. A. LYONS AND S. J. SINGER. Velocity ultracentrifugation and diffusion of silicotungstic acid. *J. Am. Chem. Soc.* **77**, 2011 (1955).
- [104] T. KURUCSEV, A. M. SARGESON AND B. O. WEST. Size and hydration of inorganic ions from viscosity and density measurements. *J. Phys. Chem.* **61**, 1567 (1957).
- [105] C. F. ZUKOSKI, D. F. ROSENBAUM AND P. C. ZAMORA. Aggregation in precipitation reactions: stability of primary particles. *Chem. Eng. Res. Des.* **74**, 723 (1996).
- [106] L. D. LANDAU AND E. M. LIFSHITZ. *Theory of Elasticity*, 3rd ed. Pergamon, Oxford, U.K., 1986.
- [107] F. OOSAWA. *Polyelectrolytes*. Marcel Dekker, Inc., New York, NY, U.S.A., 1971.
- [108] T. ODIJK. Statics and dynamics of condensed DNA within phages and globules. *Philos. Trans. R. Soc. London, Ser. A* **362**, 1497 (2004).
- [109] D. STIGTER. Interactions of highly charged colloidal cylinders with applications to double-stranded DNA. *Biopolymers* **16**, 1435 (1977).
- [110] T. ODIJK AND F. SLOK. Nonuniform Donnan equilibrium within bacteriophages packed with DNA. *J. Phys. Chem. B* **107**, 8074 (2003).
- [111] M. J. KRONMAN AND S. N. TIMASHEFF. Light scattering investigation of ordering effects in silicotungstic acid solutions. *J. Phys. Chem.* **63**, 629 (1959).

- [112] P. C. ZAMORA AND C. F. ZUKOSKI. Interactions and phase behavior of nanosized particles. *Langmuir* **12**, 3541 (1996).
- [113] G. WYROUBOFF. Untersuchungen über die Silicotungstate. *Z. Krist.* **29**, 659 (1898).
- [114] H. T. EVANS. in *Perspectives in Structural Chemistry*, ed. by J. D. Dunitz and J. A. Ibers. Wiley, New York, NY, U.S.A., 1971.
- [115] O. KRAUS. Untersuchungen über das Kristallgitter von Heteropolysäuren und deren Salzen. 3. Mitteilung. Beitrag zur Kenntnis der Isomorphieerscheinungen und der strukturellen Beziehungen bei den höheren Hydraten von Heteropolyverbindungen. *Z. Krist.* **94**, 256 (1936).
- [116] R. J. MEYER. *Gmelins Handbuch der Anorganischen Chemie, Wolfram*. Verlag Chemie, Berlin, Germany, 1933.
- [117] S. S. ALPERT AND G. BANKS. The concentration dependence of the hemoglobin mutual diffusion coefficient. *Biophys. Chem.* **4**, 287 (1976).
- [118] A. P. MINTON AND P. D. ROSS. Concentration dependence of the diffusion coefficient of hemoglobin. *J. Phys. Chem.* **82**, 1934 (1978).
- [119] R. S. HALL, Y. S. OH AND C. S. JOHNSON, JR. Photon correlation spectroscopy in strongly absorbing and concentrated samples with applications to unliganded hemoglobin. *J. Phys. Chem.* **84**, 756 (1980).
- [120] K. J. LAGATTUTA, V. S. SHARMA, D. F. NICOLI AND B. K. KOTHARI. Diffusion coefficients of hemoglobin by intensity fluctuation spectroscopy. Effects of varying pH and ionic strength. *Biophys. J.* **33**, 63 (1981).
- [121] S. BERETTA, G. CHIRICO, D. AROSIO AND G. BALDINI. Photon correlation spectroscopy of interacting and dissociating hemoglobin. *J. Chem. Phys.* **106**, 8427 (1997).
- [122] I. TINOCO, JR. AND P. A. LYONS. Diffusion of isoionic, salt-free bovine serum albumin. *J. Phys. Chem.* **60**, 1342 (1956).
- [123] T. RAJ AND W. H. FLYGARE. Diffusion studies of bovine serum albumin by quasielastic light scattering. *Biochemistry* **13**, 3336 (1974).
- [124] G. D. J. PHILLIES, G. B. BENEDEK AND N. A. MAZER. Diffusion in protein solutions at high concentrations: A study by quasielastic light scattering spectroscopy. *J. Chem. Phys.* **65**, 1883 (1976).
- [125] J. L. ANDERSON, F. RAUH AND A. MORALES. Particle diffusion as a function of concentration and ionic strength. *J. Phys. Chem.* **82**, 608 (1978).

- [126] C. LE BON, T. NICOLAI, M. E. KUIL AND J. G. HOLLANDER. Self-diffusion and cooperative diffusion of globular proteins in solution. *J. Phys. Chem. B* **103**, 10294 (1999).
- [127] S. J. GIBBS, A. S. CHU, E. N. LIGHTFOOT AND T. W. ROOT. Ovalbumin diffusion at low ionic strength. *J. Phys. Chem.* **95**, 467 (1991).
- [128] B. NYSTRÖM AND R. M. JOHNSEN. Effect of concentration and ionic strength on the translational diffusion coefficient of lysozyme. *Chem. Scripta* **22**, 82 (1983).
- [129] A. Y. MIRAREFI AND C. F. ZUKOSKI. Gradient diffusion and protein solubility: use of dynamic light scattering to localize crystallization conditions. *J. Cryst. Growth* **265**, 274 (2004).
- [130] J. ZHANG AND X. Y. LIU. Effect of protein-protein interactions on protein aggregation kinetics. *J. Chem. Phys.* **119**, 10972 (2003).
- [131] M. SKOURI, J.-P. MUNCH, B. LORBER, R. GIEGÉ AND S. CANDAU. Interactions between lysozyme molecules under precrystallization conditions studied by light scattering. *J. Cryst. Growth* **122**, 14 (1992).
- [132] W. EBERSTEIN, Y. GEORGALIS AND W. SAENGER. Molecular interactions in crystallizing lysozyme solutions studied by photon correlation spectroscopy. *J. Cryst. Growth* **143**, 71 (1994).
- [133] C. LEGGIO, L. GALANTINI, E. ZACCARELLI AND N. V. PAVEL. Small-angle X-ray scattering and light scattering on lysozyme and sodium glycocholate micelles. *J. Phys. Chem. B* **109**, 23857 (2005).
- [134] W. S. PRICE, F. TSUCHIYA AND Y. ARATA. Lysozyme aggregation and solution properties studied using PGSE NMR diffusion measurements. *J. Am. Chem. Soc.* **121**, 11503 (1999).
- [135] O. ANNUNZIATA, D. BUZATU AND J. G. ALBRIGHT. Protein diffusion coefficients determined by macroscopic-gradient Rayleigh interferometry and dynamic light scattering. *Langmuir* **21**, 12085 (2005).
- [136] P. RETAILLEAU, M. RIÈS-KAUTT, A. DUCRUIX, L. BELLONI, S. J. CANDAU AND J. P. MUNCH. Coulombic interaction and ion-protein macroion coupled diffusion evidenced by light scattering. *Europhys. Lett.* **46**, 154 (1999).
- [137] J. NARAYANAN AND X. Y. LIU. Protein interactions in undersaturated and supersaturated solutions: a study using light and X-ray scattering. *Biophys. J.* **84**, 523 (2003).

- [138] B. U. FELDERHOF. Diffusion of interacting Brownian particles. *J. Phys. A* **11**, 929 (1978).
- [139] C. VAN DEN BROECK, F. LOSTAK AND H. N. W. LEKKERKERKER. The effect of direct interactions on Brownian diffusion. *J. Chem. Phys.* **74**, 2006 (1981).
- [140] T. OHTSUKI AND K. OKANO. Diffusion coefficients of interacting Brownian particles. *J. Chem. Phys.* **77**, 1443 (1982).
- [141] B. CICHOCKI AND B. U. FELDERHOF. Diffusion coefficients and effective viscosity of suspensions of sticky hard spheres with hydrodynamic interactions. *J. Chem. Phys.* **93**, 4427 (1990).
- [142] U. GENZ AND R. KLEIN. Collective diffusion of charged spheres in the presence of hydrodynamic interaction. *Physica A* **171**, 26 (1991).
- [143] D. N. PETSEV AND N. D. DENKOV. Diffusion of charged colloidal particles at low volume fraction: theoretical model and light scattering experiments. *J. Coll. Int. Sci.* **149**, 329 (1992).
- [144] N. D. DENKOV AND D. N. PETSEV. Light scattering and diffusion in suspensions of strongly charged particles at low volume fractions. *Physica A* **183**, 462 (1992).
- [145] D. N. PETSEV, N. D. DENKOV AND K. NAGAYAMA. Diffusion and light scattering in dispersions of charged particles with thin electrical double layers. *Chem. Phys.* **175**, 265 (1993).
- [146] J. GAPINSKI, A. WILK, A. PATKOWSKI, W. HÄUSSLER, A. J. BANCHIO, R. PECORA AND G. NÄGELE. Diffusion and microstructural properties of solutions of charged nanosized proteins: Experiment versus theory. *J. Chem. Phys.* **123**, 054708 (2005).
- [147] M. A. LAMPERT AND R. S. CRANDALL. Spherical, nonlinear Poisson-Boltzmann theory and its Debye-Hückel linearization. *Chem. Phys. Lett.* **68**, 473 (1979).
- [148] M. A. LAMPERT AND R. S. CRANDALL. Fate of the Coulomb singularity in nonlinear Poisson-Boltzmann theory: The point charge as an electrically invisible object. *Phys. Rev. A* **21**, 362 (1980).
- [149] N. MARTINOV, D. OUROUSHEV AND E. CHELEBIEV. New types of polarisation following from the non-linear spherical radial Poisson-Boltzmann equation. *J. Phys. A* **19**, 1327 (1986).
- [150] G. V. RAMANATHAN. Counterion condensation in micellar and colloidal solutions. *J. Chem. Phys.* **88**, 3887 (1988).

- [151] S. ALEXANDER, P. M. CHAIKIN, P. GRANT, G. J. MORALES, P. PINCUS AND D. HONE. Charge renormalization, osmotic pressure, and bulk modulus of colloidal crystals: Theory. *J. Chem. Phys.* **80**, 5776 (1984).
- [152] W. C. CHEW AND P. N. SEN. Potential of a sphere in an ionic solution in thin double layer approximations. *J. Chem. Phys.* **77**, 2042 (1982).
- [153] H. OHSHIMA, T. W. HEALY AND L. R. WHITE. Accurate analytic expressions for the surface charge density/surface potential relationship and double-layer potential distribution for a spherical colloidal particle. *J. Coll. Int. Sci.* **90**, 17 (1982).
- [154] G. WEISBUCH AND M. GUÉRON. Polyelectrolyte theory. 3. The surface potential in mixed-salt solutions. *J. Phys. Chem.* **85**, 517 (1981).
- [155] I. A. SHKEL, O. V. TSODIKOV AND M. T. RECORD, JR. Complete asymptotic solution of cylindrical and spherical Poisson-Boltzmann equations at experimental salt concentrations. *J. Phys. Chem. B* **104**, 5161 (2000).
- [156] B. CICHOCKI AND B. U. FELDERHOF. Short-time diffusion coefficients and high frequency viscosity of dilute suspensions of spherical Brownian particles. *J. Chem. Phys.* **89**, 1049 (1988).
- [157] G. K. BATCHELOR. Brownian diffusion of particles with hydrodynamic interaction. *J. Fluid Mech.* **74**, 1 (1976).
- [158] G. K. BATCHELOR AND J. T. GREEN. The hydrodynamic interaction of two small freely-moving spheres in a linear flow field. *J. Fluid Mech.* **56**, 375 (1972).
- [159] A. J. GOLDMAN, R. G. COX AND H. BRENNER. The slow motion of two identical arbitrarily oriented spheres through a viscous fluid. *Chem. Eng. Sci.* **21**, 1151 (1966).
- [160] M. D. A. COOLEY AND M. E. O'NEILL. On slow motion of 2 spheres in contact along their line of centres through a viscous fluid. *Proc. Cambridge Philos. Soc.* **66**, 407 (1969).
- [161] A. NIR AND A. ACRIVOS. On the creeping motion of two arbitrary-sized touching spheres in a linear shear field. *J. Fluid Mech.* **59**, 209 (1973).
- [162] D. J. JEFFREY AND Y. ONISHI. Calculation of the resistance and mobility functions for two unequal rigid spheres in low-Reynolds-number flow. *J. Fluid Mech.* **139**, 261 (1984).
- [163] M. STIMSON AND G. B. JEFFERY. The motion of two spheres in a viscous fluid. *Proc. R. Soc. London, Ser. A* **111**, 110 (1926).

- [164] H. BRENNER. The slow motion of a sphere through a viscous fluid towards a plane surface. *Chem. Eng. Sci.* **16**, 242 (1961).
- [165] M. E. O'NEILL AND S. R. MAJUMDAR. Asymmetrical slow viscous fluid motions caused by the translation or rotation of two spheres. Part I: The determination of exact solutions for any value of the ratio of radii and separation parameters. *Z. Angew. Math. Phys.* **21**, 164 (1970).
- [166] M. E. O'NEILL AND B. S. BHATT. Slow motion of a solid sphere in the presence of a naturally permeable surface. *Q. J. Mech. Appl. Math.* **44**, 91 (1991).
- [167] M. CHAOUI AND F. FEUILLEBOIS. Creeping flow around a sphere in a shear flow close to a wall. *Q. J. Mech. Appl. Math.* **56**, 381 (2003).
- [168] M. FIXMAN. Variational theorem for the generalized diffusion matrix. *J. Chem. Phys.* **76**, 6124 (1982).
- [169] A. J. GOLDMAN, R. G. COX AND H. BRENNER. Slow viscous motion of a sphere parallel to a plane wall—I. Motion through a quiescent fluid. *Chem. Eng. Sci.* **22**, 637 (1967).



Summary

Statistical mechanics of protein solutions

The goal of this thesis is to develop a thermodynamic description of solutions of globular proteins in water with added monovalent salt. Current theories mainly focus on low concentrations of protein but here we also look at higher concentrations. A better understanding of the thermodynamic behavior of protein solution helps, for example, in finding the right conditions to grow protein crystals for structure determination or can assist in developing new food products.

In the first part of Chapter 1 we give an introduction to proteins. Then we show how one can build a theory to describe protein solutions and we explain which difficulties one runs into, for example the fact that one has to introduce an attractive interaction to explain the experimental data or the fact that the virial approach does not work at high concentrations, and we show how we deal with them. This part serves as an introduction to the theory in the rest of the thesis and focuses on some points that are not explained further on. The last part of the introduction deals with some issues of the theory more thoroughly. We go deeper into the one-component description and we show what the potential of mean force is, from a statistical mechanical point of view. We also show some thermodynamic properties of adhesive hard spheres, spherical particles with a hard-core repulsion and a sticky attraction, that are useful later on.

In Chapter 2, we set up a theory to describe the thermodynamic behavior of protein solutions. We assume the particles are spherical and we approximate the interaction potential by an isotropic interaction that consists of a steric interaction plus an electrostatic repulsion and a short range attraction. We then approximate the system by an adhesive hard sphere (AHS) system and we derive an approximate expression for the stickiness parameter in the AHS system as a function of ionic strength by equating second virials. We apply this to lysozyme

solutions at pH 4.5. The steric interaction is determined by the size of the protein, which is known, and the electrostatic interaction depends on the charge, which we know from titration experiments. We determine the ionic strength-independent range and strength of the short range attraction by fitting second virial data as a function of ionic strength and we show that we can also predict the second virial coefficient at pH 7.5 by using the same values for these two parameters. Thermodynamic properties of the lysozyme solution at low concentrations of protein can then be determined by using the results from the AHS model at low concentrations and the relation between the stickiness parameter and the properties of the lysozyme solution (for example ionic strength and protein charge).

Next we develop a theory to deal with protein solutions at higher concentrations of protein. We again approximate the original system by the AHS system but now we determine the stickiness by matching the free energies of the two systems. We do this by making a functional expansion of the free energy of the original system with the AHS system as the reference system. The stickiness, which now also depends on the protein concentration, is determined by putting the first order correction in the expansion equal to zero. We call this procedure the optimized Baxter model (OBM). We then use these results to predict (there are no adjustable parameters in our theory) the compressibility of lysozyme solutions at pH 4.5 as a function of protein concentration for various values of the ionic strength. We show that we can predict the experimental data pretty well.

In Chapter 2 we use the OBM to predict experimental data on lysozyme solutions. However, both the OBM and the interaction potential are approximate and it is unclear how much each approximation contributes to the error. Therefore we test the OBM in Chapter 3 on a system with a known interaction potential, the Yukawa system. We perform Monte Carlo simulations on the Yukawa system to determine thermodynamic properties such as the pressure and the chemical potential and we then compare the results to predictions of the OBM. First we show that we can predict these properties very well along the fluid line of the fluid-solid coexistence region. Then we do a consistency test in the fluid phase. For a given range of the Yukawa interaction and a given particle concentration we predict what the strength of the interaction has to be to get a certain value for the stickiness. Then we determine the pressure and chemical potential by simulation and we compare these to pressures and chemical potentials at the same stickiness and particle concentration but different ranges of the Yukawa interaction to see if they are indeed equal, as the OBM predicts. An advantage of doing this in such a way is that we then only need the accurate pair correlation function for the AHS system and not the expressions for the thermodynamic properties, which are only approximate. We show that the OBM is accurate to within 10 percent and is actually much more precise in most cases. We also show that the naive method of equating second virials performs not as well as the OBM.

In Chapter 4 we use the OBM to determine the pressure and chemical potential of protein crystals and of crystals of inorganic colloids. We do this indirectly by determining these properties for the surrounding liquid which is in equilibrium

with the crystal. We then apply this to lysozyme crystals and to crystals of Silicotungstate (STA). We then set up a theory for the crystal phase. We calculate the electrostatic part of the crystal free energy by assuming that the interstitial volumes are spherical and we solve the Poisson-Boltzmann equation to determine the effective charge of the particles in the salt-free case. Then a Donnan approximation is used to calculate the pressure and chemical potential when salt is present. We show that the salt dependence of the chemical potential agrees with experiments.

In the final chapter, Chapter 5, we study the collective diffusion of proteins. The collective diffusion coefficient describes how a protein solution reacts to a small gradient in the protein concentration. It is a non-equilibrium property and it is not clear whether we can still use the results from the OBM, since the stickiness parameter is determined by matching equilibrium properties (the second virial coefficient or the free energy). We show that one can still do this, however, since, although the method is not exact, the error is only small. We predict the collective diffusion coefficient for lysozyme at pH 4.5 as a function of ionic strength for low concentrations of lysozyme and we show that the results compare well with experimental data.

Peter Prinsen



Samenvatting

Statistische mechanica van eiwitoplossingen

Het doel van dit proefschrift is het ontwikkelen van een thermodynamische beschrijving van waterige oplossingen van globulaire eiwitten met toegevoegd enkelwaardig zout. Bestaande theorieën richten zich voornamelijk op lage concentraties eiwit maar wij bekijken hier ook hogere concentraties. Een beter begrip van het thermodynamisch gedrag van eiwitoplossingen draagt bijvoorbeeld bij aan het vinden van de juiste omstandigheden voor de groei van eiwitkristallen, die gebruikt kunnen worden voor de bepaling van de structuur van het eiwit, of het kan helpen bij het ontwikkelen van nieuwe voedselproducten.

In het eerste deel van Hoofdstuk 1 geven we een inleiding over eiwitten. Vervolgens laten we zien hoe men een theorie kan opbouwen waarmee eiwitoplossingen beschreven kunnen worden en we leggen uit tegen wat voor soort problemen men aan kan lopen, bijvoorbeeld het feit dat men een aantrekkende wisselwerking in moet voeren om de experimentele gegevens te verklaren of het feit dat de viriaalbenadering niet werkt bij hoge eiwitconcentraties, en we laten zien hoe we met deze problemen omgaan. Dit gedeelte dient als een inleiding tot de theorie in de rest van het proefschrift en het richt zich op een aantal punten dat verderop niet wordt uitgelegd. Het laatste gedeelte van de inleiding behandelt enkele onderdelen van de theorie wat uitvoeriger. We gaan wat dieper in op de één-component beschrijving en we laten zien wat een potentiaal van gemiddelde kracht is, vanuit een statistisch mechanisch oogpunt. We tonen ook enkele thermodynamische eigenschappen van plakkende harde bollen, bolvormige deeltjes met een harde afstoting en een plakkerige aantrekking, die later in het proefschrift gebruikt worden.

In Hoofdstuk 2 bouwen we een theorie op om het thermodynamisch gedrag van eiwitoplossingen mee te beschrijven. We nemen aan dat de deeltjes bolvormig zijn en we benaderen de wisselwerkingspotentiaal door een isotrope wisselwerking

die bestaat uit een sterische afstoting plus een elektrostatische afstoting en een aantrekking met korte dracht. Vervolgens benaderen we het systeem met een systeem van plakkende harde bollen (AHS-systeem) en we leiden een benaderde uitdrukking af voor de parameter die de sterkte van de plakkende kracht aanduidt als functie van de ionsterkte door tweede viriaalcoëfficiënten aan elkaar gelijk te stellen. Dit passen we vervolgens toe op oplossingen van lysozyme bij een pH van 4.5. De sterische wisselwerking wordt bepaald door de grootte van het eiwit, welke bekend is, en de elektrostatische wisselwerking hangt af van de lading, die we kennen door titratie-experimenten. We bepalen de dracht en sterkte van de aantrekkende wisselwerking, welke niet van de ionsterkte afhangen, aan de hand van experimentele gegevens van de tweede viriaalcoëfficiënt als functie van de ionsterkte, en we laten zien dat we de tweede viriaalcoëfficiënt bij een pH van 7.5 kunnen voorspellen door dezelfde waardes voor deze twee parameters te nemen. Thermodynamische eigenschappen van de lysozyme-oplossing bij lage eiwitconcentraties kunnen dan worden bepaald door resultaten van het AHS-systeem bij lage concentraties te gebruiken samen met de relatie tussen de plakkracht en de eigenschappen van de lysozyme-oplossing (bijvoorbeeld de ionsterkte en de eiwitlading).

Vervolgens ontwikkelen we een theorie die eiwitoplossingen bij hogere eiwitconcentraties beschrijft. We benaderen het oorspronkelijke systeem weer door het AHS-systeem maar nu bepalen we de plakkracht door de vrije energieën van de twee systemen aan elkaar gelijk te stellen. We doen dit door een functionaalontwikkeling van de vrije energie van het oorspronkelijke systeem te maken waarbij we het AHS-systeem als referentiesysteem gebruiken. De plakkracht, die nu ook van de eiwitconcentratie afhangt, wordt bepaald door de eerste-orde correctie in de ontwikkeling gelijk aan nul te stellen. We noemen deze methode “the optimized Baxter model” (OBM), oftewel het geoptimaliseerde Baxter model. We gebruiken dit resultaat vervolgens om de samendrukbaarheid van de lysozyme-oplossing bij een pH van 4.5 en verschillende ionsterkten te voorspellen (de theorie bevat geen aanpasbare parameters). We laten zien dat we de experimentele gegevens vrij aardig kunnen voorspellen.

In Hoofdstuk 2 hebben we het OBM gebruikt om experimentele gegevens van lysozyme-oplossingen te voorspellen. Echter, zowel het OBM zelf als de wisselwerkingspotentiaal die we gebruiken is een benadering en het is onduidelijk hoeveel elk bijdraagt aan de totale fout. Om die reden testen we het OBM in Hoofdstuk 3 op een systeem met een wisselwerking die bekend is, de Yukawa-wisselwerking. We doen Monte Carlo simulaties van het Yukawa-systeem om thermodynamische eigenschappen zoals de druk en de chemische potentiaal te bepalen en vervolgens vergelijken we deze resultaten met voorspellingen van het OBM. Eerst laten we zien dat we deze eigenschappen erg goed kunnen voorspellen langs de coëxistentielijn van de vloeistof en de vaste stof. Vervolgens testen we de consistentie van de methode. Voor een gegeven dracht van de Yukawa-wisselwerking en een gegeven deeltjesconcentratie voorspellen we wat de sterkte van de wisselwerking moet zijn om een bepaalde waarde voor de plakkracht te

krijgen. Vervolgens bepalen we de druk en de chemische potentiaal in de simulatie en we vergelijken deze met de drukken en de chemische potentialen behorende bij dezelfde plakkracht en deeltjesconcentratie maar bij andere lengtes van de dracht van de Yukawa-wisselwerking om te zien of deze inderdaad gelijk zijn, zoals het OBM voorspelt. Een voordeel van deze methode is dat men zo het OBM kan testen onafhankelijk van de uitdrukkingen voor de thermodynamische eigenschappen van het AHS-systeem, welke minder nauwkeurig bekend zijn, omdat men alleen de nauwkeurig bekende paarcorrelatiefunctie van het AHS-systeem nodig heeft. We laten zien dat het OBM binnen 10 procent nauwkeurig is en in veel gevallen zelfs een stuk nauwkeuriger. We laten ook zien dat de naieve methode waarbij men tweede viriaalcoëfficiënten aan elkaar gelijkstelt slechter presteert dan de OBM-methode.

In Hoofdstuk 4 gebruiken we het OBM om de druk en de chemische potentiaal van eiwitkristallen en van kristallen van anorganische colloïden te bepalen. We doen dit op een indirecte wijze door deze eigenschappen te bepalen voor de omringende vloeistof welke in evenwicht is met het kristal. We passen dit toe op lysozymekristallen en kristallen van siliciumwolframaat. Vervolgens ontwikkelen we een theorie voor de kristallijne fase. We berekenen het elektrostatische gedeelte van de vrije energie van het kristal door aan te nemen dat de tussenruimtes tussen de deeltjes bolvormig zijn en we lossen de Poisson-Boltzmann vergelijking op om de effectieve lading van de deeltjes in het zoutloze geval te bepalen. Vervolgens gebruiken we een Donnan-benadering om de druk en chemische potentiaal te bepalen in aanwezigheid van het zout. We laten zien dat de zoutafhankelijkheid van de chemische potentiaal overeenkomt met experimentele resultaten.

In het laatste hoofdstuk, Hoofdstuk 5, bestuderen we de collectieve diffusie van eiwitten. De collectieve diffusiecoëfficiënt beschrijft hoe een eiwitoplossing reageert op een kleine gradient in de eiwitconcentratie. Het is een niet-evenwichtseigenschap en het is onduidelijk of we de resultaten van het OBM hier kunnen gebruiken omdat de plakkracht bepaald is door evenwichtseigenschappen aan elkaar gelijk te stellen (de tweede viriaalcoëfficiënt of de vrije energie). Echter, wij laten zien dat men dit kan doen omdat, hoewel de methode niet exact is, de gemaakte fout klein is. We voorspellen de collectieve diffusiecoëfficiënt van lysozyme bij een pH van 4.5 als functie van de ionsterkte bij lage eiwitconcentraties en we laten zien dat de resultaten goed overeenkomen met experimentele resultaten.



Curriculum Vitae

Peter Prinsen is geboren op 18 december 1977 te 's-Hertogenbosch. Van 1990 tot 1996 bezocht hij het Stedelijk Gymnasium te 's-Hertogenbosch, waar hij in 1996 zijn VWO-diploma behaalde. Daarna begon hij aan een studie Technische Natuurkunde en een studie Technische Wiskunde aan de Technische Universiteit te Eindhoven. Tijdens zijn studie bracht hij drie maanden door op het Unilever Research Laboratory te Port Sunlight in het Verenigd Koninkrijk. Hij deed daar, onder begeleiding van dr. P. B. Warren, theoretisch onderzoek aan surfactanten. Vervolgens voerde hij zijn afstudeeronderzoek, getiteld “De vorm van een nematische druppel vloeibaar kristal in de isotrope fase”, uit in de vakgroep Polymerfysica onder begeleiding van dr. P. P. A. M. van der Schoot uit deze vakgroep en prof. dr. J. Molenaar van de faculteit Wiskunde en Informatica. Dit onderzoek werd bekroond met de Mignot afstudeerprijs 2003. In 2002 studeerde hij cum laude af in zowel de Technische Natuurkunde als de Technische Wiskunde.

Op 1 januari 2003 trad hij als promovendus in dienst bij de Technische Universiteit Delft. Hij verrichtte daar onderzoek onder begeleiding van prof. dr. T. Odijk in de onderzoeksgroep Theorie van Complexe Vloeistoffen van de faculteit Technische Natuurwetenschappen. Resultaten van dit onderzoek zijn onder andere gepresenteerd in Lunteren (Wetenschappelijke Vergadering Statistische Fysica, Nederland 2004, en Wetenschappelijke Bijeenkomst studiegroep Vloeistoffen en Grensvlakken, Nederland 2004), Göteborg (5th International Conference on Biological Physics, Zweden 2004), Lausanne (First international symposium on the delivery of functionality in complex systems, Zwitserland 2005) en Leiden (Lorentz workshop over “Screening, charge inversion and condensation of macroions”, Nederland 2005). Tijdens deze periode deed hij 3 maanden onderzoek met prof. dr. D. R. M. Williams aan de Australian National University (ANU) in Canberra, Australië.

In december 2006 heeft hij een Rubicon beurs van de Nederlandse Organisatie voor Wetenschappelijk Onderzoek (NWO) ontvangen waarmee hij vanaf 1 mei 2007 twee jaar lang onderzoek zal verrichten als post-doctoraal medewerker in de Virus Research Group van prof. dr. W. M. Gelbart en prof. dr. C. M. Knobler aan de University of California, Los Angeles (UCLA) in de Verenigde Staten.

Peter Prinsen was born on the 18th of December 1977 in 's-Hertogenbosch, in The Netherlands. From 1990 until 1996 he attended the Stedelijk Gymnasium in 's-Hertogenbosch, where he received his highschool diploma in 1996. He then went to Eindhoven University of Technology to study Applied Physics and Industrial and Applied Mathematics. During this time, he spent three months at the Unilever Research Laboratory in Port Sunlight in the United Kingdom. Under supervision of dr. P. B. Warren, he performed theoretical research on surfactants. He then went on to do his Master's thesis research in the section Polymer Physics under supervision of dr. P. P. A. M. van der Schoot from this section and prof. dr. J. Molenaar from the department of Mathematics and Computer Science. The title of his thesis is "De vorm van een nematische druppel vloeibaar kristal in de isotrope fase" ("The shape of a nematic tactoid in an isotropic environment"). He was awarded the Mignot prize 2003 for his thesis and in 2002 he graduated cum laude in both Applied Physics and Industrial and Applied Mathematics.

On the first of January 2003 he started his PhD research at the Delft University of Technology under supervision of prof. dr. T. Odijk from the section Complex Fluids Theory of the faculty of Applied Sciences. Results of this research were presented in Lunteren (Wetenschappelijke Vergadering Statistische Fysica (Scientific meeting Statistical Physics), Nederland 2004 and Wetenschappelijke Bijeenkomst studiegroep Vloeistoffen en Grensvlakken (Scientific meeting Liquids and Interfaces), Nederland 2004), Gothenburg (5th International Conference on Biological Physics, Sweden 2004), Lausanne (First international symposium on the delivery of functionality in complex systems, Switzerland 2005) and Leiden (Lorentz workshop on "Screening, charge inversion and condensation of macroions", The Netherlands 2005). During this period he spent three months at the Australian National University (ANU) in Canberra, Australia, where he did research with prof. dr. D. R. M. Williams.

In December 2006 he received a Rubicon grant from the Netherlands Organisation for Scientific Research (NWO) which he will use to spend two years as a postdoctoral researcher in the Virus Research Group of prof. dr. W. M. Gelbart and prof. dr. C. M. Knobler at the University of California, Los Angeles (UCLA) in the United States, starting on the first of May 2007.



List of Publications

This thesis is based on the following publications:

- P. PRINSEN AND T. ODIJK. Optimized Baxter model of protein solutions: Electrostatics versus adhesion. *Journal of Chemical Physics* **121**, 6525 (2004) (Chapter 2).
- P. PRINSEN AND T. ODIJK. Fluid-crystal coexistence for proteins and inorganic nanocolloids: Dependence on ionic strength. *Journal of Chemical Physics* **125**, 074903 (2006) (Chapter 4).
- P. PRINSEN, J. C. PÀMIES, T. ODIJK AND D. FRENKEL. Application of the optimized Baxter model to the hard-core attractive Yukawa system. *Journal of Chemical Physics* **125**, 194506 (2006) (Chapter 3).
- P. PRINSEN AND T. ODIJK. Collective diffusion coefficient of proteins with hydrodynamic, electrostatic and adhesive interactions. Accepted for publication in *Journal of Chemical Physics* (Chapter 5).

Other publications by the author:

- P. PRINSEN, P. B. WARREN AND M. A. J. MICHELS. Mesoscale simulations of surfactant dissolution and mesophase formation. *Physical Review Letters* **89**, 148302 (2002).
- P. B. WARREN, P. PRINSEN AND M. A. J. MICHELS. The physics of surfactant dissolution. *Philosophical Transactions of the Royal Society of London Series A - Mathematical Physical and Engineering Sciences* **361**, 665 (2003).
- P. PRINSEN AND P. VAN DER SCHOOT. Shape and director-field transformation of tactoids. *Physical Review E* **68**, 021701 (2003).

- P. PRINSEN AND P. VAN DER SCHOOT. Continuous director-field transformation of nematic tactoids. *European Physical Journal E* **13**, 35 (2004).
- P. PRINSEN AND P. VAN DER SCHOOT. Parity breaking in nematic tactoids. *Journal of Physics - Condensed Matter* **16**, 8835 (2004).



Dankwoord

Ten slotte wil ik nog van de gelegenheid gebruik maken om een aantal mensen te bedanken. Allereerst Cindy, voor het feit dat je met mij mee bent verhuisd naar Rotterdam toen ik met mijn promotie begon hoewel je dat eigenlijk niet zo zag zitten. Het is jammer dat het uiteindelijk allemaal anders is gelopen dan dat we toen hadden gedacht.

Iedereen van de sectie Enzymologie: Alexey, Alidin, Angela, Arminder, Barbara, Daan, Dirk, Esengül, Frankie, Fred, Jaap, Jana, Laura, Laurice, Marc, Nahid, Nuria, Peter-Leon, Ram, Sandra, Simon, Suharti, Tony, Valeria en in het bijzonder Emile, Loesje en Marieke. Ik heb het erg naar mijn zin gehad met jullie in de koffiepauzes, tijdens de lunches en in “t Keldertje”.

Ahmed, Agur, Chun, Edgar, Joris en Valeria. Ik vond het erg leuk om het laatste jaar regelmatig bij jullie in Leiden door te brengen.

Harald, als enig medegroepslid in Delft heb je me het eerste jaar wegwijs gemaakt op de TU en we zijn ook samen naar mijn eerste grote conferentie geweest. Bedankt voor je gezelschap en hulp in dat eerste jaar.

Dini, thank you for your company in the years that you were a student in our group.

Mijn kamergenoten Miranda, Ron en Rosario. Bedankt voor de fijne sfeer die er in onze kamer heerste en waarin ik altijd erg prettig heb kunnen werken.

Mijn ouders. Bedankt dat jullie me altijd de vrijheid en de mogelijkheid hebben gegeven om mijn eigen richting te kiezen.

Mijn zusjes, Heleen en Karin. Bedankt voor jullie steun tijdens de promotieplechtigheid.

David and Scott. I thank you for the three months I spent working with you at ANU, and I thank the people from the Department of Applied Mathematics for the great time I had in Canberra and for the first (and so far only) cricket match I ever played.

Paul. Bedankt dat je me na een erg leerzame afstudeerperiode bij jou naar

Theo doorverwees om met hem te gaan praten over een promotieplek.

Theo. In de ruim vier jaar bij jou heb ik enorm veel geleerd. Niet alleen over het onderwerp van dit proefschrift, maar ook over andere onderwerpen in de wetenschap en over het doen van onderzoek. Ik heb erg genoten van onze bijna wekelijkse gesprekken op woensdag in de namiddag en avond. Ik denk dat we in die tijd goede vrienden zijn geworden en dat ik ook na deze promotie zeker nog af en toe langskom voor een interessant gesprek en Thais eten. Dank je wel!

En als laatste wil ik Janine bedanken. Voor je morele steun tijdens de laatste anderhalf jaar van mijn promotie en voor het maken van de afbeelding op de omslag van dit proefschrift. Op het moment zijn we vaak verder van elkaar verwijderd dan we graag zouden willen maar ik hoop nog lang van je bijdehante opmerkingen te kunnen genieten en dat je nog vaak tijdens mijn verhalen over wetenschap precies die vraag weet te stellen waar ik geen antwoord op weet.